

**BUILDING INTER-STOREY DRIFT UNDER
PSEUDO DYNAMIC LOAD**

PANG HUI ER

UNIVERSITI TUNKU ABDUL RAHMAN

**BUILDING INTER-STOREY DRIFT UNDER
PSEUDO DYNAMIC LOAD**

PANG HUI ER

**A project report submitted in partial fulfilment of the
requirements for the award of Bachelor of Civil
Engineering with Honours**

**Lee Kong Chian Faculty of Engineering and Science
Universiti Tunku Abdul Rahman**

May 2023

DECLARATION

I hereby declare that this project report is based on my original work except for citations and quotations which have been duly acknowledged. I also declare that it has not been previously and concurrently submitted for any other degree or award at UTAR or other institutions.

Signature :  _____

Name : PANG HUI ER _____

ID No. : 18UEB04108 _____

Date : 12.5.2023 _____

APPROVAL FOR SUBMISSION

I certify that this project report entitled “**BUILDING INTER-STOREY DRIFT UNDER PSEUDO DYNAMIC LOAD**” was prepared by **PANG HUI ER** has met the required standard for submission in partial fulfilment of the requirements for the award of Bachelor of Civil Engineering with Honours at Universiti Tunku Abdul Rahman.

Approved by,

Signature : 

Supervisor : Ir. Ts. Dr. Yip Chun Chieh

Date : 12.5.2023

Signature : _____

Co-Supervisor : _____

Date : _____

The copyright of this report belongs to the author under the terms of the copyright Act 1987 as qualified by Intellectual Property Policy of Universiti Tunku Abdul Rahman. Due acknowledgement shall always be made of the use of any material contained in, or derived from, this report.

© 2023, PANG HUI ER. All right reserved.

ACKNOWLEDGEMENTS

First and foremost, I would like to express my deep and sincere gratitude to my research supervisor, Ir. Ts. Dr. Yip Chun Chieh, for his advice, motivation and enormous patience throughout the development of the research. His guidance helped me in all the time of research and writing of this report.

Secondly, I would like to thank my research mate, Mr. Khoo Li Yong as well as the UTAR lab staffs, Mr. Ho Chan Cheong, Mr. Wan Mohd Syafiq bin Wan Hanapi and Ms. Nora'aslinda binti Abd Rahman, who had helped me a lot in conducting laboratory work.

In addition, I would like to thank the students from the UTAR undergraduate research scheme, Mr. Lee Tzyy Lih, Ms. Teo Chung Jing, Ms. Chong Jnee, Ms. Leong Choi Mei and Mr. Chong Zi Yao, who gave me a lot of help and contributed to the successful completion of this project.

I would also like to express my gratitude to my loving parents and friends who have given me encouragement and support.

ABSTRACT

Earthquake is the most destructive natural disaster which causes fatalities and destruction globally. Malaysia is considered a region with a low seismicity profile. Earthquakes that happened in neighbouring countries such as Indonesia and Philippines induced impacts and the earthquake tremors may affect buildings in Malaysia. Viscous damper systems have been introduced in this research and potentially enhance the seismic resistance of the building. The main focus of this research is assessing the inter-storey drift performance and mode shape of the scaled reinforced building with and without dampers. A 1:8 downscaled model of 1 bay 3-storey reinforced concrete structure was constructed based on critical parts of a high school building's perimeter structural skeleton for the shaking table's dynamic load test. The model specifications were acquired by applying Similitude Theory and Buckingham's Pi Theorem in order to establish the correlation between the prototype and downscaled model. Failure mode and damage mechanism of the scaled model under different levels of earthquake intensity found that the inter-storey drift of the scaled model is huge when the ground is having large movement with low aggressiveness. On the other hand, when the earthquake's intensity increases, the structural movement was found to reduce gradually with intense vibration such as primary wave. The structure was found to have a higher translation mode of oscillation from single curvature to double curvature when the ground acceleration was getting intense. Three brands of viscous dampers were tested and compared in this study as well. The results showed that all viscous dampers are able to reduce the building inter-storey drift. The breakthrough of this research is the finding of the scaled models' overall rooftop displacements are lowered by 45%, 63% and 34% under different intensities of ground movement with the installation of the APIDO, SKK and ESPADA viscous dampers, respectively. Hence, the novelty of this research is that the APIDO viscous damping system is found to be the most suitable for absorbing large displacement, while SKK viscous damping system is suitable for building lateral displacement generated under intense ground vibration.

TABLE OF CONTENTS

DECLARATION		i
APPROVAL FOR SUBMISSION		ii
ACKNOWLEDGEMENTS		iv
ABSTRACT		v
TABLE OF CONTENTS		vi
LIST OF TABLES		ix
LIST OF FIGURES		x
LIST OF SYMBOLS / ABBREVIATIONS		xv
LIST OF APPENDICES		xvi
CHAPTER		
1	INTRODUCTION	1
1.1	General Introduction	1
1.2	Importance of the Study	2
1.3	Problem Statement	3
1.4	Aim and Objectives	4
1.5	Scope and Limitation of the Study	4
1.6	Contribution of the Study	5
1.7	Outline of the Report	6
2	LITERATURE REVIEW	7
2.1	Introduction	7
2.2	Characteristics of Earthquakes	7
2.3	Impacts of Earthquakes	8
2.4	Earthquakes in Malaysia	11
2.4.1	Earthquakes in West Malaysia	12
2.4.2	Earthquakes in East Malaysia	13
2.5	Similitude Theory and Buckingham's Pi Theorem	15
2.6	Earthquake Behaviour on High-Rise and Low-Rise Buildings	19

2.7	Viscous Dampers	20
	2.7.1 Operation of Viscous Dampers	20
	2.7.2 Configuration of Viscous Dampers	22
2.8	Shaking Table Test	23
2.9	Inter-Storey Drift	25
	2.9.1 Limitation of Inter-Storey Drift	26
2.10	Mode Shape	28
	2.10.1 Factors Affecting Mode Shapes	30
2.11	Summary	33
3	METHODOLOGY AND WORK PLAN	34
3.1	Introduction	34
3.2	Structural Model Details	35
	3.2.1 Geometry	36
	3.2.2 Reinforcement	37
3.3	Scale Factor Determination	38
	3.3.1 Theoretical Prediction	39
	3.3.2 Actual Measurement	40
3.4	Raw Materials	40
3.5	Mix Proportion	42
3.6	Trial Mix Design	42
	3.6.1 Concrete Mixing and Casting	43
	3.6.2 Concrete Curing	45
	3.6.3 Compressive Strength Test	46
3.7	Model Construction	48
	3.7.1 Quality Control	55
3.8	Shaking Table Test	57
3.9	Summary	63
4	RESULTS AND DISCUSSION	65
4.1	Introduction	65
4.2	Bare Frame Structure	66
4.3	Structure with APIDO Dampers	73
4.4	Structure with SKK Dampers	78
4.5	Structure with ESPADA Dampers	83

4.6	Displacement Response for Structure with and without Damper	87
4.7	Prototype Displacement Response Prediction	94
4.8	Summary	96
5	CONCLUSIONS AND RECOMMENDATIONS	97
5.1	Conclusions	97
5.2	Recommendations for Future Work	98
	REFERENCES	99
	APPENDICES	104

LIST OF TABLES

Table 2.1:	Dimensions of Basic Physical Quantities in MLT System (Hamit and Azelođlu, 2020).	17
Table 2.2:	Summary of Similitude Relations for Elastic Model (Yip, et al., 2017).	18
Table 2.3:	Importance Classes for Buildings (EN 1998-1, 2004).	27
Table 3.1:	Mixture of Concrete (Yip and Marsono, 2016).	42
Table 3.2:	Mix Proportion for Trial Mix Design.	43
Table 3.3:	Ultimate Load and Compressive Strength of Concrete Cylinders (Trial Mix Design).	48
Table 3.4:	Ultimate Load and Compressive Strength of Concrete Cylinders (First Floor).	56
Table 3.5:	Ultimate Load and Compressive Strength of Concrete Cylinders (Second Floor).	56
Table 3.6:	Ultimate Load and Compressive Strength of Concrete Cylinders (Third Floor).	56
Table 4.1:	Intensity of Each Level of Earthquake Simulation.	65
Table 4.2:	Inter-Storey Drift for Bare Frame Structure at All Levels.	70
Table 4.3:	Inter-Storey Drift for Structure with APIDO Dampers at All Levels.	77
Table 4.4:	Inter-Storey Drift for Structure with SKK Dampers at All Levels.	81
Table 4.5:	Inter-Storey Drift for Structure with ESPADA Dampers at All Levels.	86
Table 4.6:	Rooftop Displacement and Reduction Percentage of Each Damper at All Levels.	94
Table 4.7:	Prototype Inter-Storey Drift Prediction for Bare Frame Structure and Structure with APIDO Dampers at All Levels.	95
Table 4.8:	Prototype Inter-Storey Drift Prediction for Structure with SKK and ESPADA Dampers at All Levels.	96

LIST OF FIGURES

Figure 2.1:	Part of the Cypress Freeway in Oakland, California, Collapsed during the 1989 Loma Prieta Earthquake (Earle, 2015).	9
Figure 2.2:	Inter-storey Drift due to Weak Storey Mechanism during the Van Earthquake (Yon, et al., 2017).	9
Figure 2.3:	Failure Mechanism of Strong Beam-Weak Column during the Van Earthquake (Yon, et al., 2017).	10
Figure 2.4:	Pacific Ring of Fire (National Geographic Society, 2022).	11
Figure 2.5:	Earthquake Distribution in West Malaysia from 1970 to 2018 (Tongkul, 2021).	13
Figure 2.6:	Earthquake Distribution in Sarawak from 1970 to 2019 (Tongkul, 2021).	14
Figure 2.7:	Plate Tectonic Margins and Movements in Southeast Asia (Tongkul, 2017).	15
Figure 2.8:	Earthquake Distribution in Sabah from 1966 to 2019 (Tongkul, 2021).	15
Figure 2.9:	Typical Viscous Damper (Lee and Taylor, 2001)	21
Figure 2.10:	Schematic of Orifice (Constantinou and Symans, 1992).	21
Figure 2.11:	Different Configurations of Viscous Damper (a) Diagonal; (b) Chevron; (c) Upper Toggle (Pourzangbar, et al., 2020).	22
Figure 2.12:	Shaking Table Test (Kashima and Hirade, 2017).	25
Figure 2.13:	Inter-Storey Drift and Roof Displacement of Buildings (Bhat and Azam, 2020).	26
Figure 2.14:	Basic Mode Shape of Oscillation (Murty, et al., 2012).	28
Figure 2.15:	Resultant Displacement Pattern and Modal Components (Ondrej, 2019).	29
Figure 2.16:	Translational Modes of Oscillation along the X-axis of a 5-Storey Benchmark Building (Murty, et al., 2012).	30

Figure 2.17:	Effect of Flexural Stiffness of Structural Members (a) Pure Flexural Response; (b) Pure Shear Response; (c) Almost Shear Response (Murty, et al., 2012).	31
Figure 2.18:	Effect of Axial Stiffness of Vertical Members (Murty, et al., 2012).	32
Figure 2.19:	Effect of Building Height (a) 5-Storey; (b) 25-Storey; (c) 40-Storey Buildings (Murty, et al., 2012).	33
Figure 3.1:	Study Workflow.	35
Figure 3.2:	Structural Model Geometry.	36
Figure 3.3:	Footing Reinforcement Details.	37
Figure 3.4:	Column Reinforcement Details.	37
Figure 3.5:	Beam Reinforcement Details.	38
Figure 3.6:	Slab Reinforcement Details.	38
Figure 3.7:	Raw Materials of Concrete.	40
Figure 3.8:	Superplasticizer.	42
Figure 3.9:	Materials and Tools Preparation.	44
Figure 3.10:	Dry Mix.	44
Figure 3.11:	Fresh Concrete.	45
Figure 3.12:	Fresh Cylinder Concrete Specimens.	45
Figure 3.13:	Hardened Cylinder Concrete Specimens.	46
Figure 3.14:	Concrete Curing Process.	46
Figure 3.15:	Compressive Strength Test.	47
Figure 3.16:	Footing Formwork with Bolts Installed on Shaking Table.	49
Figure 3.17:	Beam and Slab Formwork.	49
Figure 3.18:	Bar Bending in the Mechanical and Timber Workshop.	50
Figure 3.19:	Footing Reinforcement with Column Starter Bar.	50
Figure 3.20:	Beam Reinforcement.	51

Figure 3.21: Slab Reinforcement Tied with Beam Reinforcement.	51
Figure 3.22: Concrete Casting for Footing.	52
Figure 3.23: Footing Cast.	52
Figure 3.24: First Floor Columns Cast.	53
Figure 3.25: Preparation of Concrete Casting for First Floor Beams and Slab.	53
Figure 3.26: Concrete Casting for Second Floor Beams and Slab.	54
Figure 3.27: Concrete Casting for Third Floor Columns.	54
Figure 3.28: Complete Model.	55
Figure 3.29: First Floor Concrete Specimen 2 After Compression Test.	57
Figure 3.30: Shaking Table in the Advanced Geotechnical Laboratory.	58
Figure 3.31: 50 mm LVDT Installed on the Third Floor of the Model.	59
Figure 3.32: Accelerometer Installed on the Third Floor of the Model.	59
Figure 3.33: Data Logger Connected with the Test Sensors.	60
Figure 3.34: Shaking Table Test Setup of the Bare Frame Structure.	60
Figure 3.35: Bare Frame Structure Installed on Shaking Table.	61
Figure 3.36: APIDO, SKK and ESPADA Dampers (from left to right).	61
Figure 3.37: Damper Connectors Fabricated for Whole Structure.	62
Figure 3.38: Damper Connectors Installed on the Structure.	62
Figure 3.39: Shaking Table Test Setup of the Model with Dampers.	63
Figure 3.40: Structure with APIDO Dampers Installed on Shaking Table.	63
Figure 4.1: Displacement – Time Graph for Bare Frame Structure at Level 1 (a) Overall; (b) Maximum; (c) Minimum.	67
Figure 4.2: Displacement – Time Graph for Bare Frame Structure at Level 5 (a) Overall; (b) Maximum; (c) Minimum.	68

Figure 4.3:	Displacement – Time Graph for Bare Frame Structure at Level 9 (a) Overall; (b) Maximum; (c) Minimum.	69
Figure 4.4:	Mode Shape for Bare Frame Structure at Different Levels.	71
Figure 4.5:	Concrete Cracking on the First Floor Beams of Bare Frame Structure.	72
Figure 4.6:	Concrete Cracks on the Second Floor Column of Bare Frame Structure.	73
Figure 4.7:	Concrete Cracks on the First Floor Column of Bare Frame Structure.	73
Figure 4.8:	Displacement – Time Graph for Structure with APIDO Dampers at Level 1 (a) Overall; (b) Maximum and Minimum.	74
Figure 4.9:	Displacement – Time Graph for Structure with APIDO Dampers at Level 5 (a) Overall; (b) Maximum and Minimum.	76
Figure 4.10:	Mode Shape for Structure with APIDO Dampers at Different Levels.	78
Figure 4.11:	Displacement – Time Graph for Structure with SKK Dampers at Level 1 (a) Overall; (b) Maximum and Minimum.	79
Figure 4.12:	Displacement – Time Graph for Structure with SKK Dampers at Level 5 (a) Overall; (b) Maximum; (c) Minimum.	80
Figure 4.13:	Displacement – Time Graph for Structure with SKK Dampers at Level 10 (a) Overall; (b) Maximum; (c) Minimum.	81
Figure 4.14:	Mode Shape for Structure with SKK Dampers at Different Levels.	82
Figure 4.15:	Displacement – Time Graph for Structure with ESPADA Dampers at Level 1 (a) Overall; (b) Maximum; (c) Minimum.	83
Figure 4.16:	Displacement – Time Graph for Structure with ESPADA Dampers at Level 5 (a) Overall; (b) Maximum; (c) Minimum.	84

Figure 4.17: Displacement – Time Graph for Structure with ESPADA Dampers at Level 9 (a) Overall; (b) Maximum; (c) Minimum.	85
Figure 4.18: Mode Shape for Structure with ESPADA Dampers at Different Levels.	87
Figure 4.19: Mode Shape for Structures at (a) Level 1; (b) Level 2.	88
Figure 4.20: Mode Shape for Structures at (a) Level 3; (b) Level 4.	89
Figure 4.21: Mode Shape for Structures at Level 5.	90
Figure 4.22: Mode Shape for Structures at Level 6.	91
Figure 4.23: Mode Shape for Structures at (a) Level 7; (b) Level 8.	92
Figure 4.24: Mode Shape for Structures at (a) Level 9; (b) Level 10.	93

LIST OF SYMBOLS / ABBREVIATIONS

A	cross-sectional area of the concrete specimen, mm ²
d_r	design inter-storey drift, mm
E_m	modulus elasticity of scaled model, Pa
E_p	modulus elasticity of prototype, Pa
F	compressive strength of the concrete specimen, MPa
h	storey height, mm
m	mass of reinforced concrete, kg
P	ultimate load applied to the concrete specimen, N
S	scale factor for linear dimension
S_a	scale factor for acceleration
S_e	scale factor for structural material elasticity
V	volume of reinforced concrete, m ³
ν	reduction factor
$\pi_j^{(m)}$	capacity of scaled model
$\pi_j^{(p)}$	capacity of prototype
ρ	density of reinforced concrete, kg/m ³
ASTM	American Society for Testing and Materials
LVDT	Linear variable differential transformers
Mw	Moment magnitude
OPC	Ordinary Portland Cement

LIST OF APPENDICES

Appendix A: Graphs	104
--------------------	-----

CHAPTER 1

INTRODUCTION

1.1 General Introduction

Earthquakes are the most destructive natural disasters in human history, resulting in more than a hundred thousand people's deaths and the destruction of property worth billions of dollars. The number of deaths due to natural disasters is lower today than in the historical case since the globe is now more adaptable. However, a high death toll is recorded annually, commonly due to earthquakes and possibly a tsunami triggered by them. The deadliest earthquake recorded in human history happened in Shaanxi, China, with a magnitude of 8 on January 23, 1556, resulting in approximately 830 000 deaths. The earthquake lasted only a few seconds, toppled mountains, shifted the course of rivers, formed cracks up to 20 m deep in the ground, and caused major landslides and devastating flooding and fire lasted for days (Zhang, et al., 2020). Over 60 % of the population was killed in this earthquake since most people in that region used soft soil to build their houses, which had no seismic performance. When the earthquake happened, their houses collapsed, and the entire hillside toppled, burying whole communities (Elhassan, 2018).

The most powerful earthquake in recorded history is the Valdivia Earthquake, also known as the 1960 Great Chilean Earthquake on May 22, 1960. The main earthquake with a magnitude of 9.5, hit approximately 160 km off the coast of Chile, causing a rupture zone of about 1000 km along the country's coast (Pasten, et al., 2021). Four foreshocks larger than magnitude 7.0 preceded this earthquake, including a magnitude 7.9 on the previous day that caused major destruction in the Concepcion region. Five aftershocks with a magnitude of 7.0 or higher were recorded till November 1. At least 3000 people were hurt, 1655 people perished, and two million were homeless due to the Valdivia earthquake. Most of the casualties and economic damages were caused by the massive tsunami triggered by the Valdivia Earthquake that raced across the Pacific. Tsunamis caused deaths and severe damage in Japan, the Philippines and Hawaii (United States Geological Survey, 2022).

Malaysia is located on the Sunda plate in the Eurasian plate and surrounded by the Philippine Plate and Indian – Australian Plate, considered a region with a low seismicity profile. However, the regional earthquakes due to Sumatra's earthquake-prone fault and subduction zones cause seismic events in Malaysia. Moreover, the movement of the Sunda Plate with an eastward movement of 10 mm/year relative to the Eurasian plate also causes local earthquakes in Malaysia (Lee, et al., 2022). From 1922 to 2020, at least 59 earthquake activities in West Malaysia have been recorded in the databases of international and national seismological centres, including the local earthquake caused by a strike-slip fault along the Bukit Tinggi Fault Zone (Nazaruddin and Duerrast, 2021). Despite the fact that Malaysia has experienced significant earthquakes in the past decade, the risk from earthquakes is currently not a concern. As our population increases and the development of buildings and infrastructures keeps improving, the potential for devastation grows daily.

Hence, the seismic performance must be improved in the structural design in order to minimize the earthquake response and eventually reduce the devastating impacts of earthquakes. The energy dissipation tools such as viscous dampers shall be utilised to protect the structure against sudden shock and destructive vibration. In conventional buildings, the earthquake energy is dissipated through the yielding of construction materials, such as the formation of plastic hinges at the beams and columns, which may lead to structural failure when the plastic deformation capacity of the structural members is insufficient (Bayrak, et al., 2022). Viscous dampers absorb earthquake energy when the compressible hydraulic fluid flows through the small orifice in an enclosed cylinder. Consequently, the ability of the structure to sustain seismic activities increases since the viscous damper systems lessen the earthquake effect.

1.2 Importance of the Study

This study examines the structural behaviour and damage mechanism of the reinforced concrete structure under pseudo dynamic load. The lab experiment conducted can be used as guidance or reference to enhance the displacement response as well as seismic resistance of the structure during an earthquake. The data collected in this study can be used in the structural design in order to

minimize the effect of seismic events and prevent structural failure that may lead to loss of life and property.

The study on viscous damping systems is also crucial to enhance the stability performance level of a building, as the seismic effect can be reduced by installing viscous dampers in the structure. The result of inter-storey drift with and without dampers is also crucial in the earthquake design since it can be used to evaluate the seismic hazard levels as well as the performance state of the building under earthquake.

1.3 Problem Statement

Malaysia is free from earthquakes as it is located in a geological stability region away from the active tectonic plates. However, the seismic events that happened in the neighbouring countries induced impacts such as tremors in Malaysia, especially in Sabah. Earthquakes can also trigger other disasters that bring destructive effects to the communities, including tsunamis, landslides and fires (Koçoğlu, et al., 2023). Nevertheless, local construction firms rarely consider the structural design under seismic loads and assess the need for viscous damping systems for reinforced concrete structures in Malaysia.

The past earthquakes that happened in Sabah prove that devastating earthquakes may occur in Malaysia one day. However, Malaysia is not yet prepared to sustain the effect of a large-scale seismic event since there is little current development considering the seismic hazard assessment. Assessing the seismic effect by constructing a real-life structural model is unrealistic as it is time-consuming and not cost-effective. Complicated testing devices are required to study the performance of a full-scale reinforced structure under dynamic loads.

There are a few design parameters that are concerned in seismic analysis in order to study the structural behaviour of the structure during seismic events. Displacement is one of the valuable and trustworthy indicators of the structural performance of a building, especially for high-rise buildings (Serras, et al., 2022). Although the substantial lateral displacement potentially causes failure in the structure, a question remains whether the viscous damper affects the inter-storey drift of a building under seismic loads.

When a building is vibrated at the natural frequency, the deformation of the structural components can be studied by observing the mode shape of the structure (Murty, et al., 2012). Hence, mode shape which is also known as vibration shape, can be used to study the structural behaviour when dynamic loads are caused by different earthquake levels. It may be interesting to compare the mode shape of a structure with and without damping systems.

1.4 Aim and Objectives

This study aims to investigate the inter-storey drift performance of the scaled reinforced building with and without dampers. Three objectives that have been determined in order to achieve the aim are listed below:

- (i) To construct a downscaled reinforced concrete 1 bay 3-storey model.
- (ii) To access the building's inter-storey drift with and without dampers.
- (iii) To compare the mode shape of the building with and without dampers.

1.5 Scope and Limitation of the Study

This study is to construct a structural model of 1 bay 3-storey reinforced concrete structure that scaled-down eight times from a full-scale high school building model prototype. Before the construction of the structural model, a trial mix design of the grade C30 concrete is done to ensure the mix proportion is able to produce concrete with desired strength. The model with a total height of 1.5 m is then placed on a shaking table to simulate unidirectional movement in the laboratory. The shaking table test will be repeated by testing the structure with a damping system that can suppress the vibration of the building during earthquake simulation. The full scale of the building is impractical due to the laboratory's cost, facility and space restrictions.

The limitation of the study is that the downscaled model is more idealised and simplified than the actual building. The structural model only consists of the structural members, which are columns, beams and slabs. Nevertheless, there should be walls constructed, finishes of walls and floors as well as furniture placed in the real building, causing more loads acting on the

structure such as dead load, live load and superimposed load. Moreover, the slab is constructed at the same level for the whole storey in the model. However, the real building typically considers dropping panels in the toilet and bathroom area. Furthermore, this study only considers seismic load as the lateral load, although other loads may exist in an actual building.

1.6 Contribution of the Study

The results obtained from the shaking table test can be used to assess the structure's condition after experiencing a seismic event. This data is necessary for retrofitting existing damaged buildings to prevent catastrophic consequences. At the same time, this study also provides information to optimise the design of new buildings with better seismic resistance that can withstand the higher intensity of earthquakes or for a longer time. The utilisation of a damping system in new buildings aids in reducing the environmental impact of earthquakes by decreasing the construction material required for seismic retrofitting.

The study on the energy dissipation device offers the consultant firm another option in designing the structure considering lateral load, including seismic load and wind load. The development of new damping technologies and systems has the potential to drive innovation in earthquake engineering, leading to new advances in Malaysia. With continual research and development, engineers and researchers can develop new materials, designs, and damping strategies to improve the performance of structures during earthquakes.

Earthquake mitigation measures are much needed and concerned in the structural design in East Malaysia, especially in Sabah, since it is predicted to have more frequent near-field earthquakes happen in the future. Developing proper earthquake mitigation measures helps improve the resilience of buildings and infrastructure during an earthquake. Seismic mitigation strategies are essential to minimize property damage, protect human life and guarantee the continued operation of vital infrastructure such as hospitals and emergency services during and after earthquakes.

1.7 Outline of the Report

This report comprises five chapters which are the introduction, literature review, methodology and work plan, results and discussion as well as conclusions and recommendations. References and appendices follow the main chapters.

Chapter 1 outlines the general introduction of the research, including the history of earthquake disasters, seismicity in Malaysia as well as the application of energy dissipation tools. Besides, the problem statement, aim and objectives of this study are mentioned in this chapter. This chapter also includes the scope and limitation of the study, the contribution of the study and the outline of the report.

Chapter 2 presents the literature review of the study. The characteristics and impacts of earthquakes will be described in this chapter. The earthquakes in Malaysia, including West and East Malaysia, will also be reviewed. The theories applied in this study which are Similitude Theory and Buckingham's Pi Theorem will be discussed in this chapter. Moreover, this chapter also mentions the operation and configuration of viscous dampers. The shaking table test with the expected outcomes of this study which are inter-storey drift and mode shape will be discussed in this chapter.

Chapter 3 focuses on the methodology and work plan of the study. A study workflow will be presented in detail. The structural model specifications and details will be stated as well. In addition, the procedures for constructing the scaled model and conducting the shaking table test will be explained in this chapter.

Chapter 4 discusses the results obtained from the shaking table test. Four structures will be tested in this study, including a structure without dampers and structures with three brands of viscous dampers. The lateral movement of each building throughout the shaking table test will be recorded to assess its inter-storey drift and mode shape under varying intensities of shaking. The experimental data will be analysed and compared among the structures to study the structure's seismic performance with and without dampers.

Chapter 5 consists of the conclusion and recommendation part. A summary of the study's aim and objectives will be outlined. Lastly, several recommendations for future work will be given.

CHAPTER 2

LITERATURE REVIEW

2.1 Introduction

Malaysia is a country in Southeast Asia that is free from natural disasters, including earthquakes, since it is located in a geologically stable region. However, the occurrence of earthquakes in Malaysia keeps increasing in this decade due to the movements of plate tectonic in Southeast Asia that are approaching Malaysia. Malaysia is now subjective to both far-field earthquakes and near-field earthquakes. Hence, it is now the trend to enhance the seismic resistance of the structure in order to reduce the devastating effects when an earthquake strikes our country, such as structural failure and collapse.

The earthquake energy is transferred to the building during the seismic event, causing the structure to vibrate. The structure vibrates continuously until all the transferred energy is dissipated. If the structure is not equipped with an energy dissipation system, the energy is dissipated through the friction in the joints of structural members at a prolonged rate. The structural members will move in large displacement if the vibration is too vigorous due to the high intensity of the earthquake. Consequently, plastic joints will be formed in the structure, increasing ductility and energy depletion. As a result, the local degradation of the structure results in a significant energy loss.

Viscous dampers are hydraulic devices that scatter seismic activity and minimize the impacts of the earthquake on the building. A viscous damper is used to disperse the dynamic loads by the mechanism of passing the hydraulic fluid through the orifice. It can be utilised in the structure to reduce the motion of the high-rise building due to wind loads and protect the structure during a seismic event. The retrofitting of the structure with the brace-viscous damper system improves the seismic resistance of the structure.

2.2 Characteristics of Earthquakes

An earthquake is a seismic event that involves intense and violent shaking of the Earth's surface resulting from the movement between tectonic plates along a fault line in the outermost layer of the Earth. It usually occurs suddenly and

without warning. The Earth is made of four major layers, which are a solid inner core, a liquid outer core, a nearly solid mantle and a solid crust. The crust and the top and stiff layer of the mantle form a region called the lithosphere, covering the Earth's surface with many giant tectonic plates. The tectonic plates constantly move slowly, causing friction between the edges of the faults. The energy that lets two blocks of the earth slip past one another is stored in the ground. When the force of moving tectonic plates is able to overcome the friction, earthquakes happen to release the energy, creating seismic waves that cause vibration on Earth's surface (Wald, 2009).

The occurrence of an earthquake cannot be avoided and is hard to predict since it occurs primarily due to the sudden rupture of geological faults. When an earthquake ruptures, it does not occur all at once. Instead, it begins at a particular location and spreads quickly to other places. Some earthquakes have foreshocks with a smaller intensity that happens before the mainshock. The main earthquake is commonly followed by a series of aftershocks (Wald, 2009). Most aftershocks have a smaller magnitude than the main shock, but some can be larger. It can be happened anytime after the main shock, within seconds, minutes, hours, days, weeks or even years (Earle, 2015).

2.3 Impacts of Earthquakes

The earthquakes in recorded history have caused much destruction and millions of deaths globally. The common impacts of an earthquake include structural damage to structures, damage to bridges and highways, landslides, fire hazards, liquefaction and tsunamis. The extent of destruction and effects of an earthquake depends on the intensity and location of the earthquake's epicentre, the population in the affected area, the risk management of the area, and the seismic resistance of the structure (Earle, 2015). Figure 2.1 show the impacts of the earthquake in a past seismic event.



Figure 2.1: Part of the Cypress Freeway in Oakland, California, Collapsed during the 1989 Loma Prieta Earthquake (Earle, 2015).

Earthquakes also lead to structural failure in reinforced concrete buildings due to inappropriate design. The most frequent failure mode in a reinforced concrete building is the soft and weak storey mechanism, notably on the structure's first floor. When the wall is not constructed continuously along the height of the building, the structure may experience a sudden change in lateral strength between adjacent storeys during the earthquake. This unexpected inter-storey drift will cause brittle failures at the end of the columns and eventually lead to partial or total collapse in the weak storey of the building (Yon, et al., 2017). The structural damages due to the weak storey mechanism can be seen in Figure 2.2.



Figure 2.2: Inter-storey Drift due to Weak Storey Mechanism during the Van Earthquake (Yon, et al., 2017).

Other than the weak storey mechanism, the strong beam and weak column concept is undesirable in the seismic design of the reinforced concrete structure. When the earthquake loads act on the structure, the deep and rigid beams resist more moments than weak columns (Yon, et al., 2017). Consequently, these beams behave elastically, causing the plastic hinges to be formed at the flexible columns. The column will transfer all the forces from the structural members to the foundation. The failure of a column in the structure eventually leads to global structural damage, and the whole structure may be collapsed due to this concept (Irfani and Vimala, 2019). Figure 2.3 shows the structural failure due to the strong beam-weak column effect during an earthquake.



Figure 2.3: Failure Mechanism of Strong Beam-Weak Column during the Van Earthquake (Yon, et al., 2017).

Moreover, inadequate transverse reinforcement in columns and beams will reduce the ductility of the reinforced concrete structures. The structural members are not capable of resisting the increment of shear forces and dynamic loads during an earthquake, especially at the columns and beam-column joints. Furthermore, shear failure is possible to be experienced by a short column in the structure during earthquakes. This is because the short column will carry more shear forces since it is stiffer and more brittle than the other columns (Yon, et al., 2017).

2.4 Earthquakes in Malaysia

Malaysia is considered a region with a low seismicity profile since it is not in the Ring of Fire. The Ring of Fire is also known as the Circum-Pacific Belt, an active zone of earthquakes and volcanic eruptions around the edges of the Pacific Ocean (National Geographic Society, 2022). It is a 40,000 km path formed due to the interactions of the massive Pacific Plate with several surrounding tectonic plates, which are relatively less dense, as shown in Figure 2.4. Malaysia is located on the Eurasian plate, the Australian plate in the west, and the Philippine plate near East Malaysia (Marto, et al., 2013).

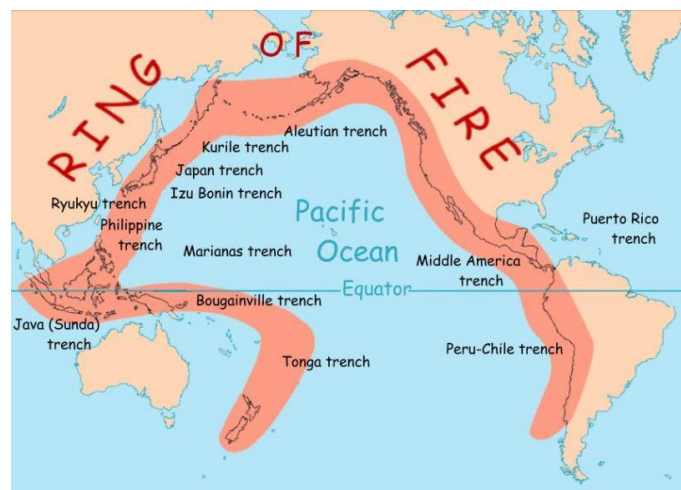


Figure 2.4: Pacific Ring of Fire (National Geographic Society, 2022).

Although Malaysia is not included as a country in the Ring of Fire, Malaysia experiences tremors and is affected by the neighbouring countries with active seismic events. Most of the earthquakes from the neighbouring nations bring minor effects to Malaysia. According to the recorded history, the 2004 Indian-Ocean Earthquake with a magnitude of 9.1 Mw is one of the most significant regional earthquakes that caused devastating effects on Malaysia and other countries. This earthquake led to an unexpected tsunami, causing 68 deaths in Malaysia and thousands of deaths in Indonesia, Sri Lanka and Thailand (Marto, et al., 2013).

2.4.1 Earthquakes in West Malaysia

West Malaysia is affected by local and regional earthquakes, also known as long-distance earthquakes. There are two major sources of earthquakes that cause seismic activities in West Malaysia, which are the Sumatra subduction zone and the great Sumatra fault. Most significant earthquakes in West Malaysia originated from the Sumatra subduction zone, which is one of the most active plate tectonic boundaries globally. Malaysia is located northeast of Sumatra Island with the closest distance of 450 km from the subduction zone. Nevertheless, the far-field earthquake caused by the subduction zone can travel up to 1,000 km and create tremors in the regions (Nabilah and Balendra, 2012).

The second feature of far-field earthquakes is the Sumatra strike-slip fault, which is 275 km from Malaysia. Sumatra fault is one of the tremendous dextral faults on the surface of Earth with a 1,900 km length running through the entire Sumatra Island. This fault consists of 19 segments and moves at 6 to 27 mm every year. Less energy is stored on Earth due to the movement of faults, thus the intensity of earthquakes caused by the Sumatra fault zone is lower than the earthquake that originated from the Sumatra subduction zone (Marto, et al., 2013).

Even though Malaysia is not in the Ring of Fire, local earthquakes that originated within Malaysia have been recorded since 1970 (Tongkul, 2021). The reactivations of inactive faults are believed to be due to the intraplate stress developed after the 2004 Mega seismic event. Bentong Fault Zone, which covers Bukit Tinggi Fault and Kuala Lumpur Fault, is recognized as the major active seismic feature in West Malaysia (Marto, et al., 2013). Figure 2.5 shows the historical near-field earthquakes located in Peninsular Malaysia. The earthquakes are mainly in Bukit Tinggi, Kuala Pilah, Temenggor, Kuala Pilah, Kenyir and Manjung. Most of the local earthquakes have a magnitude of less than 4 Mw, only cause some tremors and shaking of high-rise buildings in Malaysia but do not lead to any devastating changes (Tongkul, 2021).

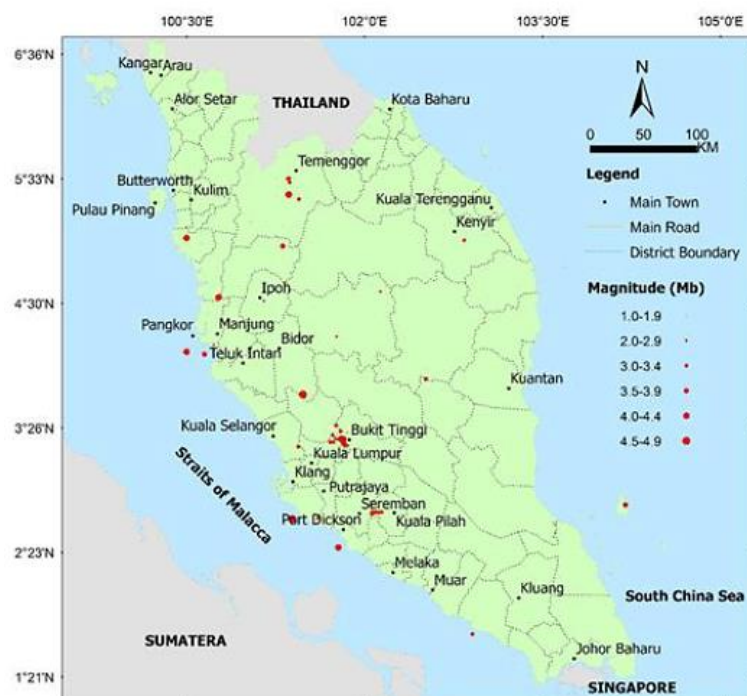


Figure 2.5: Earthquake Distribution in West Malaysia from 1970 to 2018 (Tongkul, 2021).

2.4.2 Earthquakes in East Malaysia

East Malaysia consists of two states which are Sabah and Sarawak as well as the Federal Territory of Labuan. East Malaysia has more seismic activities compared to West Malaysia as it is located near the active fault lines. The seismic events that occurred in East Malaysia are due to the active faults, including normal faults, thrust faults and strike-slip faults.

Most of the earthquakes in Sarawak are due to local earthquakes. About 20 light to moderate earthquakes less than 5 Mw in magnitude were recorded in Sarawak from 1970 to 2019. Figure 2.6 shows that the earthquakes surround Selangau and Niah in Sarawak. The local earthquakes mainly happened after 2006 due to the NW-SE trending dextral strike-slip faults near the Bukit Mersing area and the N-S trending sinistral strike-slip faults in the Niah area (Tongkul, 2021).

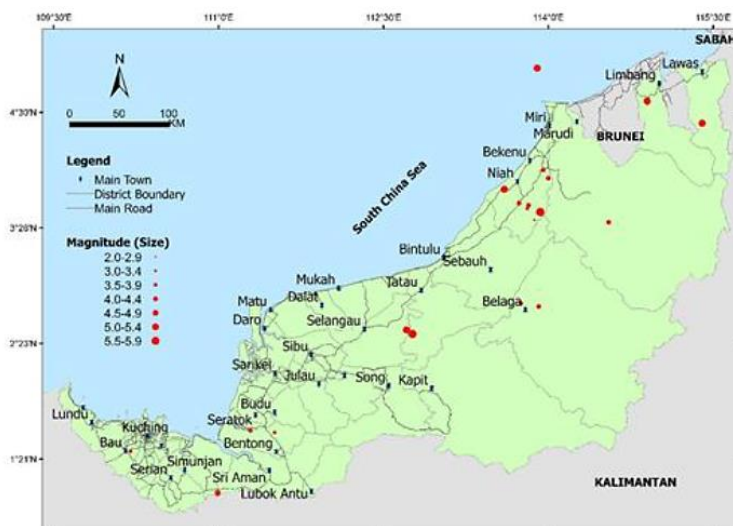


Figure 2.6: Earthquake Distribution in Sarawak from 1970 to 2019 (Tongkul, 2021).

Sabah is the most tectonically active region in Malaysia, as it is close to the main plate boundary faults. It is surrounded by the Indian-Australian Plate, Eurasian Plate and Philippine Plate while these tectonic plates are approaching each other from different directions and at varying rates, as shown in Figure 2.7 (Tongkul, 2017). The movement and interaction of three major tectonic plates cause the subduction zone and initiate an earthquake in Sabah. The active subduction zones identified by the Cotabato, Manila, Negros, Philippine, Sulu, and North Sulawesi Trench are the feature of regional earthquakes in Sabah (Tongkul, 2021). It can be noticed that small earthquakes with a magnitude greater than 2.0 Mw frequently happen in Darvel Bay and Ranau areas, as shown in Figure 2.8.

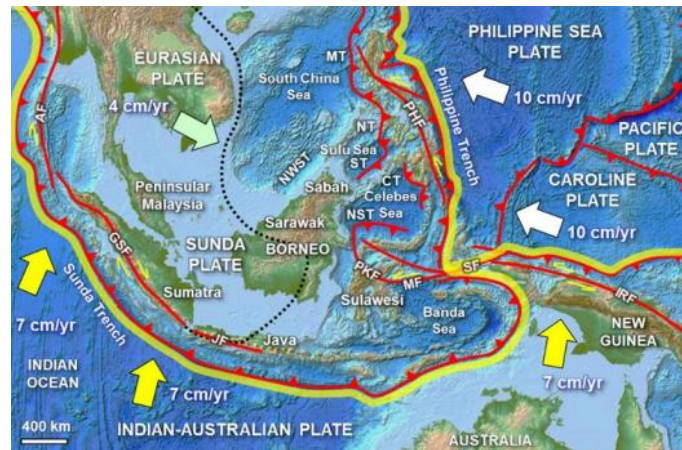


Figure 2.7: Plate Tectonic Margins and Movements in Southeast Asia (Tongkul, 2017).

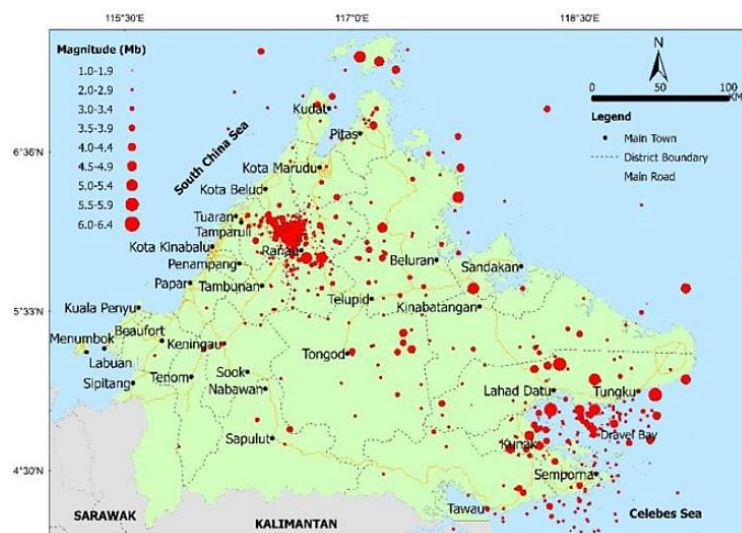


Figure 2.8: Earthquake Distribution in Sabah from 1966 to 2019 (Tongkul, 2021).

2.5 Similitude Theory and Buckingham's Pi Theorem

Experimental testing is essential for the development of technology and validation of the prediction of new approaches in the field of structural engineering (Casaburo, et al., 2019). Since full-scale structure testing is complicated and required more time and cost to construct the structure, a small-scale model is commonly used to conduct the experimental testing in the laboratory. Moreover, a repeated test is always needed due to unexpected conditions or errors that happen during the test. Other than that, testing facilities and equipment for the full-scale model are always limited. Consequently, scale

models are utilised by many researchers to study the behaviour of the full-scale model (Yip, et al., 2017).

However, even if it is perfectly scaled down or up, the scaled model is still another structure that may have its ultimate capacities. The static and dynamic responses of the scaled model do not coincide with its full-scale structure. Hence, the full-scale system's structural behaviour sometimes cannot be represented in the scaled model (Casaburo, et al., 2019).

Similitude theory is applied to design a scaled-down or up model for a full-scale prototype in order to predict its structural response by using the scaled results. Similitude theory is a concept that focuses on determining the necessary conditions for establishing similarity between two or more systems. In structural engineering, a prototype is referred to as the full-scale system while the scaled system is known as a model, regardless of whether it is scaled up or down. When the model achieves the similitude condition, the model is expected to behave as the prototype (Casaburo, et al., 2019).

Three types of similitude can be established between the model and prototypes, which are geometric, kinematic and dynamic similitude. The scaled model and the prototypes are considered full similitude when all the similitude exists simultaneously. Nevertheless, this condition is hard to satisfy due to the ambient environment and testing conditions. Hence, it is essential to determine the testing conditions in order to scale the basic variables accordingly (Hamit and Azeloğlu, 2020).

Similitude methods are applied to derive the theoretical relationships between the physical variable (Yip, et al., 2017). Various types of similitude methods were established, such as the dimensional analysis, energy method, asymptotical scaled modal analysis, similitude theory applied to governing equations, sensitivity analysis and empirical similarity method. Dimensional analysis is the common method applied in structural engineering since it is simple, fast and suitable to be used without determining the governing equations (Casaburo, et al., 2019).

Buckingham's Pi theorem is used in dimensional analysis. By applying this theorem, the number of parameters involved in the systems is reduced since the dimensionless group is determined. The common fundamental dimension used to describe the physical variables are length (L), time (T) and either mass

(M) or force (F). Table 2.1 summarises the dimensions of a basic physical quantity in the MLT base, which only utilised mass, length and time.

Table 2.1: Dimensions of Basic Physical Quantities in MLT System (Hamit and Azeloğlu, 2020).

Symbol	Physical Quantity	Unit	Symbol	Physical Quantity	Unit
[L]	Length	L	[M]	Mass	M
[T]	Time	T	[v]	Velocity	LT ⁻¹
[a]	Acceleration	LT ⁻²	[F]	Force	MLT ⁻²
[ρ]	Density	ML ⁻³	[P]	Pressure	ML ⁻¹ T ⁻²
[α]	Angle	1	[E]	Energy	ML ² T ⁻²

Based on this theorem, the equation must be equivalent despite the units involved in the physical variables (Yip, et al., 2017). For instance, the functional relation of physical variables is shown in Equation 2.1, while the equation is rewritten in terms of pi products, as shown in Equation 2.2. Each pi group is then determined as shown in Equation 2.3, Equation 2.4 and Equation 2.5.

$$f_1(P_1, P_2, \dots, P_N) = 0 \quad (2.1)$$

$$f_2(\pi_1, \pi_2, \dots, \pi_{N-K}) = 0 \quad (2.2)$$

$$\pi_1 = f_3(P_1, P_2, \dots, P_K, P_{K+1}) = 0 \quad (2.3)$$

$$\pi_2 = f_4(P_1, P_2, \dots, P_K, P_{K+2}) = 0 \quad (2.4)$$

$$\pi_{N-K} = f_5(P_1, P_2, \dots, P_K, P_N) = 0 \quad (2.5)$$

where

P denotes the physical variable

N denotes the number of physical variables

π denotes the dimensionless product

K denotes the number of fundamental dimensions

After the pi groups are determined for the systems, Buckingham's Pi theorem is incorporated with the similitude theory. As a result, the dimensionless pi products are equally scaled as they will be similar for the capacity of the scaled model (m) and full-scale prototypes (p), as shown in the equation below.

$$\pi_j^{(m)} = \pi_j^{(p)} \quad (2.6)$$

for $j = 1, 2, \dots, (N - K)$

Furthermore, the capacity of the full-scale prototype and the scaled model is affected by the fundamental scale factors. Scale factor must be taken into account in each equation in order to determine prototype and scaled factor capacity for similitude conditions (Yip, et al., 2017). The scale factors of the common parameters are shown in Table 2.2.

Table 2.2: Summary of Similitude Relations for Elastic Model (Yip, et al., 2017).

Parameter	Scale Factor
Dimension ($h_p = \text{height}$ or $t_p = \text{thickness}$)	S
Area A_p	S^2
Volume V_p	S^3
Linear displacement U_p	S
Moment of inertia I_p	S^4
Frequency f	$S^{-1/2}$ or $(S/Sa)^{-1/2}$
Time	$(S/Sa)^{1/2}$
Density ρ_p	Se/SaS
Point load F_p	SeS^2
Line load F_L	SeS
Uniform distributed load P_p	Se
Shear force V_p	SeS^2

Table 2.2 (Continued)

Moment M or Torque T	SeS^2
Stress σ_p	Se
Velocity V	$(S)^{1/2}$
Acceleration a	Sa or S/S = 1
Curvature C	1/S
Mass M	SeS^2/Sa
Stiffness K	SeS
Spectral acceleration S_A	$SeS^2/(SeS^2/Sa)$

The scale factor, S is vital for the scaling of linear dimensions, including height, width, length and thickness. The acceleration scale factor, S_a is equal to the product of time and velocity dimension and it can be determined by using Equation 2.7. It is equal to 1 when the system is under constant gravitational. The stress scale factor, S_e is related to the elasticity of structural material, as shown in Equation 2.8. It is essential to define the strength effects of downscaled material (Yip, et al., 2017).

$$S_a = \left(\frac{1}{S^{1/2}}\right) \left(\frac{S}{S^{1/2}}\right) \quad (2.7)$$

$$S_e = \frac{E_p}{E_m} \quad (2.8)$$

where

E_p = modulus elasticity of prototype, Pa

E_m = modulus elasticity of scaled model, Pa

2.6 Earthquake Behaviour on High-Rise and Low-Rise Buildings

The seismic behaviour of high-rise buildings is generally different from low-rise buildings to a certain extent. The earthquake load distribution is affected by the properties of the building, such as its mass, shape and size, ground acceleration, and dynamic characteristics. High-rise buildings usually are more flexible and typically experience lesser ground acceleration than low-rise

buildings (Rajmani and Guha, 2015). Nevertheless, high-rise buildings are more susceptible to shaking longer, which causes them to magnify the long-period ground motion (Aly and Abburu, 2015). This means that high-rise buildings are at risk of damage when the duration of an earthquake is long. Thus, one of the mitigation methods to reduce the seismic impact on high-rise buildings is to use a tuned mass damper. The tuned mass damper is the most efficient when the first mode contribution to earthquake response is dominant, which happens in high-rise buildings (Elias and Matsagar, 2015). However, the tuned mass damper is more effective in helping the building dissipate energy in low earthquake shaking levels compared to medium to strong earthquakes (Gutierrez Soto and Adeli, 2013).

Low-rise buildings are shorter and more rigid compared to high-rise buildings. The performance of low-rise buildings during an earthquake might not be as effective as high-rise buildings. This is because low-rise buildings have higher inter-storey drift and lateral displacement compared to high-rise buildings (Yel, et al., 2022). In low-rise buildings, ground motion duration does not impact its seismic response, although a slightly higher inter-storey drift can be seen in a short duration of ground motion (Martineau, et al., 2020). Besides, high-rise buildings are usually designed to resist lateral loads such as seismic loads and wind loads. In contrast, these designs are usually not emphasized in low-rise buildings, which makes them more prone to destruction during earthquakes. Therefore, a viscous damper is usually used in low-rise buildings to resist seismic impact.

2.7 Viscous Dampers

2.7.1 Operation of Viscous Dampers

Viscous dampers, also known as seismic dampers, are hydraulic devices used in a structure to dissipate energy during seismic events. Damping devices were initially designed for the shock isolation of military equipment and transitioned to the industry field since viscous dampers are able to protect buildings, bridges and other structures against sudden vibration and violent shock (Constantinou and Symans, 1992). Viscous dampers absorb most of the seismic energy before the formation of plastic hinges in the structural members to absorb the energy (Lee and Taylor, 2001).

Figure 2.9 shows the longitudinal cross-section of a typical viscous damper. There are six components in a viscous damper, including a stainless-steel piston rod, a cylinder made from seamless steel tubing, a piston head connected to the piston rod that divides the cylinder into two pressure chambers, a compressible hydraulic fluid, an internal accumulator for smooth fluid circulation and a seal to ensure zero leakage. Silicone fluid typically serves as the hydraulic fluid since it is non-toxic, non-flammable, thermally stable, and will not degrade after a long period (Lee and Taylor, 2001).

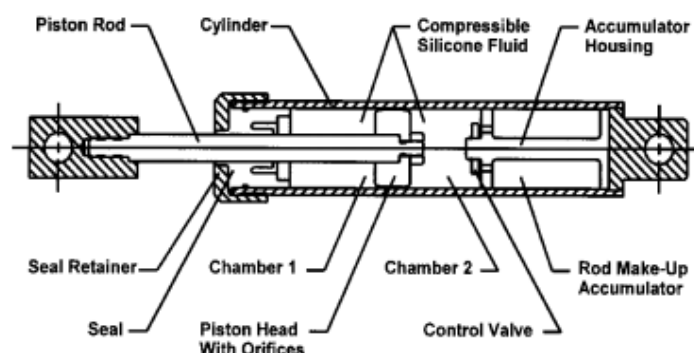


Figure 2.9: Typical Viscous Damper (Lee and Taylor, 2001)

When the piston strokes through the fluid-filled cylinder, silicone fluid is forced to flow from chamber 2 towards chamber 1 through the orifice at a very high speed. The orifice connected to the piston head is designed for the fluid control mechanisms, as shown in Figure 2.10. It uses several uniquely shaped channels to adjust flow patterns in response to the fluid velocity (Constantinou and Symans, 1992).

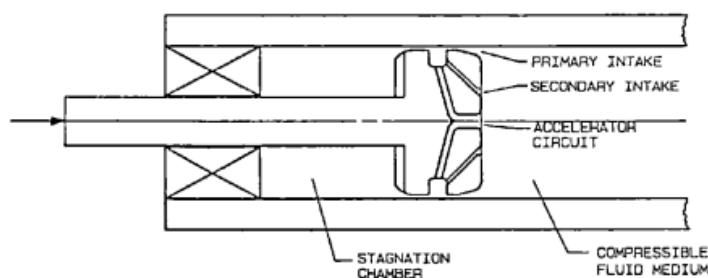


Figure 2.10: Schematic of Orifice (Constantinou and Symans, 1992).

The movement of hydraulic fluid from the chamber to the orifice and then to another chamber with different opening areas cause the dissipation of

energy due to the loss of the pressure head. In short, the dynamic energy is mitigated by the movement of the piston through the silicone fluid in viscous cylinders (Pourzangbar, et al., 2020). Viscous dampers create a force that is directly proportional to the axial velocity of the dampers in order to resist the dynamic motion of the structure (Lee and Taylor, 2001).

2.7.2 Configuration of Viscous Dampers

The efficiency of brace-viscous damper systems is governed by dynamic parameters such as the brace stiffness and the arrangement of viscous dampers in the structure. The damper with a greater brace stiffness is more capable of absorbing and dissipating energy. When the brace is stiffer, the brace is able to hold the damper at the fixed position firmly. Hence, there is less interaction between the brace and the viscous damper, enhancing the functionality of the damper. The dynamic response of the structure is reduced by the brace-viscous damper system (Pourzangbar, et al., 2020).

The configuration of viscous dampers in a structure also brings a significant impact on the seismic performance of the building. Different configurations of damper-brace systems are suggested to be applied in different structures to enhance the mitigation of displacement caused by seismic energy. For instance, K-shape and diagonal brace-viscous damper systems are not suitable to be used in high-rise and shear wall structures since they are not cost-effective. Figure 2.11 shows the typical configurations of viscous dampers, including the diagonal, chevron and upper toggle brace-viscous damper system.

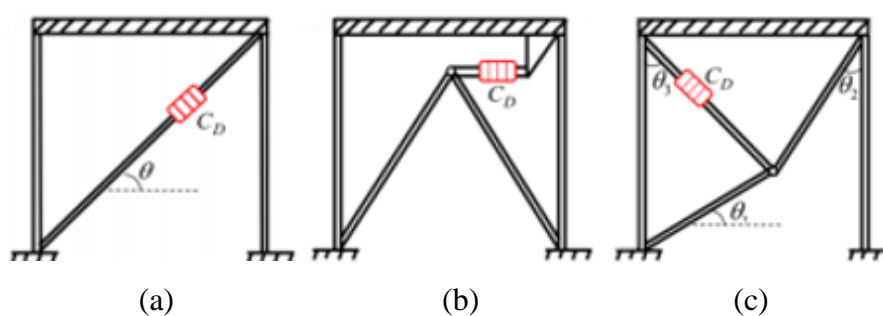


Figure 2.11: Different Configurations of Viscous Damper (a) Diagonal; (b) Chevron; (c) Upper Toggle (Pourzangbar, et al., 2020).

The damper is installed along the brace axis in the diagonal brace mechanism while the damper is placed at the upper part of the braces in the chevron arrangements. The chevron damper does not incline since it is parallel to the floor (Pourzangbar, et al., 2020). Hence, the magnification factor of the displacement in the chevron brace system is equal to one, and the chevron damper's displacement represents the storey's drift. Nevertheless, the axial displacement of the diagonal damper is less than the storey drift of the structure as the magnification coefficient is always smaller than one due to the inclination of the damper (Constantinou, et al., 2001). The damping ratio in the chevron bracing damper arrangement is greater than the diagonal configuration since the damping ratio is directly proportional to the displacement coefficient (Pourzangbar, et al., 2020).

For the toggle configuration, one of the ends of the damper is connected to the beam-column connection, while the other end is attached to the brace connection. Since the value of the magnification factor in the toggle bracing damper is more than one, the displacement of the damper is much larger than the structural drift. Hence, the toggle braced-damper system is suitable to be utilised when the storey drift is relatively small, including the application of wind response reduction and seismic hazard mitigation in stiff structural systems. Toggle configuration is preferable to the diagonal and chevron damper arrangements since it not only mitigates dynamic loads efficiently in the structure but also saves the cost of the energy dissipation system due to its significant magnification coefficient of displacement (Constantinou, et al., 2001).

2.8 Shaking Table Test

The shaking table test is one of the techniques that is widely used to investigate the dynamic behaviour of the structure in earthquake engineering (Boron, et al., 2023). It is conducted to assess the response of the building under linear and nonlinear dynamic loads during seismic events. The shaking table is able to perform realistic earthquake simulations in order to study the seismic performance of the test model. This test is performed to study the failure mode, damage mechanism and the weak parts of the structure under different levels of earthquake intensity in order to analyse and evaluate the effectiveness of the

shock absorption and isolation of the structure. Furthermore, the mechanical performance of the bracing system in the structure can be investigated by performing the shaking table test using a scaled model (Wang, et al., 2021).

Sometimes, field testing is carried out to verify the results of the shaking table tests after the structure is completed. For instance, the dynamic characteristics and seismic performance of high-rise buildings, Shanghai Tower (632 m high) and the Famen Temple (147 m high) in Shaanxi Province, China, were investigated and evaluated from the data obtained from field experiments as well as the shaking table tests conducted on the scaled model (Boron, et al., 2023). Moreover, the multidirectional shaking table test was conducted on a scaled model of a 33-storey reinforced concrete building, and the results were then verified in the field testing after the construction was completed to study the dynamic similitude between the prototype and scaled model (Lu, et al., 2008).

Currently, the shaking table test is the only experimental method that can be conducted to simulate real earthquake loadings in the laboratory (Nama, et al., 2023). There are various types of shaking tables that operate using different methods, including electrical shaking tables, hydraulic shaking tables, and manually driven shaking tables. The earliest known shaking table developed in Japan was driven by manual power in Japan at the end of the 19th century. At the beginning of the 20th century, the shaking table driven by an electric motor that was capable of producing unidirectional refined oscillatory motion was developed by Stanford University (Severn, 2011).

The shaking table driven by a hydraulic system also had been developed in recent years. The shaking table is recently developed from single-directional movement to two and even three-dimensional vibrations that actuated in the global x, y and z-axis. There is a study that developed a shaking table that is unique from the current shaking table, which is able to simulate the earthquake in a true manner. The designed shaking table capable to mimic an earthquake with high energy, then gradually decreases until reaching the zero value (Nama, et al., 2023). Hence, the dynamic motions generated by the shaking table in more direction capable of reproducing the actual earthquake motions more realistic and faithfully than the one-dimensional shaking table.

Steady state and random shaking can be performed using a shaking table by generating different wave motions. A harmonic wave is used in performing steady state shaking, while a random wave of white noise is utilised in the random shaking. Different frequencies of the harmonic wave with low amplitude keep the test model in the elastic range in order to study its dynamic properties. Intense movements are involved in the random shaking to reproduce the actual situation during an earthquake. The amplitude of motions is adjusted to test the limit of the test model to sustain the seismic loads (Kashima and Hirade, 2017). Figure 2.12 illustrates the shaking table driven by the actuator.

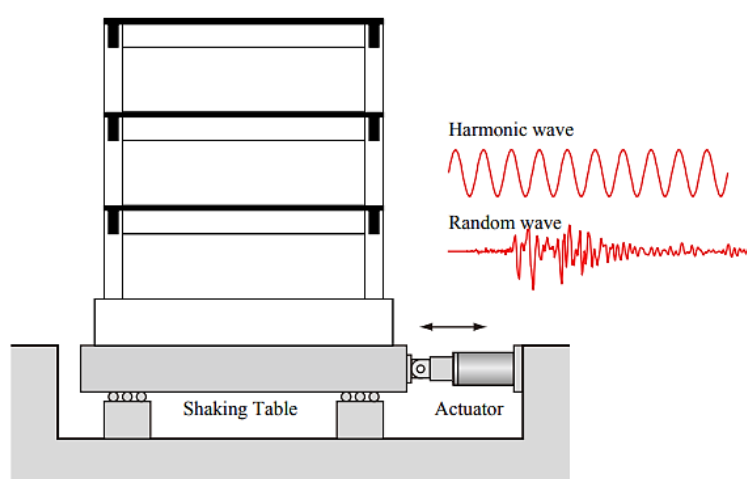


Figure 2.12: Shaking Table Test (Kashima and Hirade, 2017).

There are a few indicators that are concerned in seismic analysis in order to study the structural behaviour of the structure during seismic events. The response indicators are separated into local and global indicators. Local indicators refer to the parameters used to locate the possible damage in the structure and assess the degree to which stress and strain threshold values are attained at various performance levels. On the other hand, global indicators are mainly used in determining the fundamental characteristic of the structures, such as displacements, forces and moments.

2.9 Inter-Storey Drift

Inter-storey drift is one of the valuable and essential indicators of the deformations of a building, especially for high-rise buildings. Inter-storey drift is defined as the difference in lateral displacement between two consecutive

storeys caused by wind and seismic forces. It must be taken into account when analysing a structure since lateral displacement will cause failure in the structure.

The resultant drift of any storey in the structure is the addition of the axial deformation of the slab, shear deformation of the respective storey, the global buckling of the building as well as the rotation of the foundation (Bhat and Azam, 2020). However, the flexural curvatures and rotations are not taken into consideration in evaluating the framing system. Figure 2.13 shows the deformation of a 4-storey building.

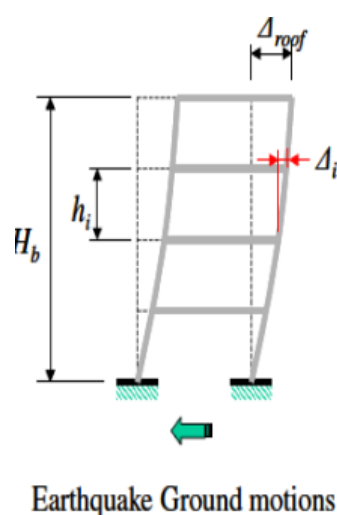


Figure 2.13: Inter-Storey Drift and Roof Displacement of Buildings (Bhat and Azam, 2020).

2.9.1 Limitation of Inter-Storey Drift

Eurocode 8: Design of structures for earthquake resistance – Part 1: General rules, seismic actions and rules for buildings (EN 1998-1:2004) is a European standard that provides guidelines for the seismic design of buildings and structures. It provides a comprehensive set of guidelines for the seismic design of structures, including the seismic hazard assessment, seismic analysis and design of structures to resist seismic forces in varying intensities and magnitudes, as well as other forms of ground motion such as aftershocks and soil liquefaction.

Clause 4.4.3.2 in EN 1998-1:2004 states that the limitation of inter-storey drift for buildings without non-structural elements can be determined by using Equation 2.9:

$$d_r v \leq 0.010h \quad (2.9)$$

where

d_r = design inter-storey drift, mm

v = reduction factor

h = storey height, mm

The value of the reduction factor depends on the importance class of the building. According to EN 1998-1:2004, buildings can be classified into four importance classes, from Class I to Class IV, as shown in Table 2.3. The classification of buildings is based on the consequences of collapse for human life, the significance of a building for immediate post-earthquake public safety and civil protection and the economic and social effects of collapse. The recommended values for the reduction factor are 0.5 for importance classes I and II and 0.4 for importance classes III and IV of the building. In this study, the building is classified as a Class III building since the experimental prototype is obtained from a high school building.

Table 2.3: Importance Classes for Buildings (EN 1998-1, 2004).

Importance class	Buildings
I	Buildings of minor importance for public safety, e.g. agricultural buildings, etc.
II	Ordinary buildings, not belonging in the other categories.
III	Buildings whose seismic resistance is of importance in view of the consequences associated with a collapse, e.g. schools, assembly halls, cultural institutions etc.
IV	Buildings whose integrity during earthquakes is of vital importance for civil protection, e.g. hospitals, fire stations, power plants, etc.

In late 2017, the first national code of practice for the seismic design of buildings which is the Malaysia National Annex to Eurocode 8 (MS EN 1998-1) was published by the Department of Standards Malaysia. MS EN 1998-1 states that only Class IV buildings need to be checked for damage limitation limit state based on a return period of 475 years. Since the Class III building is involved in this research, checking for displacement at the damage limitation limit state is not required.

2.10 Mode Shape

When a building is oscillated or vibrated at the natural frequency, the deformed shape of the building can be studied by observing the mode shape of the structure (Murty, et al., 2012). Hence, mode shape which is also known as vibration shape can be used to study the structural behaviour when dynamic loads are caused by different earthquake levels. Generally, each regular building has three basic mode shapes of oscillation, which are pure translational along the X-axis and Y-axis as well as pure rotation about the Z-axis, as shown in Figure 2.14. For the buildings with irregular geometry or non-uniform load distribution and different stiffness along the height and in plan, a mixture of basic mode shapes can be observed (Murty, et al., 2012).

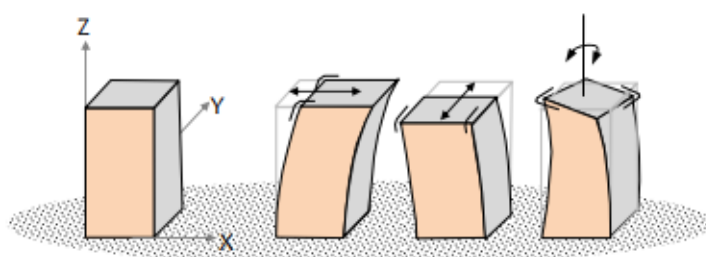


Figure 2.14: Basic Mode Shape of Oscillation (Murty, et al., 2012).

Mode shape is used in investigating the linear dynamic response and describing the displacement patterns, especially in the lateral direction of the structure. It is utilised to study the permutations that a structure will inevitably dispense. The mode shape of low-order mathematical expressions typically contributes more to structural response, meaning the mode shape is less reliable when the orders increase. Nevertheless, the modal analysis is terminated, and the results are accepted when sufficient mode shapes are obtained.

The number of mode shapes for a structure is governed by its number of degrees of freedom (Ondrej, 2019). For instance, the structure with four degrees of freedom will generate four corresponding mode shapes. Each mode shape is independent and normalized, which needs to be amplified and superimposed in order to obtain the final displacement pattern, as shown in Figure 2.15. The combination of all mode shapes represents the overall response of the building (Murty, et al., 2012).

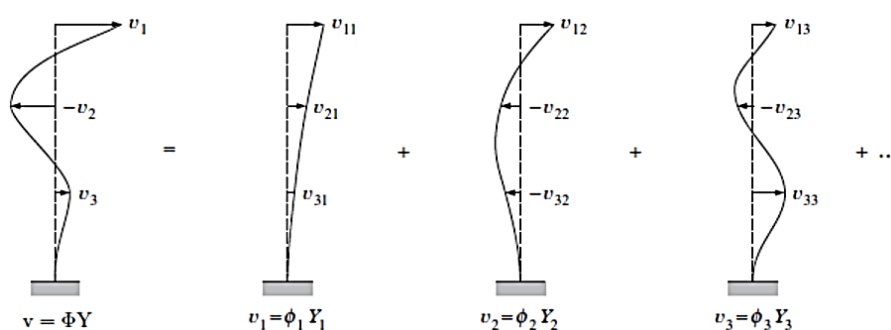


Figure 2.15: Resultant Displacement Pattern and Modal Components (Ondrej, 2019).

When a building oscillates along one direction, the mode shape of the building along that direction can be varied. When the building oscillates in its fundamental mode, it has the least resistance to the oscillation, showing a single curvature mode shape with one zero crossing of the original position. The building with a higher translational mode of oscillation offers a better resistance to motion (Murty, et al., 2012). Therefore, the building is more stable and able to absorb more seismic loads during an earthquake. The building with the second translational mode of oscillation poses a double curvature mode shape, while a double S curvature shape with three zero crossings shows a building with the third translational mode of oscillation. Figure 2.16 shows the mode shape of oscillation of a building oscillating along the X-direction.

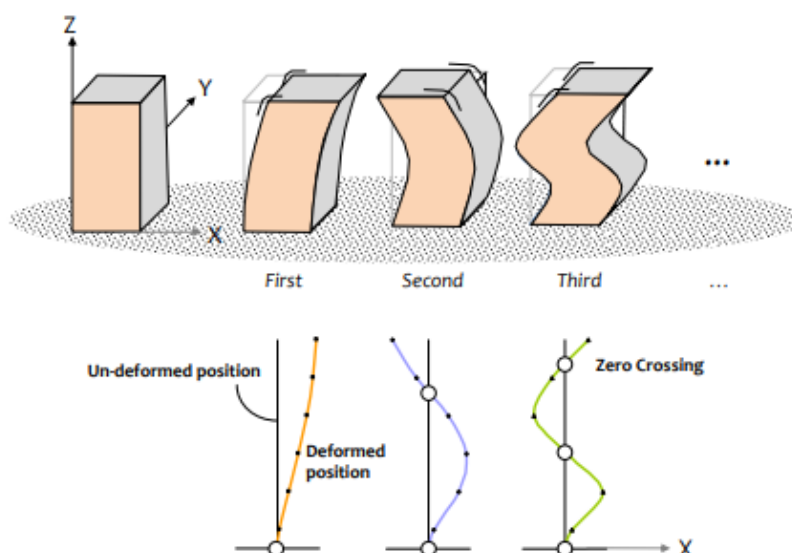


Figure 2.16: Translational Modes of Oscillation along the X-axis of a 5-Storey Benchmark Building (Murty, et al., 2012).

2.10.1 Factors Affecting Mode Shapes

The mode shape of the buildings is influenced by the geometry of the building, the material and geometric properties of structural members, the connections between the structural members and the base connection of the building. The relative flexural stiffness of beams in relation to the adjacent columns determines the building's overall lateral translational mode shape. When the beam is stiffer relative to the adjacent column, the fundamental mode shape of the buildings tends to change from flexural to shear mode shape (Murty, et al., 2012).

Figure 2.17 (a) shows the pure shear response of the building that the column deformed mainly in single curvature mode shape due to the small flexural stiffness of beams relative to the columns. On the other hand, the column deformed primarily in double curvature, showing an overall shear-type deformation behaviour of the building when the flexural stiffness of the beams is significant compared to the adjacent column, as shown in Figure 2.17 (b). For the low-rise and mid-rise buildings, it is common for the relative stiffness of the structural members to fall between the aforementioned two extreme cases, showing an almost shear-type behaviour of the structure where both beams and columns bend in a double curvature shape, as shown in Figure 2.17 (c).

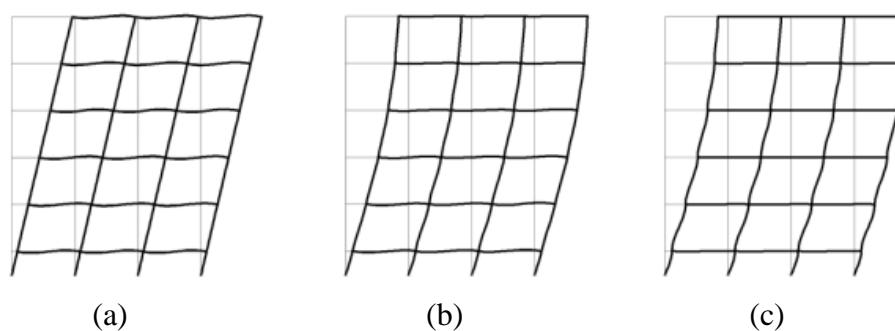


Figure 2.17: Effect of Flexural Stiffness of Structural Members (a) Pure Flexural Response; (b) Pure Shear Response; (c) Almost Shear Response (Murty, et al., 2012).

Other than that, the axial stiffness of vertical members such as columns and structural walls will also influence the mode shape of the building. Columns with small axial stiffness experience considerable axial compressive and tensile deformations. The increment of axial deformations in columns will cause the fundamental mode shape of the buildings to change from flexural-type to shear-type. The flexural behaviour of the building is not desirable in seismic design since it causes a significant horizontal sway, especially in high-rise buildings, thus large axial areas of columns and structural walls in the building are essential to enhance the building's stability (Murty, et al., 2012). Figure 2.18 shows the fundamental translational mode of oscillation of a 25-storey building changes from flexural response to shear response.

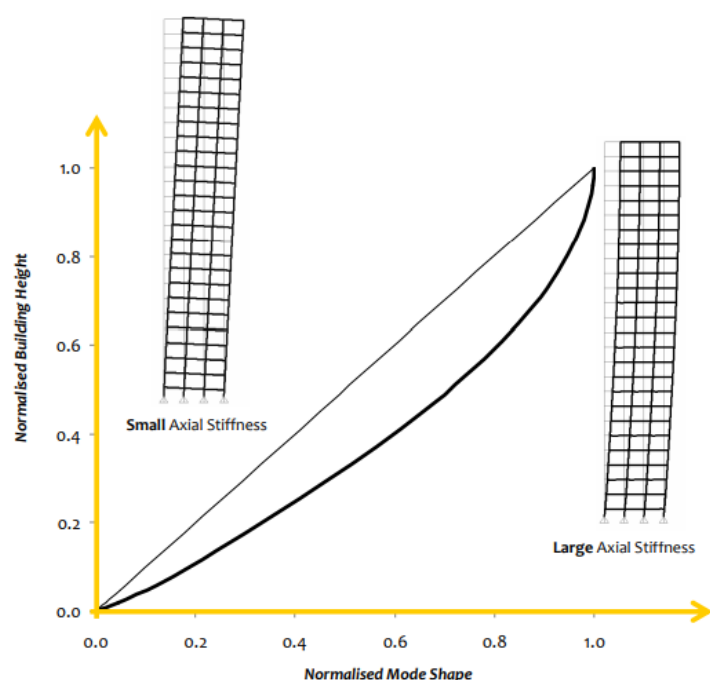


Figure 2.18: Effect of Axial Stiffness of Vertical Members (Murty, et al., 2012).

The height of a building is also one of the factors influencing its mode shape. The fundamental mode shape of a well-designed low-rise building is shear-type behaviour. While the height increases, the building is more flexible in the horizontal direction, adding its natural period. Nevertheless, the type of the mode shape does not have any significant changes. For high-rise buildings, the mode shape of the lower floors behaves in flexural-type deformation, while the higher floors tend to have a shear-type response since the axial deformation in the columns is more significant on lower floors (Murty, et al., 2012). Figure 2.19 shows the fundamental mode shape of the building with different heights.

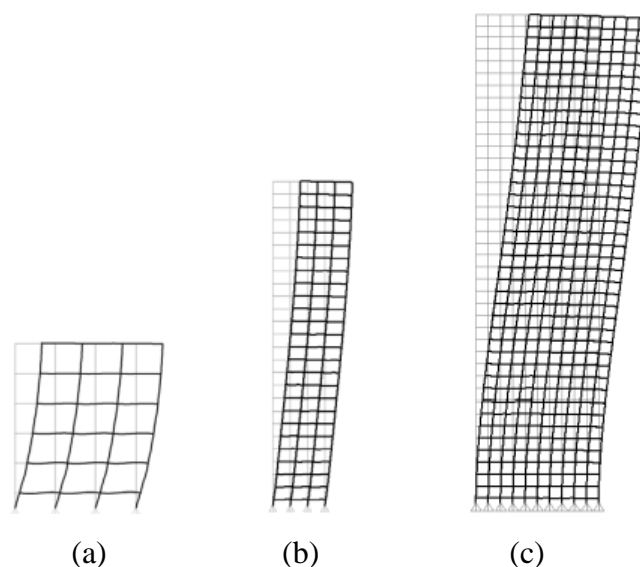


Figure 2.19: Effect of Building Height (a) 5-Storey; (b) 25-Storey; (c) 40-Storey Buildings (Murty, et al., 2012).

2.11 Summary

Earthquakes cause devastating impacts on the structure and environment, thus seismic resistance of structures and buildings must be taken into consideration during construction. Since the rate of earthquakes in West and East Malaysia keeps increasing, there is a severe need for the local government and structural engineers to study the structural behaviour under seismic loads. In order to conduct the experimental testing in the laboratory, a downscaled model is preferable since a lower cost is involved and the laboratory preparation is easier. Buckingham's Pi Theorem and similitude theory must be applied to prepare the scaled model in order to ensure the recovery of the prototype. The energy dissipation tool, such as a viscous damper, shall be utilised to absorb the earthquake loads, strengthening the stability of the structure. The shaking table test is conducted to investigate the structure's seismic performance, such as interstorey drift, mode shape and spectral acceleration. The structural behaviour with braced-damper systems shall be investigated under the ground-shaking motion generated by the earthquake simulation table.

CHAPTER 3

METHODOLOGY AND WORK PLAN

3.1 Introduction

Before the preparation of the structural model, the drawing of the 1 bay 3-storey reinforced concrete building was obtained. Next, the structure was scaled to 1:8 for the structural model. Other than the dimension of the structural members, the steel reinforcement bar diameter was scaled down to ensure it could fit into the structure with desired strength. After that, the downscaled model's detailing was prepared using Autodesk AutoCAD software and served as the reference for the construction work.

Prior to the construction of the downscaled structural model, a trial mix was performed to ensure the mix proportion of the concrete was capable of providing sufficient compressive strength. Three 200 mm height cylinders with 100 mm diameter were cast in order to conduct the compressive strength test after 14 days of curing. The concrete mix proportion was acceptable to be used in the structural model since grade C30 concrete compressive strength was achieved.

The structural model with a total height of 1.5 m was constructed in the Civil Engineering Lab. The construction of the structural model started with the fabrication of formwork and the bending of steel reinforcement bars. The formwork was made of plywood, while a 3 mm steel bar was selected as the reinforcement bar of the structure. The formworks were prepared according to the dimension of each structural member for the model casting. The steel bars were tied following the reinforcement detailing prepared to ensure adequate material strength.

After casting the structural model, the structural model was left for 28 days before the shaking table test. The model was then placed on the shaking table in the Advanced Geotechnical Laboratory to simulate dynamic loads. The linear variable differential transformers (LVDTs) and accelerometers were installed on the structure and connected to the data loggers to record the data of the shaking table test. The shaking table test was repeated on the structural model equipped with viscous dampers. Three brands of viscous dampers which

are APIDO, SKK and ESPADA dampers, were used in this study. After the shaking table test, the results were analysed and discussed in this study. Figure 3.1 illustrates the workflow of the entire study.

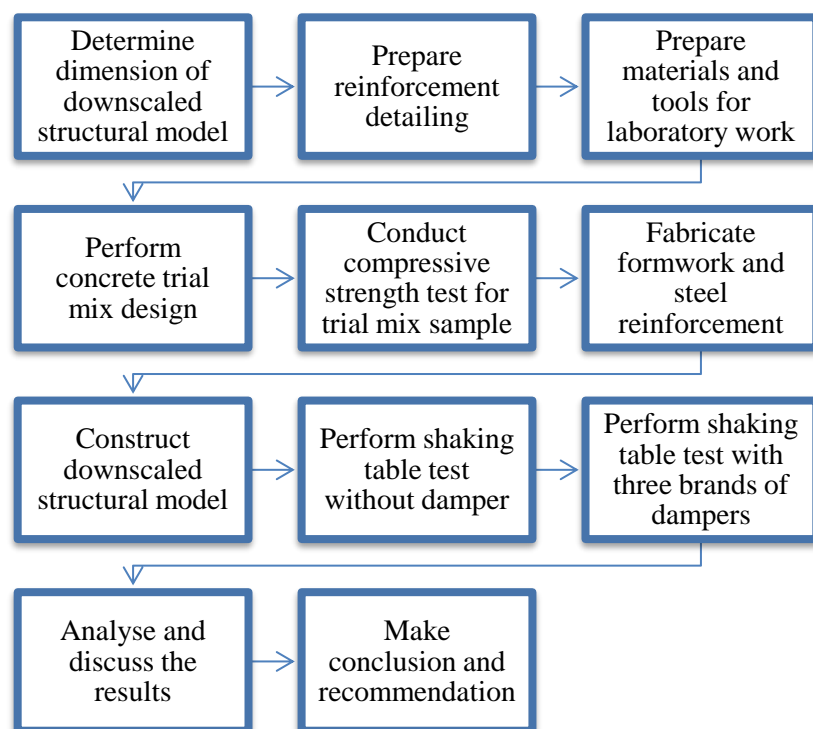


Figure 3.1: Study Workflow.

3.2 Structural Model Details

Since it is not practical to construct a whole building for seismic analysis study, a downscaled model is typically constructed to study the structural behaviours of a structure in the laboratory. After the full-scale drawing of the structure was obtained, the prototype was scaled down to prepare the 1 bay 3-storey reinforced concrete structural model for shaking table test. Due to the limitation of testing equipment, a scale factor of 1:8 was applied to the structure. A few crucial parameters need to be taken into consideration when preparing a miniature structural model in order to ensure the results obtained are applicable in real-life situations. For instance, the geometry of the buildings, the material properties of structural members and the construction approaches are essential in the study.

3.2.1 Geometry

The dimension of the structural members of the structural model was scaled down accordingly. Figure 3.2 shows the structural geometry of the model. The total height of the 3-storey structure is 1.5 m while each storey is 0.5 m. The footings bolted on the shaking table have a dimension of 175 mm in width and length, while the footing depth is 50 mm. The dimension of the scaled beam is 31 mm in width and 75 mm in depth. The column in the model is a square column with a dimension of 40 mm. The slab is scaled to 16 mm in thickness, 830 mm in width and length for the whole structure. According to the dimension of scaled structural elements, the total volume of concrete in the structural model is around 0.072 m^3 , equivalent to 170 kg of mass. Since the shaking table in the Advanced Geotechnical Laboratory is capable of sustaining 3000 kg, the shaking table test is able to be performed using this model. Moreover, the model is able to be placed on the shaking table as there is a 2.5 m height clearance of the shaking table. Consequently, the dimension of the downscaled 1 bay 3-storey reinforced concrete model is acceptable.

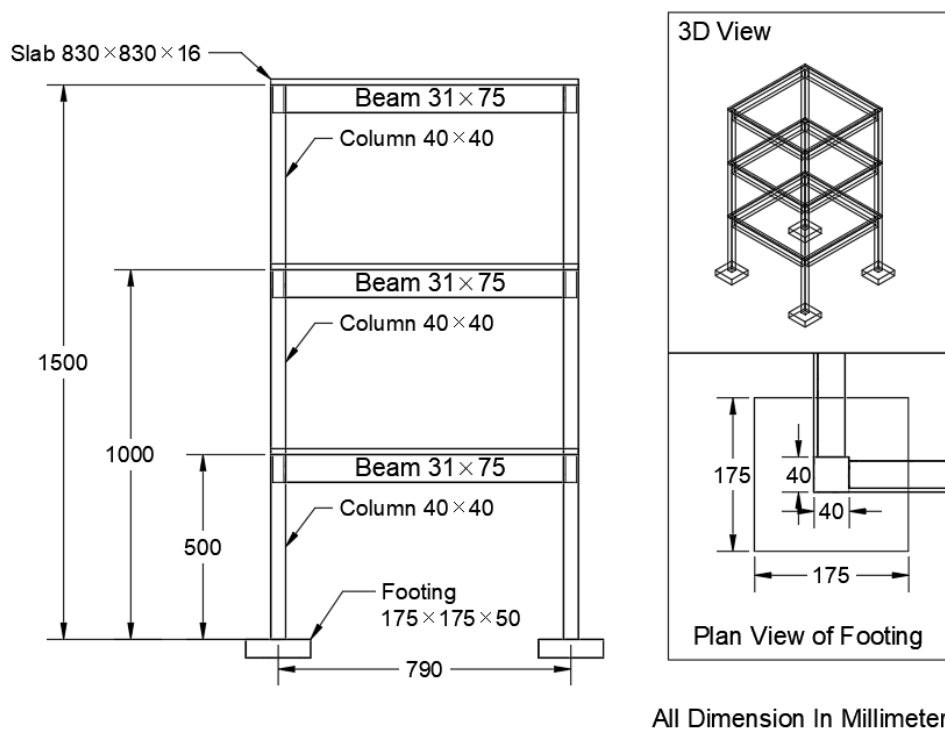


Figure 3.2: Structural Model Geometry.

3.2.2 Reinforcement

Other than the geometry of the structural model, the reinforcement details were scaled down to ensure the rebars fit into the concrete. The rebar arrangement of the structural elements was designed as in the actual reinforced concrete structure to ensure sufficient strength is provided. Since the structural member was relatively small in dimension, 3 mm steel bars were used as reinforcement bars to allow the coarse aggregate to fill between the rebars. Main reinforcement and shear reinforcement were provided for all the structural members, and the lapping of rebar was essential to ensure the structure's stability. Figure 3.3, Figure 3.4, Figure 3.5 and Figure 3.6 show the reinforcement bars arrangement for footing, column, beam and slab, respectively.

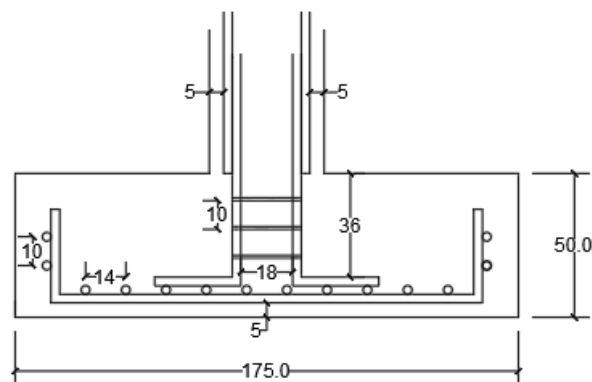


Figure 3.3: Footing Reinforcement Details.

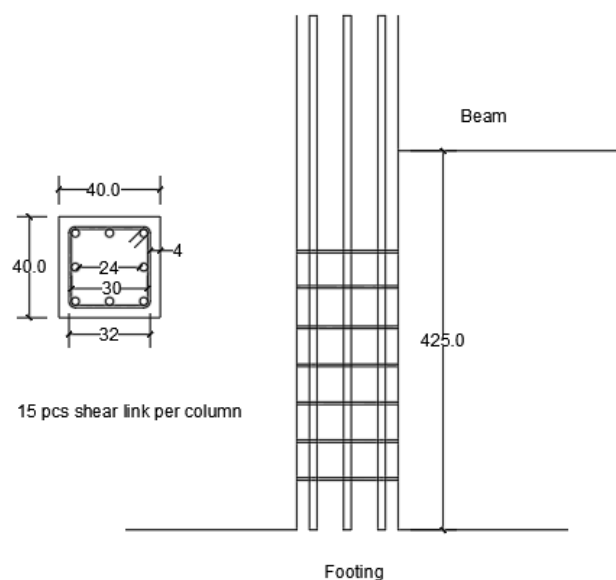


Figure 3.4: Column Reinforcement Details.

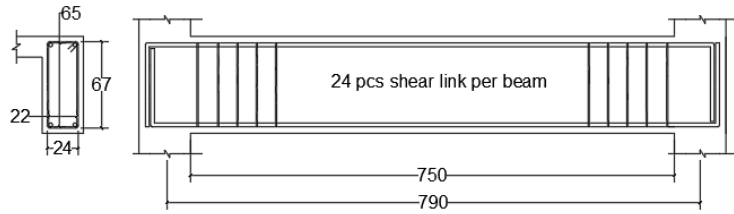


Figure 3.5: Beam Reinforcement Details.



Figure 3.6: Slab Reinforcement Details.

3.3 Scale Factor Determination

In order to assess the correlation between the full-scale prototype and the downscaled model, the scale factor must be determined before the experiment test with the aid of Similitude and Buckingham's Pi theorem. According to the theorem, three basic scale factors, which are the dimensional scale factor, S , acceleration scale factor, S_a and stress scale factor, S_e are necessary for conducting a scaled model test to obtain feasible performance and structural behaviour.

Since the prototype was scaled down eight times to the structural model in this study, the dimensional scale factor, $S = 8$. The acceleration scale factor, $S_a = 1$ since the testing was conducted under a constant gravitational environment. Based on Similitude and Buckingham's Pi theorem, the scale factor for mass is $S_e S^2 / S_a$, thus the value of S_e can be determined when the mass is known. The mass of the full-scale prototype and downscaled model were calculated by multiplying density and volume, as shown in Equation 3.1.

$$m = \rho \times V \quad (3.1)$$

where

m = mass of reinforced concrete, kg

ρ = density of reinforced concrete, kg/m^3

V = volume of reinforced concrete, m^3

3.3.1 Theoretical Prediction

For full-scale prototype,

$$\begin{aligned} \text{Density of reinforced concrete, } \rho &= 2500 \text{ kg/m}^3 \\ \text{Volume of each column} &= 0.32 \text{ m} \times 0.32 \text{ m} \times 4 \text{ m} \times 3 \text{ floors} \\ &= 1.229 \text{ m}^3 \\ \text{Volume of each footing} &= 1.4 \text{ m} \times 1.4 \text{ m} \times 0.4 \text{ m} \\ &= 0.784 \text{ m}^3 \\ \text{Mass of each column with} &= 2500 \text{ kg/m}^3 \times \\ \text{footing} &= (1.229 + 0.784) \text{ m}^3 \\ &= 5032.5 \text{ kg} \end{aligned}$$

For downscaled 1:8 structural model,

$$\begin{aligned} \text{Density of reinforced concrete, } \rho &= 2500 \text{ kg/m}^3 \\ \text{Volume of each column} &= 0.04 \text{ m} \times 0.04 \text{ m} \times 0.5 \text{ m} \times 3 \text{ floors} \\ &= 0.0024 \text{ m}^3 \\ \text{Volume of each footing,} &= 0.175 \text{ m} \times 0.175 \text{ m} \times 0.05 \text{ m} \\ &= 0.0015 \text{ m}^3 \\ \text{Mass of each column with} &= 2500 \text{ kg/m}^3 \times \\ \text{footing} &= (0.0024 + 0.0015) \text{ m}^3 \\ &= 9.75 \text{ kg} \end{aligned}$$

$$S = 8$$

$$S_a = 1$$

$$\begin{aligned} S_e &= \frac{\text{Mass} \times S_a}{S^2} \\ &= \frac{5032.5 \text{ kg} \times 1}{9.75 \text{ kg} \times 8^2} \\ &= 8.1 \end{aligned}$$

3.3.2 Actual Measurement

For downscaled 1:8 structural model,

$$\begin{aligned}
 \text{Density of reinforced concrete, } \rho &= 2500 \text{ kg/m}^3 \\
 \text{Volume of each column} &= 0.04 \text{ m} \times 0.041 \text{ m} \times 0.52 \text{ m} \\
 &\quad \times 3 \text{ floors} \\
 &= 0.00256 \text{ m}^3 \\
 \text{Volume of each footing,} &= 0.176 \text{ m} \times 0.177 \text{ m} \times 0.05 \text{ m} \\
 &= 0.00156 \text{ m}^3 \\
 \text{Mass of each column with} &= 2500 \text{ kg/m}^3 \times \\
 \text{footing} &\quad (0.00256 + 0.00156) \text{ m}^3 \\
 &= 10.3 \text{ kg}
 \end{aligned}$$

$$S = 8$$

$$S_a = 1$$

$$\begin{aligned}
 S_e &= \frac{\text{Mass} \times S_a}{S^2} \\
 &= \frac{5032.5 \text{ kg} \times 1}{10.3 \text{ kg} \times 8^2} \\
 &= 7.6
 \end{aligned}$$

3.4 Raw Materials

The raw materials used in the concrete mix proportion were Ordinary Portland Cement (OPC), coarse and fine aggregate, water and superplasticizer that acts as water reducing agent. Figure 3.7 shows the raw materials used in this research.



Figure 3.7: Raw Materials of Concrete.

There are ten types of Portland cement available in the market, while OPC used in this study is categorized as Type I Portland cement (ASTM Standard C150, 2012). Since there was no exposure to sulphate or extreme weather during the casting, Type I cement was suitable for the model construction and was commonly used for most residential development. The cement was stored in an airtight container since it is highly sensitive to moisture. The cement clinker will form when the cement is exposed to moisture in the air for a time.

Both gravel and sand were used in the manufacture of concrete. According to ASTM Standard C33 (2018), the size of fine aggregate must be less than 5 mm. Otherwise, it will be classified as coarse aggregate. This study used 5 mm coarse aggregates to make up the majority of the concrete mix, while the 600 μm fine aggregates were utilised to fill the voids between the coarse aggregate. Gravels and sands help increase the concrete volume and eventually reduce the construction cost. Furthermore, coarse aggregates determine the concrete's strength and limit the concrete's drying shrinkage during the curing process.

Water is necessary for the production of concrete to lubricate the concrete mix. The mixing water added must be clean to prevent the interference of the cement hydration process by the pollutants, which may affect the long-term durability of the concrete. Hence, clean tap water was used in this study. The strength of the concrete is inversely proportional to the water-to-cement ratio. Concrete mix with less water content produces concrete with a higher strength but lower workability. In order to enhance the workability of the concrete mix, the water-reducing admixture was utilised. In this study, superplasticizer was added to the concrete mix to reduce the water-to-cement ratio without affecting the quality of the concrete. Figure 3.8 shows the type of superplasticizers used in this study.



Figure 3.8: Superplasticizer.

3.5 Mix Proportion

In this study, the concrete was designed to achieve a compressive strength of 30 N/mm² at 28 days. The mix proportion of the materials to produce 1 m³ concrete mix is shown in Table 3.1. The density of concrete produced is 2380 kg/m³ while the water-to-cement ratio is 0.42, which is relatively low, thus superplasticizer was added in a small dosage equal to 1.2 % of the concrete weight in order to increase the workability of the concrete mix. This concrete mix design was adopted as the trial mix design of the structural model in this study.

Table 3.1: Mixture of Concrete (Yip and Marsono, 2016).

Water / cement ratio	Cement (kg/m ³)	Water (kg/m ³)	Fine aggregate (kg/m ³)	Coarse aggregate (kg/m ³)	Density (kg/m ³)	Admixture 1.2 % (kg)
0.42	550.0	233.0	511.0	1086.0	2380.0	6.6

3.6 Trial Mix Design

The trial mix design in this study was conducted based on the water-to-cement ratio and quantity of raw materials shown in Table 3.1. In order to ensure the mix proportion is able to produce grade C30 concrete, three cylinder samples were prepared for the compressive strength test. Each cylinder specimen has a diameter of 100 mm and a height of 200 mm. 15 % of the concrete mix wastage was considered since the concrete is prepared by hand mix. The calculation of

the total concrete volume required for the trial mix design is shown below, while the concrete mix proportion to produce concrete with a density of 2380 kg/m³ for the trial mix design is shown in Table 3.2. The water-to-cement ratio used in the trial mix design is 0.42.

Diameter of each cylinder specimen	=	100 mm
Height of each cylinder specimen	=	200 mm
Volume of each cylinder specimen	=	$\pi (0.05 \text{ m})^2 (0.2 \text{ m})$ = 0.00157 m ³
Volume of three cylinder specimens	=	0.00157 m ³ × 3 = 0.00471 m ³
Volume of three cylinder specimens with 15 % wastage	=	0.00471 m ³ × 1.15 = 0.00542 m ³

Table 3.2: Mix Proportion for Trial Mix Design.

Concrete volume	Cement (kg)	Water (kg)	Fine aggregate (kg)	Coarse aggregate (kg)	Superplasticizer (ml)
Per m ³	550.0	233.0	511.0	1086.0	6600
0.00542 m³	2.98	1.26	2.77	5.89	36

3.6.1 Concrete Mixing and Casting

Firstly, all the raw materials required to cast three cylinder specimens with grade C30 characteristic strength were prepared and weighed according to the calculated amount. The drum mixer in the Civil Engineering Laboratory can mix concrete up to 160 L, equivalent to 0.16 m³. Since the total volume of concrete required for the trial mix design is 0.00542 m³ which is relatively small compared to the capability of the drum mixer, the concrete mixing process was done by hand instead of using a drum mixer to ensure a homogenous mix of concrete. Other than the raw materials, the cylinder moulds were screwed tightly, and a thin layer of oil was applied to their internal surface in order to facilitate

the demoulding process. Figure 3.9 shows all the materials and tools required in concrete mixing and casting.



Figure 3.9: Materials and Tools Preparation.

Next, the concrete mixing was started by dry mixing the sand and coarse aggregate, followed by the OPC. When the dry materials were mixed evenly on the mixing tray, as shown in Figure 3.10, half of the water was added to the mixture. After that, the superplasticizer was mixed with the remaining water and poured into the mixture. Continuous mixing was carried out until the fresh concrete reached the desired workability to ensure the water was distributed evenly in the fresh concrete. The fresh concrete was ready to be used when it turned into a dense and gooey texture, as shown in Figure 3.11. The concrete casting was done within 30 minutes to ensure the quality of the fresh concrete.



Figure 3.10: Dry Mix.



Figure 3.11: Fresh Concrete.

The fresh concrete was then poured into the cylinder mould prepared. The compaction work is compulsory to avoid any air voids inside the concrete, which may cause honeycomb and eventually affect the strength of hardened concrete. The fresh concrete was compacted uniformly over the cross-section using a tamping rod. After that, the fresh concrete's top surface was flattened using a trowel and placed in an air-dry area for at least 24 hours to allow the hardening process of concrete. Figure 3.12 shows the concrete cylinder specimens cast in the laboratory.



Figure 3.12: Fresh Cylinder Concrete Specimens.

3.6.2 Concrete Curing

After 24 hours of concrete casting, the cylinder concretes were demoulded and labelled. Figure 3.13 shows the hardened concrete specimens after the cylinder moulds are dismantled. The concrete samples were air dried for 2 hours in order

to remove the moisture on the concrete surface before the curing process. When there was no more oil and water on the surface of the concrete cylinders, the hardened concrete specimens were placed in the water tank, as shown in Figure 3.14. The concrete cylinders must be fully submerged in the water for 14 days to prevent moisture loss from the concrete samples due to the cement hydration process. The curing process is important for concrete strength development as well as to ensure the durability of hardened concrete.



Figure 3.13: Hardened Cylinder Concrete Specimens.



Figure 3.14: Concrete Curing Process.

3.6.3 Compressive Strength Test

After 14 days of curing, the concrete specimens were removed from the curing tank. The concrete cylinders were left for another 2 hours to dry the concrete surface before conducting the compressive strength test. The cylinder specimens with a diameter of 100 mm and height of 200 mm were used to perform the

compressive strength test. The weight of each concrete sample was recorded since it serves as an input for the compressive strength test machine. Next, the concrete cylinder was installed on the testing machine while the flat surface of the sample was placed upward to ensure the load was applied evenly to the sample, as shown in Figure 3.15. The pacing rate of the load increment was set to 1 kN/s, and the necessary parameters were input to the machine. When the compression test machine started to operate, the compression load applied to the concrete cylinder kept increasing until the specimen failed. The ultimate load sustained by the concrete specimen was recorded, and the compressive strength was calculated by using the equation below:

$$F = \frac{P}{A} \quad (3.2)$$

where

F = compressive strength of the concrete specimen, MPa

P = ultimate load applied to the concrete specimen, N

A = cross-sectional area of the concrete specimen, mm²



Figure 3.15: Compressive Strength Test.

The compressive strength test was conducted for the trial mix design to check whether the mix proportion produces concrete with adequate strength.

Since the concrete grade of the structural model is grade C30, the characteristic strength of the concrete was designed as 30 MPa. The strength of 14 days ages of concrete is about 90 % of the final strength, thus the concrete cylinders need to achieve a target strength of 27 MPa. If the concrete cylinders fail to develop sufficient compressive strength in 14 days, the mix proportion is unsuitable for the structural model. In contrast, the trial mix design is acceptable. Table 3.3 shows the results of the compressive strength test.

Table 3.3: Ultimate Load and Compressive Strength of Concrete Cylinders (Trial Mix Design).

Concrete specimen	Ultimate load, P (kN)	Compressive strength (MPa)	Target Strength at 14 days (MPa)	Status
1	224.8	28.62	27	Pass
2	216.6	27.58	27	Pass
3	213.3	27.16	27	Pass

The results show that the compressive strength of the cylinder specimens was sufficient, thus the mix proportion was considered satisfactory. The mix proportion was used to construct the structural model in this study.

3.7 Model Construction

Before model casting, the formwork was prepared by using timber plywood. The marking was done on the plywood, including the dimension of the formwork as well as the location of bolt holes required for the damper connector and the fixing point on the shaking table. The formwork was cut accordingly in the Mechanical and Timber Workshop. The plywood was then wrapped by a layer of plastic in order to provide water resistance so that the formwork was reusable for the following casting process. At the same time, the plastic layer prevents the concrete from sticking to the formwork and eases the formwork dismantling. After that, the plywood was assembled and screwed. Figure 3.16 shows the formwork prepared for footing, while Figure 3.17 shows the formwork for the beam and slab.



Figure 3.16: Footing Formwork with Bolts Installed on Shaking Table.



Figure 3.17: Beam and Slab Formwork.

After the formwork preparation, the model construction was followed by the fabrication of reinforcement. 3 mm steel bars were cut into suitable lengths and bent into the desired shape according to the reinforcement details prepared. Bar bending was performed using the hammer in the Mechanical and Timber Workshop, as shown in Figure 3.18. Bar bending machine is not required in this study since the diameter of the steel bar is relatively small.



Figure 3.18: Bar Bending in the Mechanical and Timber Workshop.

After the steel bars were fabricated into the desired length and shape, cable ties were used to assemble the reinforcement. 3 mm steel bars were used as the main reinforcement of the structural elements, while 1 mm steel wires served as the stirrups of the shear reinforcement. Spaced shear links were provided for the column and beam reinforcements to resist the shear forces as well as confine the concrete. Figure 3.19 shows the footing reinforcement together with the starter bar of the column.



Figure 3.19: Footing Reinforcement with Column Starter Bar.

Figure 3.20 shows the beam reinforcement with adequate shear links, and Figure 3.21 shows the slab reinforcement tied with beam reinforcement.



Figure 3.20: Beam Reinforcement.

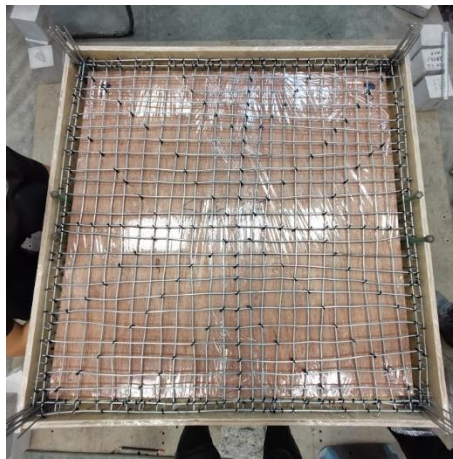


Figure 3.21: Slab Reinforcement Tied with Beam Reinforcement.

The reinforcement of footing with the column starter bar was then placed into the footing formwork, and the casting process was carried out. Three concrete cylinders were cast for each batch of fresh concrete. After 14 days of curing, the compressive strength test was conducted to ensure the structural model's concrete grade fulfilled the design requirement. Figure 3.22 shows the casting of the footing.



Figure 3.22: Concrete Casting for Footing.

After 24 hours, the footing formwork was dismantled, and the footing was checked to ensure no honeycomb that would reduce the concrete strength was formed. The sample of the footing cast is shown in Figure 3.23. After that, the footing was cured by spraying water on the concrete surface for seven days.



Figure 3.23: Footing Cast.

The model construction was then continued by casting columns, beams and slab for the first floor. Figure 3.24 shows the concrete columns cast for the first floor. Sika grout was utilised near the bolt holes prepared for the damper connector due to the limited space. The main reinforcement and shear reinforcement were congested at that location, thus aggregates used in typical concrete casting were not able to pass through the reinforcement and sika grout was selected to ensure concrete quality.

After the columns were cast, the top surface of the columns was smoothed by using the grinder to provide an even surface for beam casting work. The beams and floor slab were cast together to ease the construction work. The formworks of the beams and slab were screwed while the reinforcement bars were tied together. Figure 3.25 shows the preparation of beams and slab casting for the first floor.



Figure 3.24: First Floor Columns Cast.



Figure 3.25: Preparation of Concrete Casting for First Floor Beams and Slab.

The casting work was then repeated for the second and third floors, as shown in Figure 3.26 and Figure 3.27. The formworks and reinforcements of the remaining parts of the model were fabricated in the Civil Engineering Laboratory as well as the Mechanical and Timber Workshop.



Figure 3.26: Concrete Casting for Second Floor Beams and Slab.



Figure 3.27: Concrete Casting for Third Floor Columns.

After all the structural elements had been cast, the model was painted white for appearance and to ease the marking. Marking shall be done when

cracking is observed during the shaking table test. Figure 3.28 shows the model constructed in this study.



Figure 3.28: Complete Model.

3.7.1 Quality Control

It is important to conduct compressive strength tests for casting work to ensure the quality and durability of the concrete used in the model construction. If the concrete mixing and casting work is not performed well, it may reduce the compressive strength of concrete. The concrete may not be able to withstand the expected loads when its final strength does not meet the requirement, leading to structural integrity issues. Although the downscaled model constructed in this study is not expected to carry any extra loads, ensuring the cast structure reaches the desired grade C30 concrete as the prototype is essential. Since the similitude relation had been established between the scaled model and the full-scale prototype, it is crucial to ensure the model meets the design criteria so that its structural behaviour is similar to the prototype.

Three concrete cylinders were cast for each batch of fresh concrete to perform the compressive strength test. The cylinder samples were cured and tested at the age of 14 days. The concrete cylinders shall achieve a target strength of 27 MPa, which is 90% of the final strength for quality control. Table

3.4, Table 3.5 and Table 3.6 show the compressive strength test results for each floor's casting.

Table 3.4: Ultimate Load and Compressive Strength of Concrete Cylinders (First Floor).

Concrete specimen	Ultimate load, P (kN)	Compressive strength (MPa)	Target Strength at 14 days (MPa)	Status
1	263.1	33.50	27	Pass
2	157.7	20.08	27	Fail
3	240.4	30.61	27	Pass

Table 3.5: Ultimate Load and Compressive Strength of Concrete Cylinders (Second Floor).

Concrete specimen	Ultimate load, P (kN)	Compressive strength (MPa)	Target Strength at 14 days (MPa)	Status
1	314.8	40.08	27	Pass
2	283.7	36.12	27	Pass
3	317.4	40.41	27	Pass

Table 3.6: Ultimate Load and Compressive Strength of Concrete Cylinders (Third Floor).

Concrete specimen	Ultimate load, P (kN)	Compressive strength (MPa)	Target Strength at 14 days (MPa)	Status
1	241.9	30.80	27	Pass
2	241.7	30.77	27	Pass
3	263.8	33.59	27	Pass

Based on the results, there was one cylinder for the first floor casting work did not pass the compressive strength test, but the compressive strength of another two cylinders was greater than 27 MPa. Hence, the compressive

strength test was considered a pass. The insufficient compressive strength of concrete specimen 2 of the first floor may be caused by the presence of air voids in concrete that reduce the final strength of hardened concrete. The concrete mixture was suspected to contain more water when casting this specimen. This may happen when the concrete mixture is not mixed thoroughly. The excessive water does not involve in the cement hydration process, forming pores during the concrete hardening. Figure 3.29 shows the cylinder concrete specimen 2 of the first floor after the compression test, and pores can be seen inside the concrete.

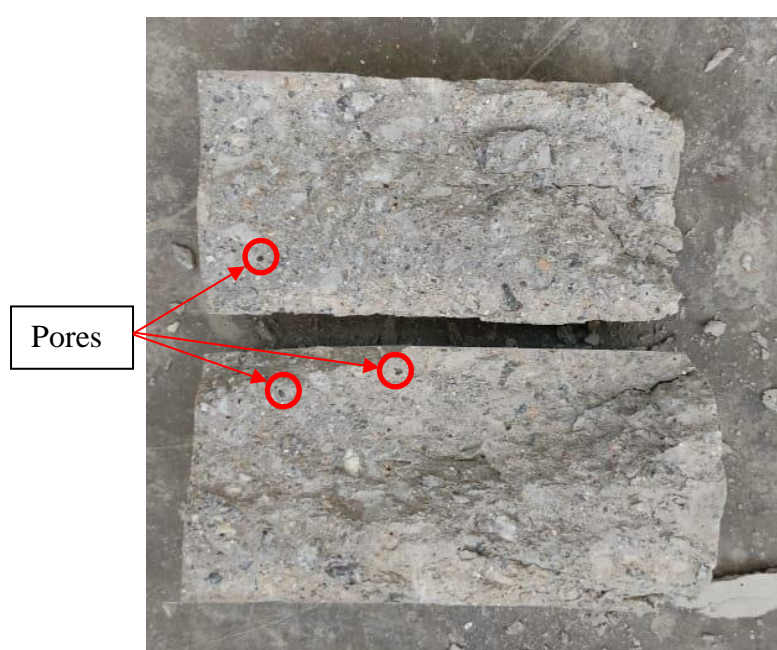


Figure 3.29: First Floor Concrete Specimen 2 After Compression Test.

All the concrete cylinders for the second and third floors passed the compressive strength test. Thus, no additional measure was needed in the model construction.

3.8 Shaking Table Test

After the model casting was completed, the model was transferred to the Advanced Geotechnical Laboratory and fixed on the shaking table. The shaking table in the laboratory is electrically driven by a direct drive motor, also known as a torque motor. It is a uniaxial shaking table that is able to generate seismic movement in one dimension only. When the frequency and displacement of the

shaking are keyed into the computer, the actuator produces linear movement according to the input, emulating the ground-shaking motions during earthquakes. Figure 3.30 shows the shaking table used in the test. This shaking table is able to simulate movement from 0.1 Hz to 20 Hz of frequency and from 0.5 mm to 15 mm of unit displacement.



Figure 3.30: Shaking Table in the Advanced Geotechnical Laboratory.

The testing sensors used in this study, LVDTs and accelerometers, were installed on the shaking table and each level of the structural model to measure the horizontal displacement and acceleration of the structural model during shaking. There were two 25 mm LVDTs installed on the first floor of the model and the shaking table that represents the ground floor. Another two 50 mm LVDTs were installed on the second and third floors of the model. During the test, four accelerometers were installed on the first, second, and third floors of the structure as well as the shaking table. Figure 3.31 and Figure 3.32 show the setup of 50 mm LVDT and accelerometer during the shaking table test.



Figure 3.31: 50 mm LVDT Installed on the Third Floor of the Model.



Figure 3.32: Accelerometer Installed on the Third Floor of the Model.

The test sensors were then connected to the data logger, as shown in Figure 3.33. Dynamic Measurement Software DRA-730AD was used in this study. The experimental data were recorded automatically on the computer. Different peak ground accelerations were used to evaluate and analyse the seismic performance of the structural model. The frequency and displacement of the shaking were adjusted at each level of the earthquake simulation. There was a total of 10 levels of earthquake simulation performed in this study.



Figure 3.33: Date Logger Connected with the Test Sensors.

The shaking table test was first conducted on the bare frame structure, which refers to the model without a damper. Figure 3.34 and Figure 3.35 show the experimental setup of the bare frame structure with testing sensors. The structural behaviour and damage mechanism were observed during the test. The cracking that occurred was marked and recorded after every level of earthquake simulation.

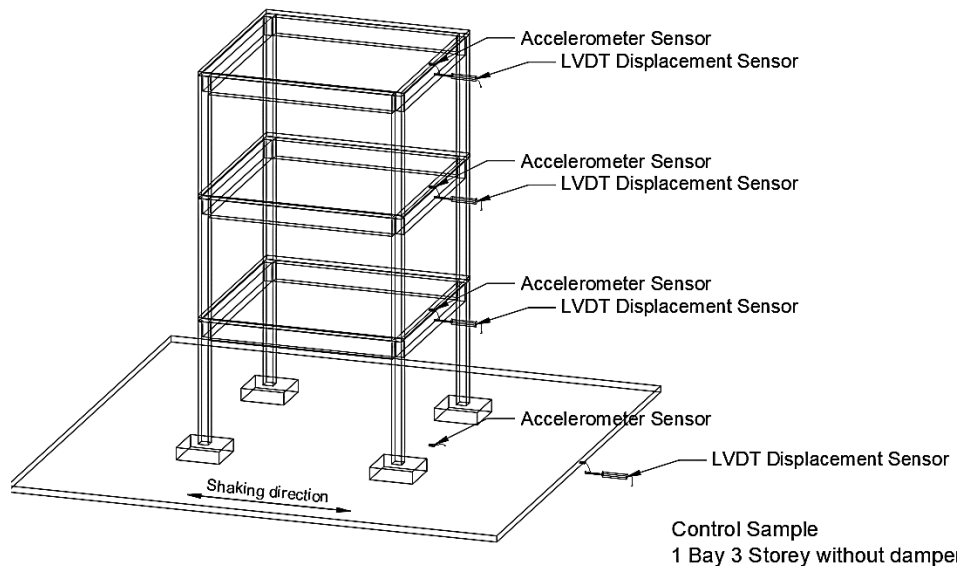


Figure 3.34: Shaking Table Test Setup of the Bare Frame Structure.



Figure 3.35: Bare Frame Structure Installed on Shaking Table.

The test was then repeated on the model equipped with a damping system. Three brands of viscous dampers were selected in this study, as shown in Figure 3.36. The shaking table test was carried out on the structure with an inverted V diagonal braced-damper system of APIDO, SKK and ESPADA dampers. The length of the cylinder containing compressible fluid for each damper is varied, while the total length of each damper is constant. Different brands of dampers were utilised to compare their performance during shaking.



Figure 3.36: APIDO, SKK and ESPADA Dampers (from left to right).

Twelve viscous dampers were installed on the structural model using connectors fabricated using steel plates. There were eighteen damper connectors fabricated for the whole structure, as shown in Figure 3.37. The steel plates were fixed to the respective locations using the bolts while the bolt holes were prepared during the model casting. Figure 3.38 shows the damper connectors installed on the structure before the installation of dampers.



Figure 3.37: Damper Connectors Fabricated for Whole Structure.

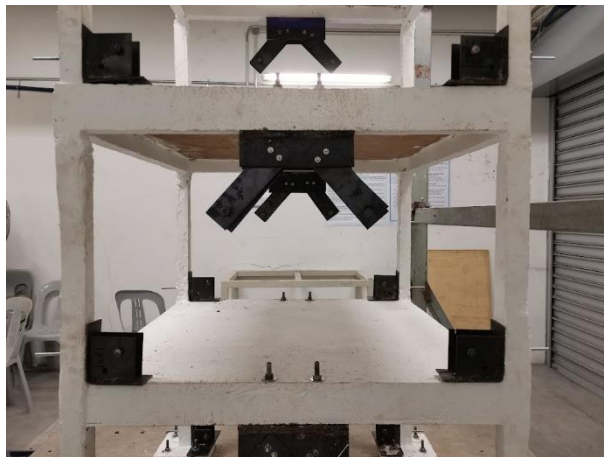


Figure 3.38: Damper Connectors Installed on the Structure.

The shaking table test was conducted on the structural model with APIDO dampers, followed by SKK dampers and ESPADA dampers. Figure 3.39 illustrates the experimental setup of the structure with an inverted V diagonal braced-damper system, and Figure 3.40 shows the braced structure with testing sensors in the shaking table test. All the experimental data was recorded by the data logger.

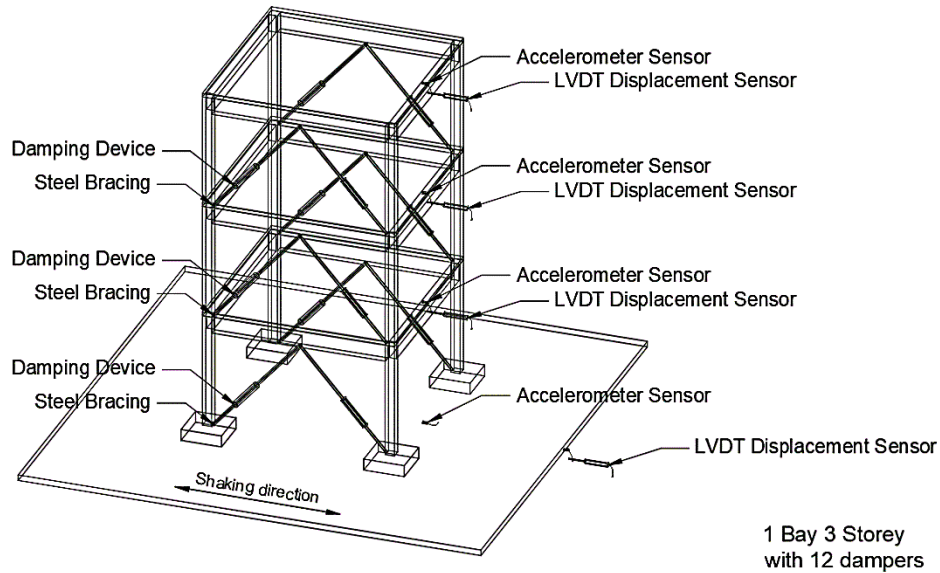


Figure 3.39: Shaking Table Test Setup of the Model with Dampers.



Figure 3.40: Structure with APIDO Dampers Installed on Shaking Table.

3.9 Summary

The prototype was scaled down eight times to the structural model using Buckingham's Pi Theorem and similitude theory. The raw materials used in concrete casting were OPC, coarse aggregate, fine aggregate, water as well as water-reducing admixture, which is the superplasticizer. The concrete mix proportion with a water-to-cement ratio of 0.42 was able to produce cement with a density of 2380 kg/m^3 . The trial mix design was performed using cylinder moulds with a dimension of 200 mm in height and 100 mm in diameter. The

concrete cylinders were cured for 14 days before compressive strength testing. The formwork was fabricated using plywood and 3 mm steel bars were selected as the reinforcement bar to construct the downscaled reinforced concrete 1 bay 3-storey model. The shaking table test was performed four times on the bare frame structure and structure with three brands of viscous dampers. LVDTs and accelerometers were installed on the model in order to record the data of the shaking test. The inverted V diagonal braced-damper system was installed on the structure to study the structural behaviour and mode shape of the structure.

CHAPTER 4

RESULTS AND DISCUSSION

4.1 Introduction

In this study, ten levels of earthquake simulation were selected to conduct the shaking table test. The earthquake simulation was carried out randomly without predetermination of peak ground acceleration. Each level has a varying intensity in terms of displacement and aggressiveness of shaking, as shown in Table 4.1. The earthquake simulation gets intense when the shaking is more aggressive with a shorter displacement. Unit displacement and frequency of each level were determined and served as the input in the operating shaking table.

Table 4.1: Intensity of Each Level of Earthquake Simulation.

Level	Intensity		Shaking Table Inputs	
	Displacement	Aggressiveness	Displacement (mm/mm)	Frequency (Hz)
1	Large	Very low	3	1
2	Large	Low	3	2
3	Moderate	Low	1.5	3
4	Moderate	Low	1.9	3
5	Moderate	Aggressive	1	5
6	Short	Aggressive	0.7	7
7	Short	Aggressive	0.6	8
8	Short	Aggressive	0.6	10
9	Short	Very high	0.3	15
10	Short	Very high	0.5	15

When the shaking level increases, the shaking frequency generally increases while the unit displacement of shaking decreases. Level 1 and Level 2 have the same unit displacement but a different shaking frequency, similar to Level 7 and Level 8. Moreover, the frequency of shaking at Level 3 and Level 4 is constant with an increment in unit displacement, and same goes for Level 9

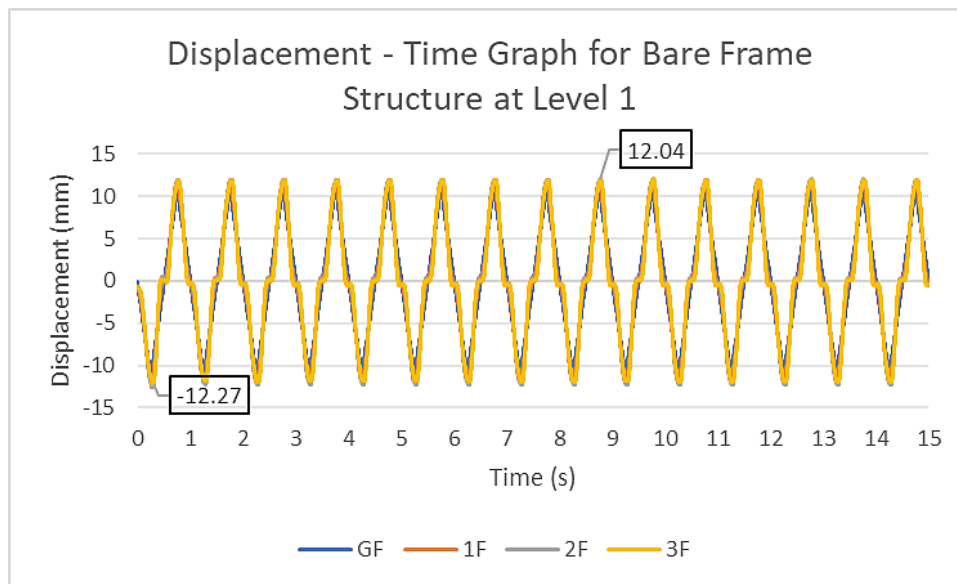
and Level 10. Hence, the relationship between the displacement response of the downscaled model and the research parameters can be observed.

Each round of pseudo dynamic load testing lasted for 15 seconds to collect the displacement response of the downscaled model. The experimental data are focused on the rooftop displacement, inter-storey drift and mode shape of the structure fixed on the shaking table. The results were measured by the LVDTs and collected by the data logger. Two 25mm LVDTs were used to collect data from the shaking table and first floor of the structure, while two 50 mm LVDTs were installed on the second and third floors of the structure. Prior to data analysis, the value obtained from the shaking table test was corrected by multiplying with the coefficient of the testing sensors, which are 2×10^{-3} for 25 mm LVDT and 5×10^{-3} for 50 mm LVDT.

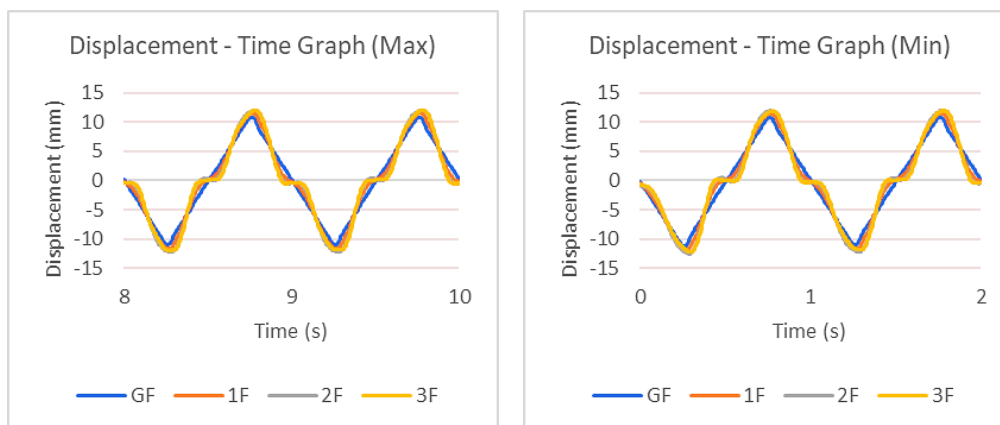
4.2 Bare Frame Structure

The shaking table test was carried out on the bare frame structure from Level 1 to Level 10 of the earthquake simulation. No viscous damping system is installed on the structure. Based on the data obtained from the LVDTs, the displacement of each floor of the structure at each level of shaking can be analysed.

Figure 4.1 shows the complete displacement over time graph for the bare frame structure at Level 1. Since the frequency of Level 1 is 1 Hz, only one cycle occurred every second. A different sign of the displacement value represents the different directions of the movement of the structure. The model moves forwards and backwards during the shaking. The displacement – time graph shows that each floor of the structure is moved in the same direction at Level 1 since the sign of displacement for each floor is similar throughout the shaking. The displacement of the ground floor represents the movement of the shaking table. The whole structure is moved following the shaking direction at Level 1. The maximum rooftop displacement throughout the shaking is found to be 12.27 mm.



(a)

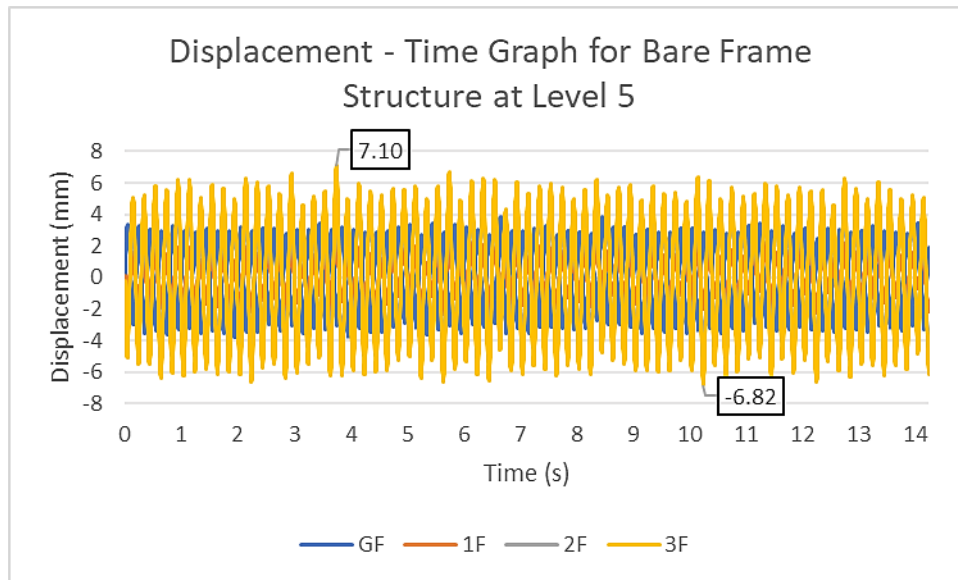


(b)

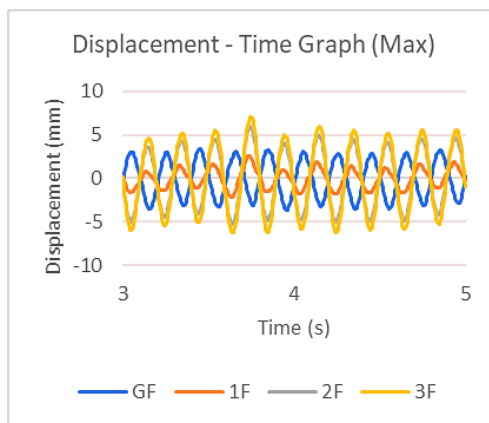
(c)

Figure 4.1: Displacement – Time Graph for Bare Frame Structure at Level 1 (a) Overall; (b) Maximum; (c) Minimum.

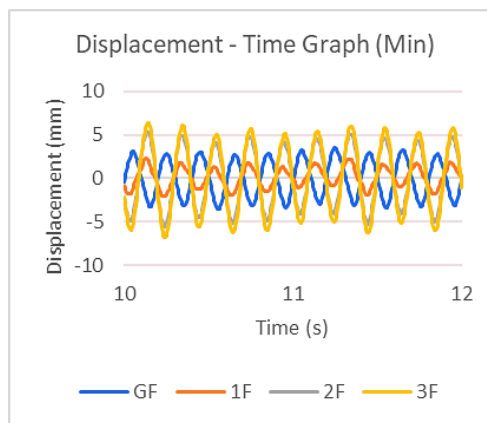
Figure 4.2 shows the complete displacement over time graph for the bare frame structure at Level 5. Starting from this level, the intensity of the shaking increases from low aggressiveness to high aggressiveness. The displacement of the first, second and third floors of the structure is found to have a positive sign, while the ground floor displacement is negative, indicating the downscaled structure is moved against the shaking direction at this level. The maximum rooftop displacement throughout Level 5 is 7.10 mm, lower than Level 1, showing that the movement observed on the rooftop has decreased.



(a)



(b)

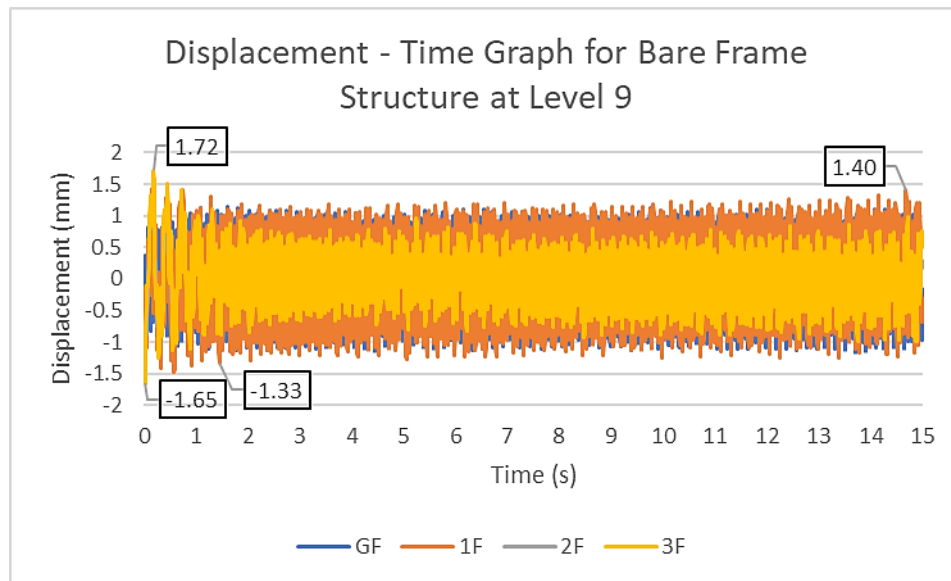


(c)

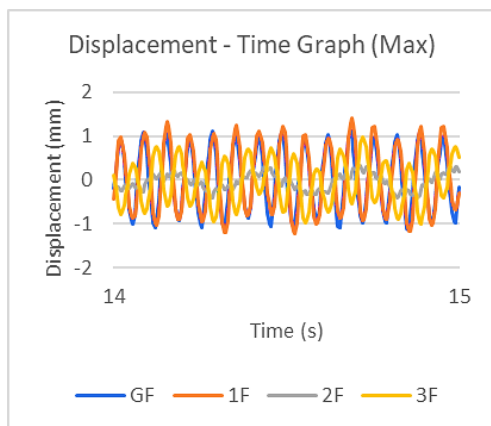
Figure 4.2: Displacement – Time Graph for Bare Frame Structure at Level 5 (a) Overall; (b) Maximum; (c) Minimum.

Level 9 and Level 10 have a very high aggressiveness of shaking with a shaking frequency of 15 Hz, which is 15 times larger than Level 1. Figure 4.3 shows the displacement over time graph for the bare frame structure at Level 9. At the beginning of the shaking, the structure moves with a large displacement of 1.72 mm on the highest floor. The rooftop displacement reduces gradually until the structure reaches a stable motion. The stable structural behaviour is analysed, and the results indicate that the displacement on the top floor is smaller than on the lower floors of the building. The structure experiences vigorous vibrations with small lateral movements at this level. The maximum

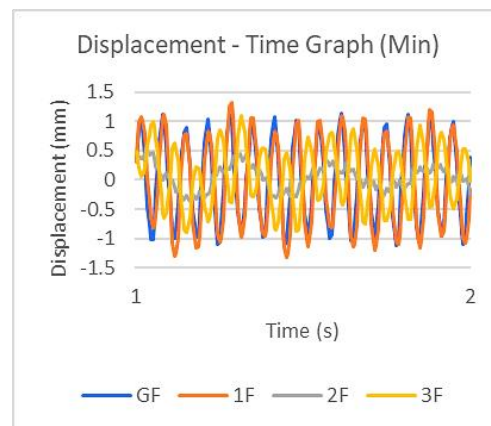
displacement of 1.40 mm is observed on the first floor, while the rooftop displacement of the structure is found to be 1.10 mm at Level 9.



(a)



(b)



(c)

Figure 4.3: Displacement – Time Graph for Bare Frame Structure at Level 9 (a) Overall; (b) Maximum; (c) Minimum.

Based on the maximum displacement for each floor at each level of shaking obtained, the inter-storey drift between floors is calculated and tabulated in Table 4.2. Based on the results of Level 1 and Level 2, the overall maximum displacement of the structure at Level 2 is found to be larger than at Level 1. The unit displacement of the simulation is consistent at both levels, which is 3 mm/mm, but the frequency of shaking at Level 2 is 1 Hz higher than Level 1, thus the structure exhibits more significant motion at Level 2.

Moreover, the overall displacement or movement of the structure at Level 4 is greater than at Level 3, despite the shaking frequency remaining the same, which is 3 Hz. This observation was likely due to the more significant unit displacement of shaking at Level 4 for 0.4 mm/mm. This observation can be seen in the results obtained from Level 9 and Level 10. When either the shaking frequency or unit displacement is increased while the other parameter is held constant, there is a corresponding increase in the maximum displacement observed in the system.

Table 4.2: Inter-Storey Drift for Bare Frame Structure at All Levels.

Level	Maximum displacement (mm)				Inter-storey drift (mm)		
	GF	1F	2F	3F	GF - 1F	1F - 2F	2F - 3F
1	11.28	11.93	12.63	12.27	0.65	0.70	- 0.36
2	11.76	13.21	15.28	15.16	1.45	2.08	- 0.13
3	7.91	12.60	16.31	17.53	4.69	3.71	1.22
4	8.52	13.68	17.46	18.26	5.16	3.77	0.80
5	3.85	2.59	5.96	7.10	- 1.26	3.37	1.13
6	2.43	2.05	2.98	3.71	- 0.38	0.94	0.73
7	2.52	2.47	3.27	3.58	- 0.06	0.80	0.31
8	2.61	2.62	2.99	3.45	0.01	0.36	0.47
9	1.16	1.40	0.55	1.10	0.25	- 0.86	0.56
10	1.54	2.00	1.96	2.36	0.46	- 0.04	0.40

Level 5 is the intermediate level, where the intensity of the shaking is increased to simulate more aggressive seismic activity. The maximum displacement on all floors decreases significantly at this level compared to the previous levels. The building behaviour changes from large lateral movement to intense vibration from this level.

The structure is observed to have the highest inter-storey drift of 5.16 mm at Level 4, shown in the yellow highlighted. The rooftop displacement of the bare frame structure is greater than the ground displacement by about 10 mm at these levels. The results indicate that the higher floors of the structure experience the largest displacement amplitudes compared to the lower floors

when the shaking displacement is moderate with low aggressiveness. This can result in significant damage or collapse of the upper floors during an earthquake.

Based on the outcome of the shaking table test, the mode shape for the bare frame structure at each level is investigated by plotting the graph, as shown in Figure 4.4. The mode shape of the bare frame structure from Level 1 to Level 4 shows a single curvature shape. The building experiences translational motion and sways in one direction only with minimal torsional or rotational motion. When the shaking level increase until Level 8, the mode shape of the structure changes to double curvature, which means the mode shape has two different curvatures in different directions. At Level 9 and Level 10, the mode shape of the building alters to a double S curvature shape. This type of mode shape can be observed when the maximum displacement of the second floor is lower than the first and third floor during shaking.

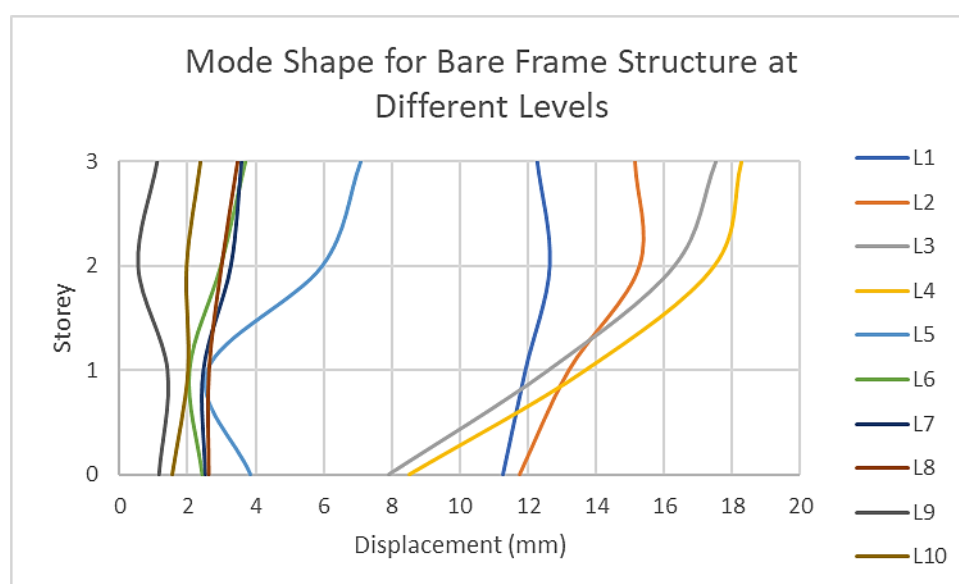


Figure 4.4: Mode Shape for Bare Frame Structure at Different Levels.

Throughout the shaking table test conducted on the bare frame structure, the structure is damaged where cracking is found on the concrete surface. The ground motion simulated causes the structure to oscillate and rotate, which induces forces and moments in the structural elements. When the internal forces exceed the yield strength of the member, plastic bending occurs, causing plastic deformation of the structural member. A plastic hinge is formed at the location where the maximum bending moment occurs, making the structure

more flexible since it allows free rotation. The formation of a plastic hinge allows the structural member to deform plastically without causing a catastrophic failure. Hence, it is also a type of energy dissipation device, and it enhances the seismic performance of the building.

Generally, the formation of a plastic hinge in a reinforced concrete member will not cause concrete cracks since it occurs in the steel reinforcement rather than in the concrete itself. However, the plastic deformation may cause the concrete cover to spall or crack in certain conditions. This can happen when the bond strength between the reinforcement and the surrounding concrete is weaker than the tension in the reinforcement. Insufficient steel reinforcement or inadequate concrete cover may also cause concrete spalling and cracking.

In a 1 bay frame structure, the plastic hinges are typically formed at the beam-to-column connections where the maximum bending moment is found. The beams are normally designed with appropriate plastic hinges to dissipate the seismic energy without collapsing. In contrast, the columns are designed to remain elastic and stabilise the structure during an earthquake.

In this study, the beams of the first floor start to crack and form plastic hinges at Level 3 of shaking. As the structure undergoes further shaking, more cracking is observed, as shown in Figure 4.5. The hinges formed allow the column-beam joints of the first floor to rotate in conjunction with the lower columns.

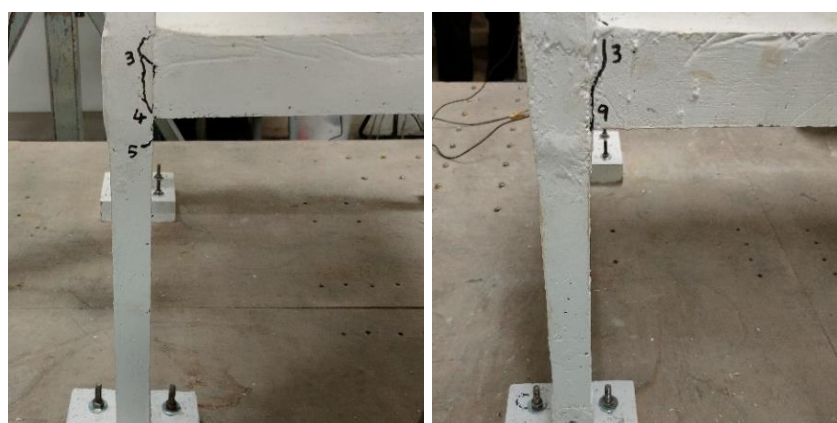


Figure 4.5: Concrete Cracking on the First Floor Beams of Bare Frame Structure.

The plastic hinges on the top of the columns of the second floor are observed starting from Level 4, as shown in Figure 4.6, while Figure 4.7 shows the formation of plastic hinges on the top of the first floor column after Level 5 of the earthquake simulation. The plastic deformation of the structural members allows the structure to absorb more energy before collapsing during earthquake events.



Figure 4.6: Concrete Cracks on the Second Floor Column of Bare Frame Structure.

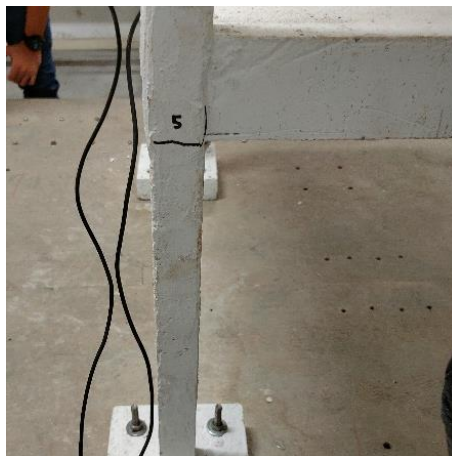
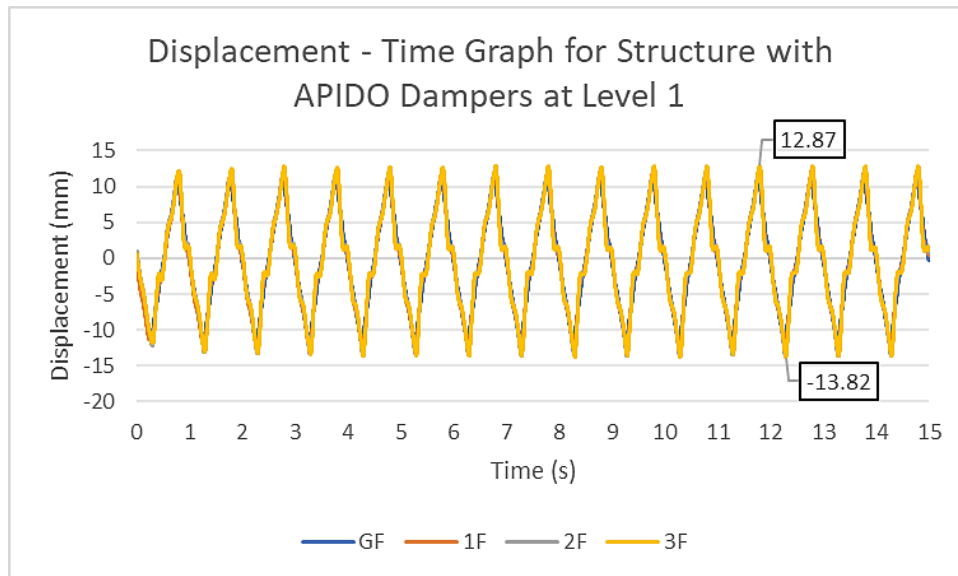


Figure 4.7: Concrete Cracks on the First Floor Column of Bare Frame Structure.

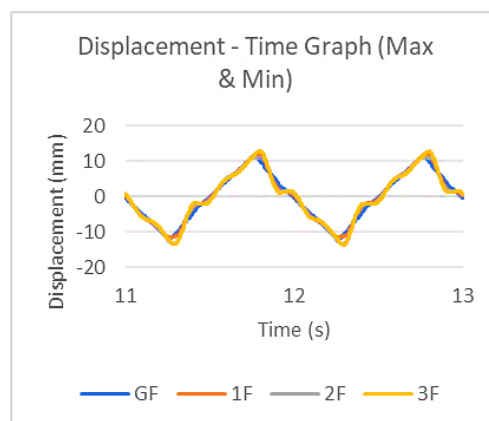
4.3 Structure with APIDO Dampers

The shaking table test was then carried out on the structure with the APIDO damping system. The horizontal movement on each floor of the structure was measured using the LVDTs to analyse the performance of viscous dampers in improving the dynamic response of the structure during earthquake simulation.

Figure 4.8 shows the complete displacement over time graph for the structure with APIDO dampers at Level 1. The displacement-time graph indicates that the whole structure moves in the direction of shaking, showing similar structural behaviour to the bare frame structure at this level. The maximum rooftop displacement obtained from the structure with an inverted V diagonal braced-damper system of APIDO dampers is 13.82 mm at Level 1.



(a)

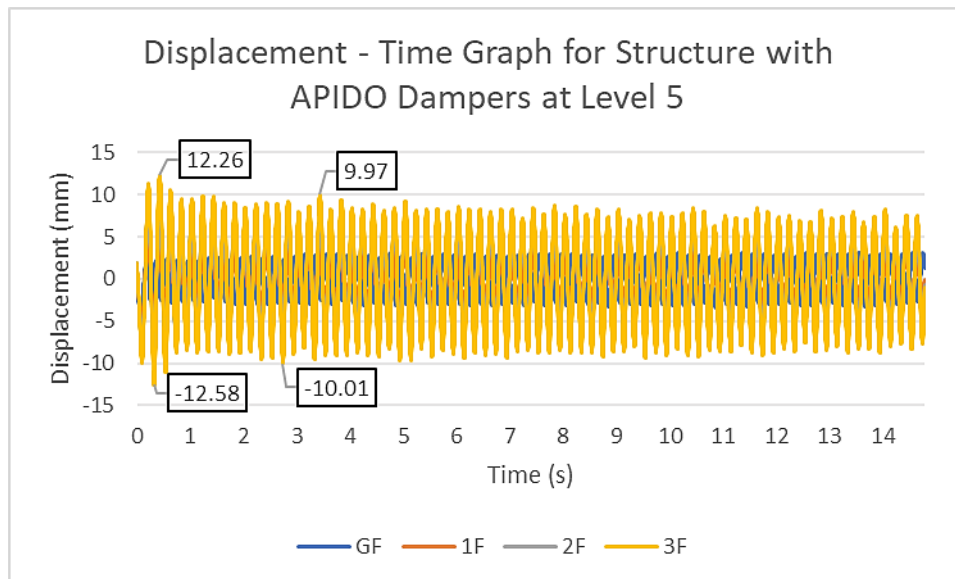


(b)

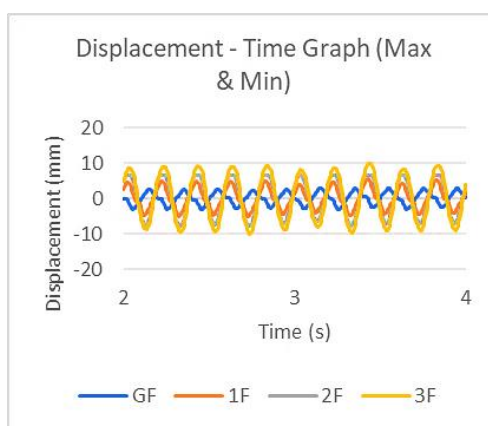
Figure 4.8: Displacement – Time Graph for Structure with APIDO Dampers at Level 1 (a) Overall; (b) Maximum and Minimum.

Starting from Level 5 of shaking, the displacement-time graph shows a high displacement in the first second, followed by a relatively constant structural behaviour. Figure 4.9 shows that the maximum rooftop displacement

of the structure within the first second at Level 5 is 12.58 mm, while the maximum rooftop displacement found after that is 10.01 mm. The research results indicate that the pseudo dynamic load activated the damping system and started to absorb and dissipate the energy of seismic waves. Hence, the amount of energy transferred to the building decreases, reducing the motion of the building in the earthquake simulation. The constant displacement of the structure indicates that the damping system has provided a consistent amount of resistance to the ground motion, thus the structure is settled into a more stable motion. The damping system stabilises the building and enhances its seismic performance. Nevertheless, the activation phase of the damping system is not considered in the data analysis to investigate the improvement of seismic resistance of the building when energy dissipation tools are utilised. Therefore, the maximum rooftop displacement of the structure with APIDO dampers obtained at Level 5 is 10.01 mm.



(a)



(b)

Figure 4.9: Displacement – Time Graph for Structure with APIDO Dampers at Level 5 (a) Overall; (b) Maximum and Minimum.

The maximum displacement for each floor and the inter-storey drift between floors of the structure with APIDO dampers at each level of shaking are tabulated in Table 4.3. The outcome of the shaking table test shows a similar observation with the bare frame structure, which is the maximum displacement of the structure increase when either the shaking frequency or unit displacement is increased. This can be proven by the larger displacement obtained at Level 2 and Level 8 compared to the respective levels, which have the same unit displacement of shaking but a lower shaking frequency. At the same time, the inter-storey drift of the structure at Level 4 and Level 10 is found to be larger than Level 3 and Level 9, respectively, indicating the structure experiences more considerable motion at a more extensive unit displacement of shaking while shaking frequency remains constant.

The structure is observed to have the highest inter-storey drift at Level 5, which is 2.27 mm between the second and first floors of the structure, as highlighted in yellow. About 2 mm of inter-storey drift is obtained from two adjacent floors of the structure with APIDO dampers at Level 5. The results indicate that the whole structure is leaned in one direction during the shaking.

Table 4.3: Inter-Storey Drift for Structure with APIDO Dampers at All Levels.

Level	Maximum displacement (mm)				Inter-storey drift (mm)		
	GF	1F	2F	3F	GF - 1F	1F - 2F	2F - 3F
1	11.96	12.28	13.60	13.82	0.33	1.32	0.22
2	11.92	12.46	14.15	14.86	0.54	1.69	0.70
3	6.32	8.54	7.86	9.57	2.22	- 0.68	1.71
4	8.05	10.24	11.29	11.88	2.20	1.05	0.59
5	3.40	5.64	7.91	10.01	2.25	2.27	2.10
6	2.09	1.56	2.50	3.36	- 0.53	0.94	0.86
7	1.84	1.46	2.18	3.09	- 0.38	0.72	0.91
8	2.44	2.51	2.72	3.82	0.07	0.21	1.10
9	0.49	1.00	0.69	0.97	0.51	- 0.31	0.28
10	1.22	1.35	0.70	1.14	0.13	- 0.65	0.44

Figure 4.10 shows the mode shape for the structure equipped with an inverted V diagonal braced-damper system of APIDO dampers at each level of shaking. The mode shape of the structure at Level 1 and Level 2 shows a double curvature shape. At Level 3, the structure has a double S curvature shape, which changes to a single curvature shape at Level 4 of shaking. A straight mode shape with a large gradient is observed at Level 5 due to the sizeable inter-storey drift of the structure in the same direction. From Level 6 to Level 8, the building experiences translational motion and sways in one direction only with minimal torsional or rotational motion, showing a single curvature mode shape. At Level 9 and Level 10, which have high intensity of shaking, the mode shape of the structure alters to a double S curvature.

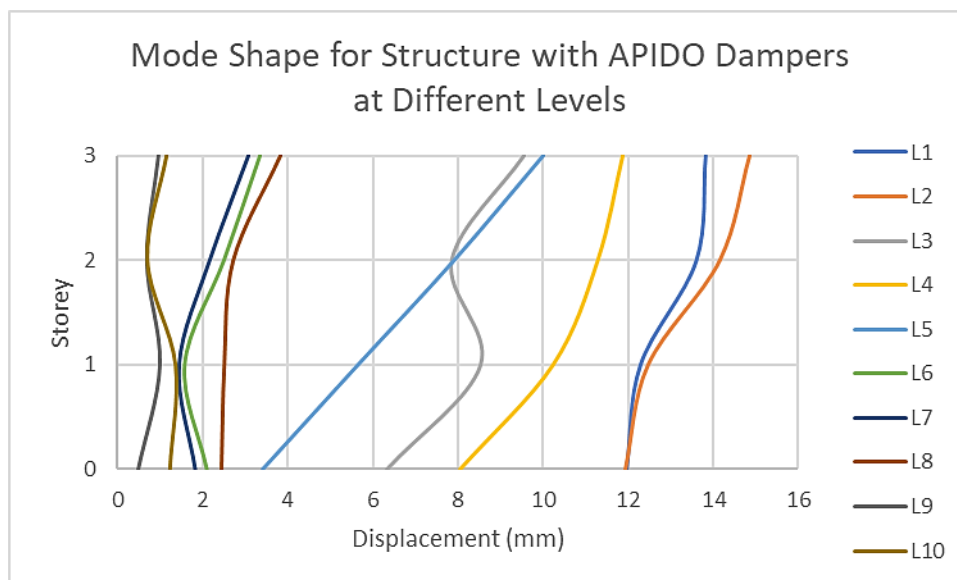
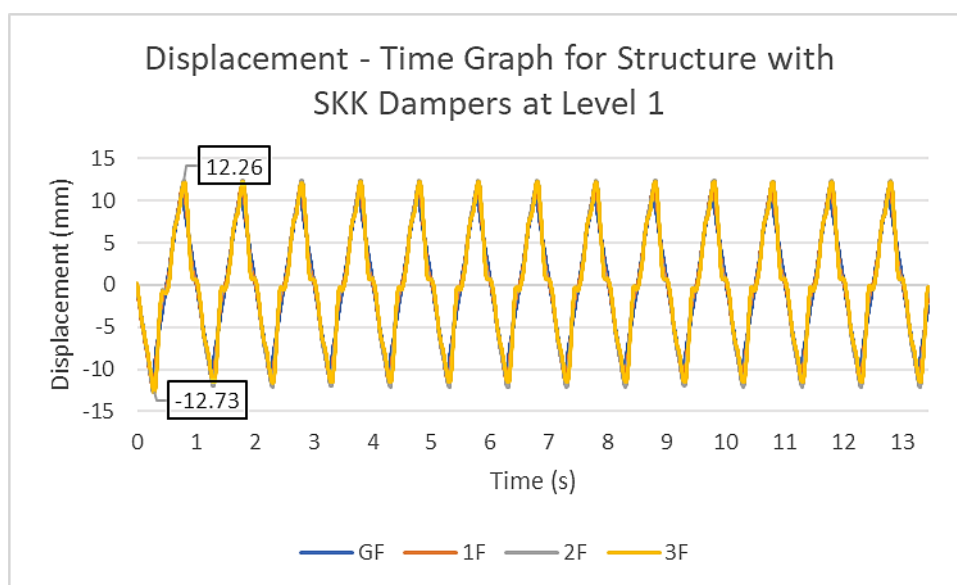


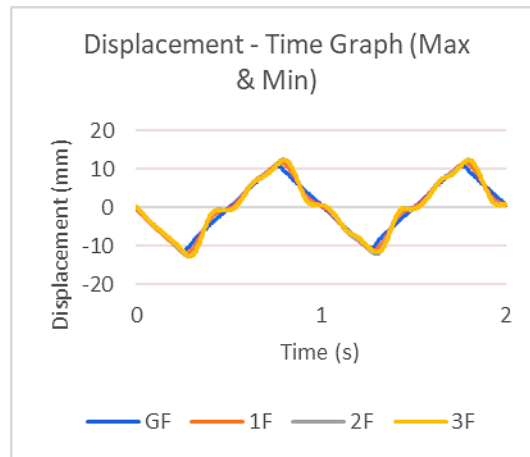
Figure 4.10: Mode Shape for Structure with APIDO Dampers at Different Levels.

4.4 Structure with SKK Dampers

Next, the structure was tested with an inverted V diagonal braced-damper system of SKK dampers. Figure 4.11 shows the lateral displacement over time for the structure at Level 1 measured using LVDTs. The graph shows that the movement of the structure follows the direction of shaking at this level, similar to previous testing. The maximum rooftop displacement obtained from the structure with SKK dampers at Level 1 of shaking is 12.73 mm.



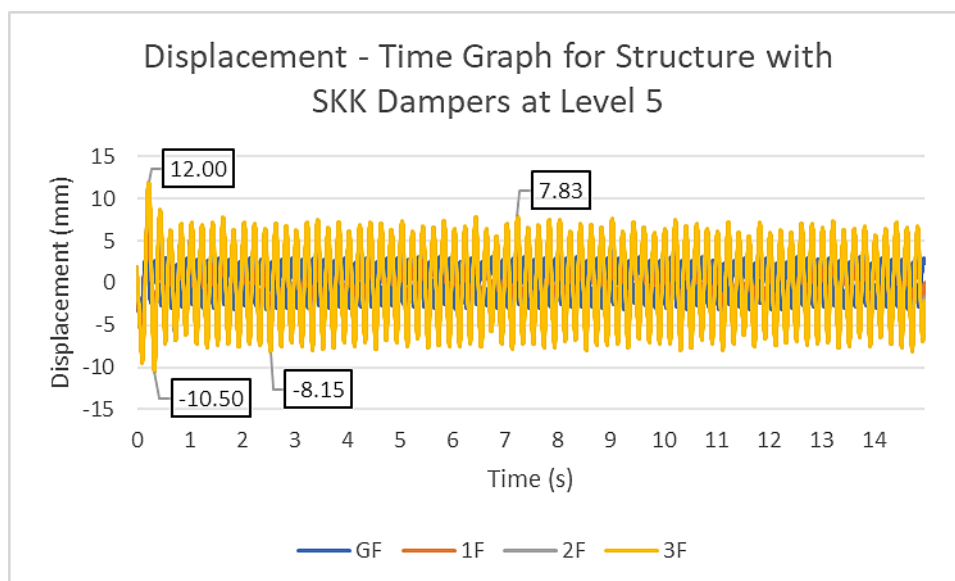
(a)



(b)

Figure 4.11: Displacement – Time Graph for Structure with SKK Dampers at Level 1 (a) Overall; (b) Maximum and Minimum.

The activation phase is also observed on the structure with the SKK damping system at Level 5 of shaking, as shown in Figure 4.12. The damping system is activated within 1 second of shaking and contributes to stabilising the structure and reducing the lateral movement due to the dynamic response of the building. The maximum displacement observed from the structure in the activation phase is 12.00 mm, while the rooftop displacement obtained from the structure in stable motion is 8.15 mm.



(a)

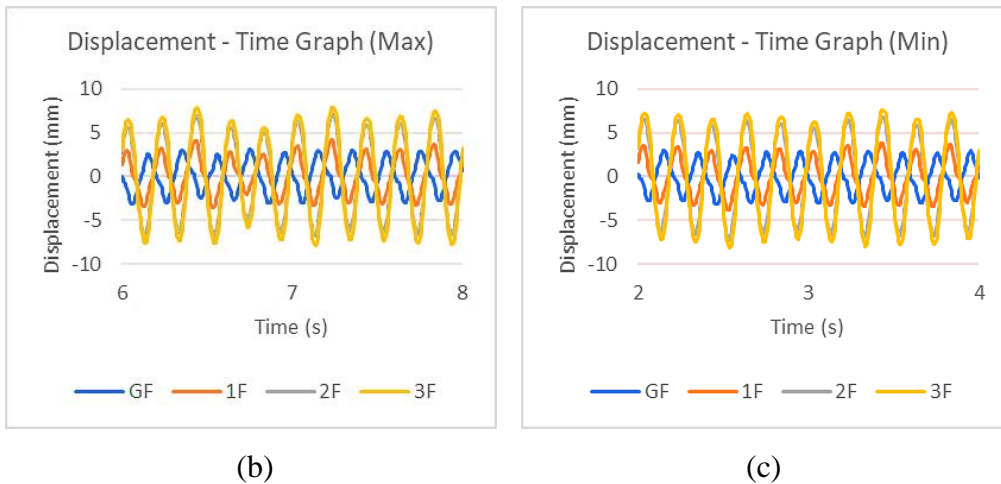
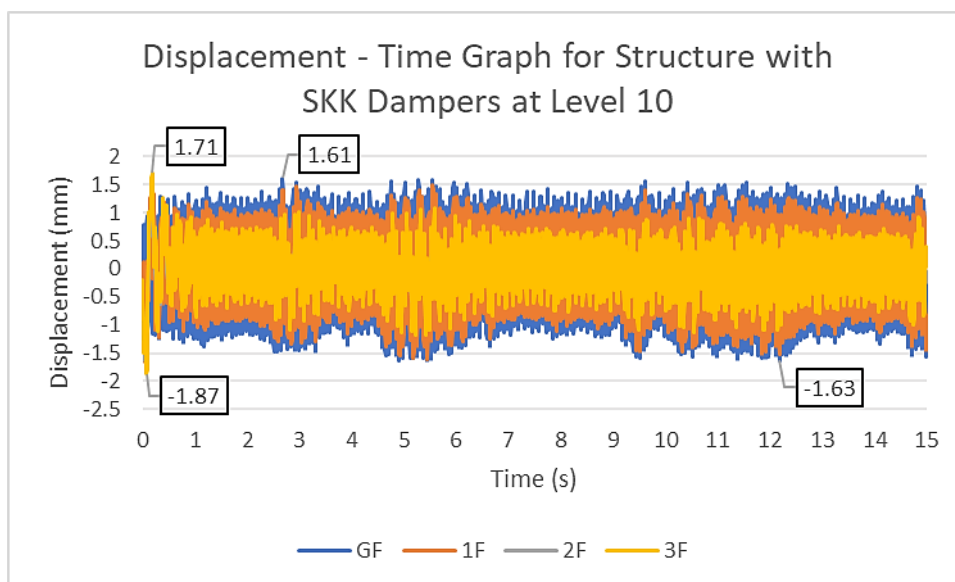


Figure 4.12: Displacement – Time Graph for Structure with SKK Dampers at Level 5 (a) Overall; (b) Maximum; (c) Minimum.

Based on the research results obtained from the shaking table test of the structure with an inverted V diagonal braced-damper system of SKK dampers, the rooftop displacement of the structure is found to be smaller than the lower floors at Level 10 as shown in Figure 4.13. The lateral movement on the third floor is the largest in the damping system's activation phase, which is about 1.87 mm. The rooftop displacement obtained during the stable motion of the structure is 1.27 mm which is smaller than the maximum ground motion of 1.63 mm. The structure experiences intense vibrations due to the high shaking frequency at Level 10.



(a)

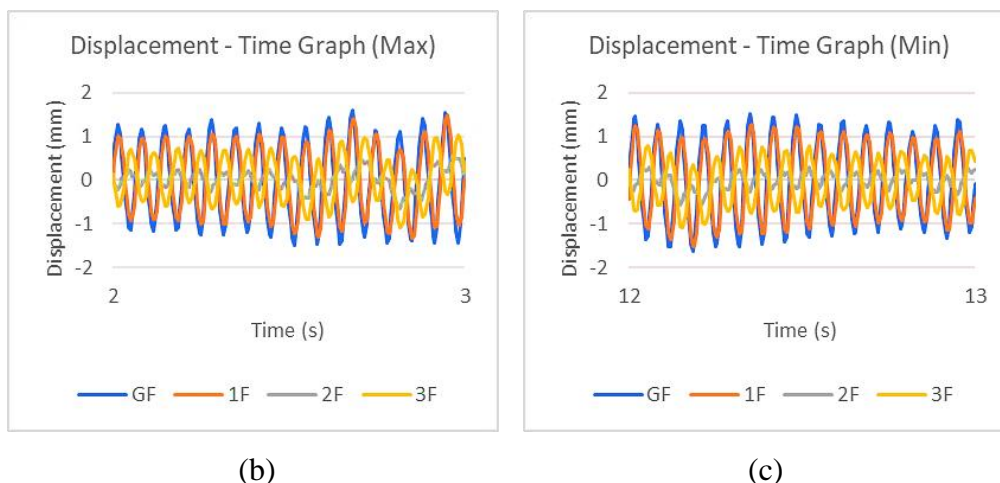


Figure 4.13: Displacement – Time Graph for Structure with SKK Dampers at Level 10 (a) Overall; (b) Maximum; (c) Minimum.

The maximum displacement for each floor and the differential lateral movement between floors of the structure with SKK dampers at each level of shaking are tabulated in Table 4.4. Similar to the previous testing, the experimental data show an increment in maximum displacement on each floor when either the shaking frequency or unit displacement is magnified. The yellow highlight in the table below shows the largest inter-storey drift of 3.54 mm between the first and ground floor of the structure at Level 3 of shaking. The rooftop displacement of the structure with the SKK damping system is greater than the ground motion by about 6.5 mm at Level 3 and Level 4. There is substantial lateral movement of the whole structure at these levels.

Table 4.4: Inter-Storey Drift for Structure with SKK Dampers at All Levels.

Level	Maximum displacement (mm)				Inter-storey drift (mm)		
	GF	1F	2F	3F	GF - 1F	1F - 2F	2F - 3F
1	11.36	11.82	12.80	12.73	0.46	0.97	- 0.07
2	11.33	12.76	13.79	13.97	1.43	1.02	0.18
3	6.18	9.72	12.29	12.61	3.54	2.57	0.32
4	8.10	11.40	14.15	14.85	3.30	2.75	0.70
5	3.19	4.16	7.25	8.15	0.97	3.10	0.90
6	2.00	1.48	2.56	3.05	- 0.51	1.08	0.49
7	1.97	1.48	2.20	2.18	- 0.49	0.72	- 0.02

Table 4.4 (Continued)

8	2.22	2.12	2.60	3.15	- 0.10	0.49	0.54
9	0.20	0.32	0.33	0.40	0.11	0.01	0.07
10	1.63	1.60	0.82	1.27	- 0.03	- 0.79	0.45

Figure 4.14 shows the mode shape for the structure with the SKK damper at each level of the earthquake simulation. The structure has a double curvature mode shape at Level 1. Starting from Level 2 to Level 4, the mode shape of the structure shows a single curvature shape, indicating that the building sways in one direction. The mode shape of the structure with SKK dampers at Level 5 is a double curvature shape where the rooftop displacement has a massive difference with ground movement. The mode shape has two different curvatures in different directions, showing a double S curvature shape until Level 8. The mode shape observed at Level 9 is a very steep straight line with a rooftop displacement smaller than 1 mm, indicating the structure has minimal inter-storey drift during the shaking. At the last level of shaking, the building experiences motion with torsion or rotation, showing a double S curvature mode shape.

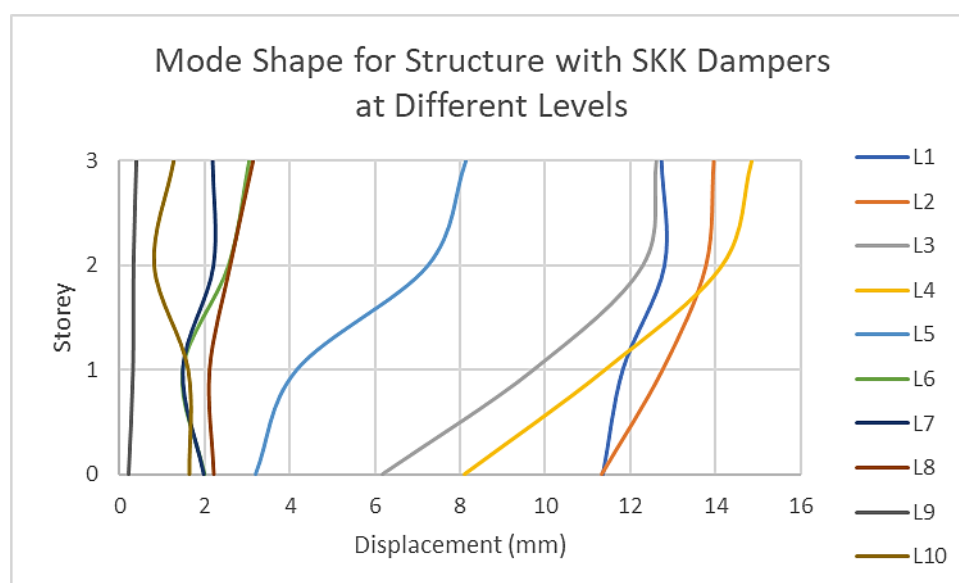
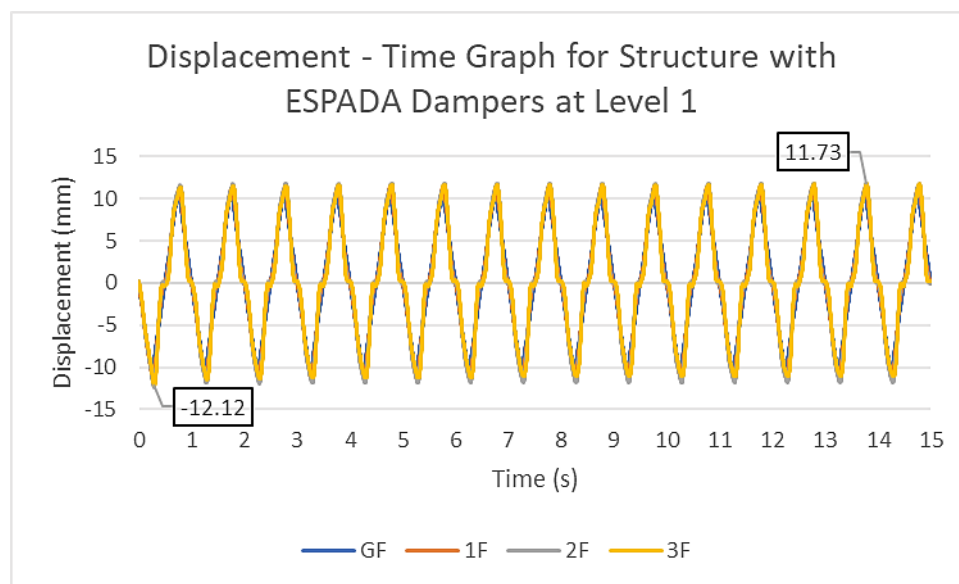


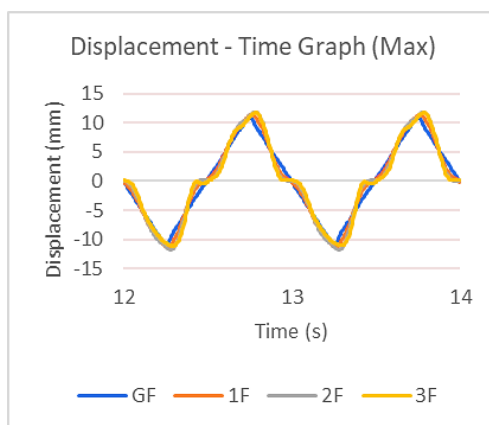
Figure 4.14: Mode Shape for Structure with SKK Dampers at Different Levels.

4.5 Structure with ESPADA Dampers

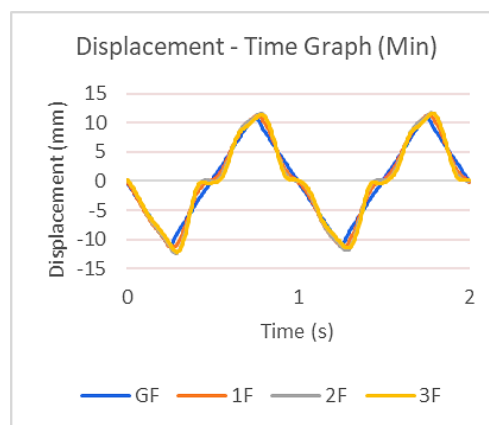
The downscaled model on the shaking table was then installed with an ESPADA damping system and subjected to 10 levels of ground motions. Figure 4.15 shows the structure's lateral movement over time at Level 1. The displacement-time graph shows that the structure moves in the direction of shaking at this level, like in the previous testing. The maximum rooftop displacement of the structure under simulated earthquake ground motion is found to be 12.12 mm.



(a)



(b)

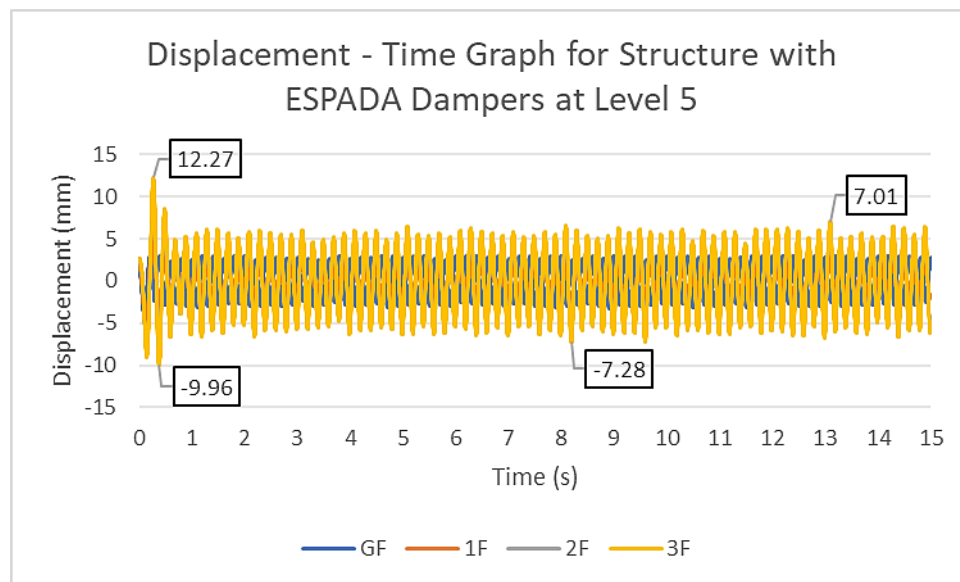


(c)

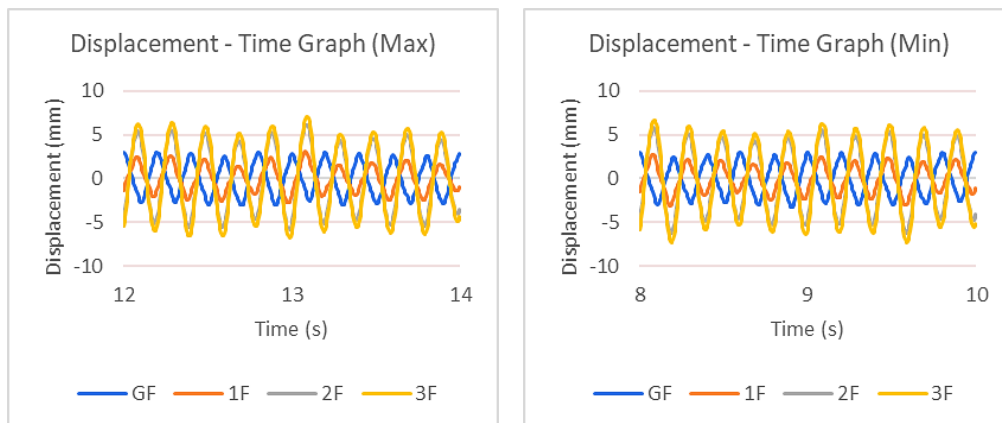
Figure 4.15: Displacement – Time Graph for Structure with ESPADA Dampers at Level 1 (a) Overall; (b) Maximum; (c) Minimum.

Like the other damping system, ESPADA dampers require an activation force to reduce the dynamic response of the structure starting from

Level 5 of shaking. Figure 4.16 shows that the maximum displacement within 1s is 12.27 mm, while the maximum movement on the third floor afterwards is found to be 7.28 mm during stable motion of the structure. The damping system stabilises the structure and reduces the amplitude of vibrations induced by the pseudo dynamic loads.



(a)



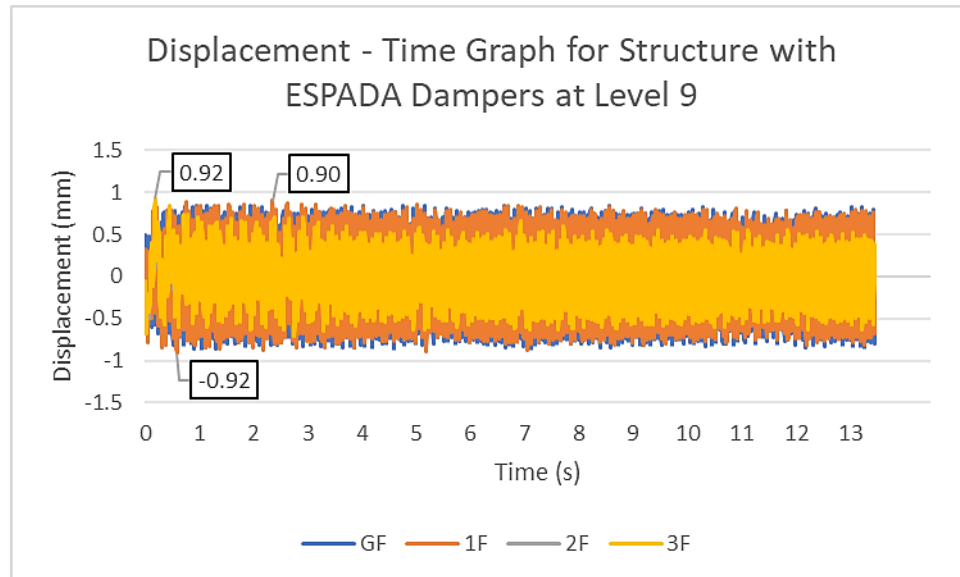
(b)

(c)

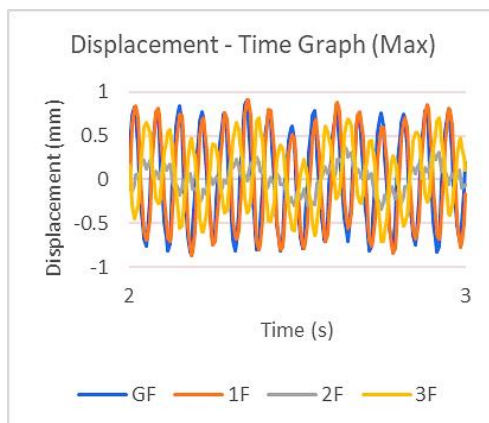
Figure 4.16: Displacement – Time Graph for Structure with ESPADA Dampers at Level 5 (a) Overall; (b) Maximum; (c) Minimum.

During the simulated earthquake level with high intensity, the lateral movement on the top floor is found to be smaller than on the lower floors. Figure 4.17 shows the horizontal displacement on each floor throughout Level 9 of earthquake motion. The most significant displacement is found on the structure's

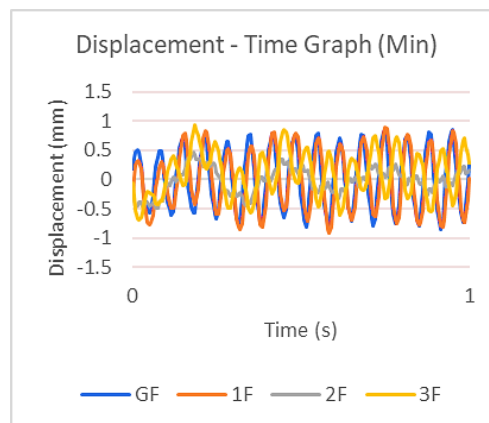
first floor, which is 0.92 mm. The overall movement of the structure is smaller than 1 mm, which is not significant to the structure, indicating the structure vibrates with high frequency when experiencing frequent back-and-forth motions.



(a)



(b)



(c)

Figure 4.17: Displacement – Time Graph for Structure with ESPADA Dampers at Level 9 (a) Overall; (b) Maximum; (c) Minimum.

The experimental results of the shaking table test conducted on the structure with ESPADA dampers are tabulated in Table 4.5. The structural behaviour is found to be similar to the bare frame structure as well as the structure equipped with other brands of dampers. The maximum displacement of the structure is found larger when either shaking frequency or unit

displacement of the shaking is larger while the other parameter is maintained constant. The largest inter-storey drift of this structure is observed between the first and ground floor at Level 3, which is 4.54 mm, as shown in yellow highlighted, followed by a difference in lateral movement of 4.45 mm found between the same location at Level 4. The rooftop displacement of the structure with ESPADA dampers is found to be more than 8 mm greater than the displacement on the ground floor at these levels of shaking.

Table 4.5: Inter-Storey Drift for Structure with ESPADA Dampers at All Levels.

Level	Maximum displacement (mm)				Inter-storey drift (mm)		
	GF	1F	2F	3F	GF - 1F	1F - 2F	2F - 3F
1	10.86	11.32	12.38	12.12	0.46	1.06	- 0.25
2	11.84	13.22	14.85	14.45	1.38	1.63	- 0.41
3	7.50	12.04	15.72	16.25	4.54	3.69	0.53
4	8.44	12.89	16.29	16.86	4.45	3.41	0.56
5	3.23	3.09	6.28	7.28	- 0.13	3.19	1.00
6	2.10	1.41	2.62	3.16	- 0.70	1.21	0.54
7	2.02	1.87	2.36	2.83	- 0.15	0.50	0.47
8	2.34	2.43	2.60	3.43	0.08	0.17	0.83
9	0.90	0.92	0.50	0.92	0.01	- 0.42	0.43
10	1.19	1.25	0.64	1.10	0.05	- 0.61	0.46

The experimental data was then used to investigate the mode shape of the structure observed at each level. Single curvature mode shapes are observed from the movement of the structure at Level 1 to Level 4, as shown in Figure 4.18, indicating the structure vibrates in a single direction during the shaking. The mode shape changes to a double curvature shape at Levels 5 and 6 and then alters to a single curvature shape at Levels 7 and 8. The mode shape shows a double S curvature with a small amplitude at the remaining levels. The double curvature mode shape shows that the building vibrates in two directions with twisting movements, while the double S curvature mode shape indicates the building has a significant twisting movement.

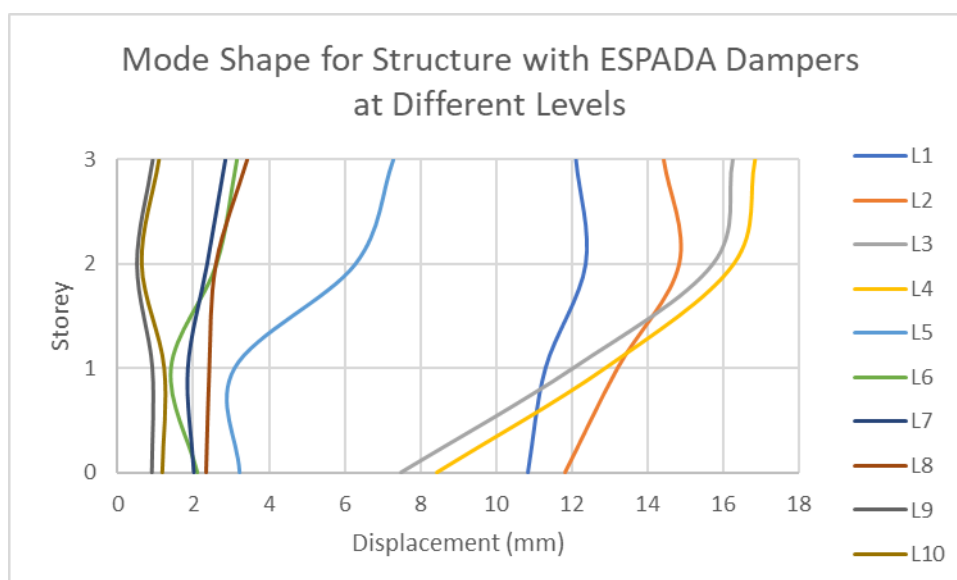


Figure 4.18: Mode Shape for Structure with ESPADA Dampers at Different Levels.

4.6 Displacement Response for Structure with and without Damper

From the experimental results obtained from the LVDTs installed to the downscaled model, the displacement response for the structure with and without a damping system can be analysed and compared. The structural behaviour and mode shape of each system had been discussed previously. The mode shapes of each system at ten levels of shaking are discussed respectively to investigate the efficiency of the viscous dampers when the building is subjected to seismic events in varying intensities. The displacement of the shaking decreases, and the aggressiveness of the shaking increases when the shaking level increases, which means a higher level of shaking has a more intense ground motion.

The first two shaking levels in this study have a large displacement motion with very low and low aggressiveness of shaking. Figure 4.19 (a) and Figure 4.19 (b) show the mode shape comparison between the structures at Level 1 and Level 2 of shaking, respectively. By comparing the mode shapes of the bare frame structure and the structures with dampers, there is no apparent improvement in the lateral displacement reduction seen from the structure with dampers at Level 1. Nevertheless, the bare frame structure has a single curvature mode shape at Level 1, while all other structures pose a double curvature mode shape which is preferable in seismic design. Double curvature mode shapes enable the structure to absorb more earthquake energy and deform more before

the ultimate failure during an earthquake since it can be more ductile than a single curvature mode shape.

Only the structure with APIDO dampers shows a double curvature mode shape at Level 2 of earthquake simulation. All the structures with dampers show a slight reduction in the rooftop displacement at Level 2. The results show that the damping system can marginally reduce the structure's dynamic response when the shaking displacement is large with low aggressiveness. When the structure is subjected to a large lateral ground motion, the whole structure tends to sway in the direction of shaking. The inverted V shape of the braces provides some stiffness and strength to the structure, improving the structural resistance to the lateral loads. Hence, the inverted V diagonal braced-damper system can reduce the structure's response to ground movement and restrain the building's sway during an earthquake.

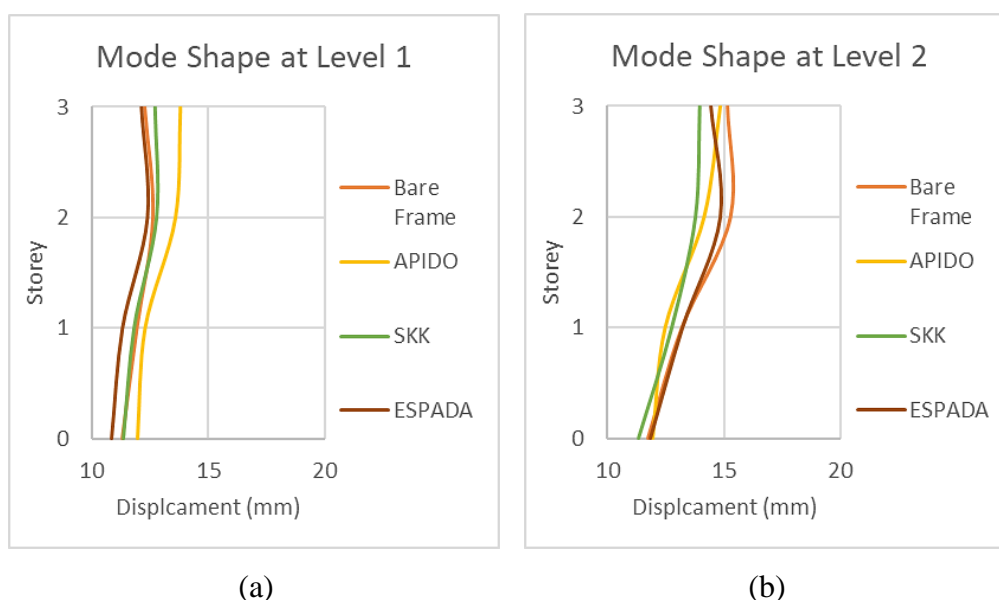


Figure 4.19: Mode Shape for Structures at (a) Level 1; (b) Level 2.

During the shaking table test with moderate displacement and low aggressiveness, the lateral movement for the structure with dampers is smaller than the bare frame structure at Levels 3 and 4, as shown in Figure 4.20. The inverted V diagonal braced-damper system installed on the structure reduces the dynamic response of the building effectively, no matter which brands of viscous dampers are utilised. The inter-storey drift of the structure also reduces as compared with the bare frame structure, indicating that the viscous dampers

successfully absorb some energy induced by the earthquake. The energy dissipation device reduces the pseudo dynamic load acting on the building and increases its seismic performance.

Based on the experimental data obtained from Level 3 and Level 4, the structure with the APIDO damping system has the best performance among all the testing models since it shows not only the least rooftop displacement but also the least inter-storey drift at both levels. A double S curvature mode shape is observed from the structure with APIDO dampers at Level 3. A double S curvature mode shape is more desired during an earthquake since it provides more excellent stability to the building than a single curvature mode shape. The double S curvature mode shape behaves similarly to the double curvature mode shape, distributing the lateral load more evenly throughout the structure. Therefore, the earthquake loads and stresses are less concentrated on one floor, which may cause the structure to collapse.

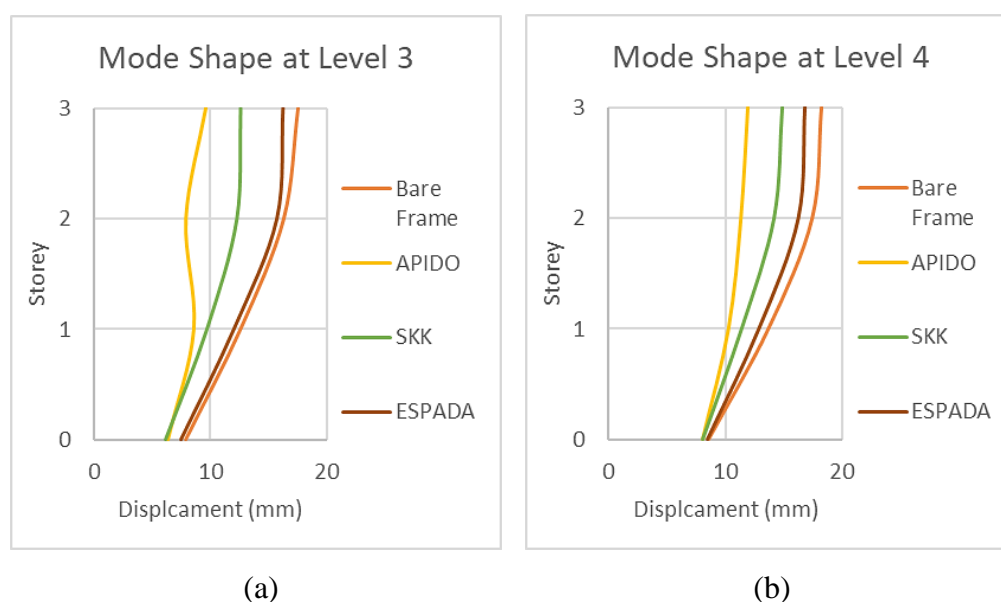


Figure 4.20: Mode Shape for Structures at (a) Level 3; (b) Level 4.

Figure 4.21 shows the mode shape for the testing models at Level 5 with moderate displacement and high aggressiveness of earthquake motion. Based on the mode shape obtained from the shaking table test, the bare frame structure tends to perform better than the structure with a damping system at this level. The structure with ESPADA dampers and the bare frame structure shows a similar structure behaviour at this level since the mode shape of both structures

is alike. The structure with APIDO dampers has the poorest performance, showing a straight mode shape with a large rooftop displacement. The structure sways heavily in one direction during the earthquake simulation, which may cause structural damage and eventually lead to collapse. At this level, the damping system is found not effective as it fails to dissipate the seismic energy and reduce the lateral movement of the structure due to ground motion.

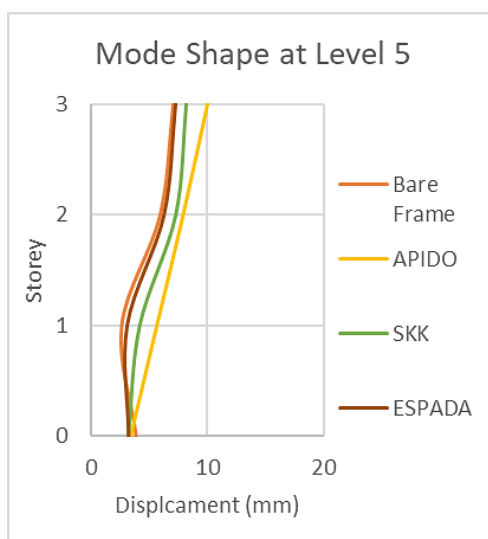


Figure 4.21: Mode Shape for Structures at Level 5.

The ground movement of the shaking changes from moderate displacement to short displacement at the next shaking level. The mode shape of the structures shows a significant improvement in the dynamic response of the structure with a damping system from the bare frame structure. Figure 4.22 shows that there is a notable reduction in the horizontal movement of the structures with a damping system at Level 6 of shaking. Thus, the inverted V diagonal braced-damper system is able to absorb seismic energy and reduce the amplitude of vibrations of the building effectively at this level, regardless of brand. The movement of the piston of the viscous dampers within the compressible fluid successfully creates a resistance force to oppose the motion of the building. Eventually, it improves the structural behaviour during the seismic event.

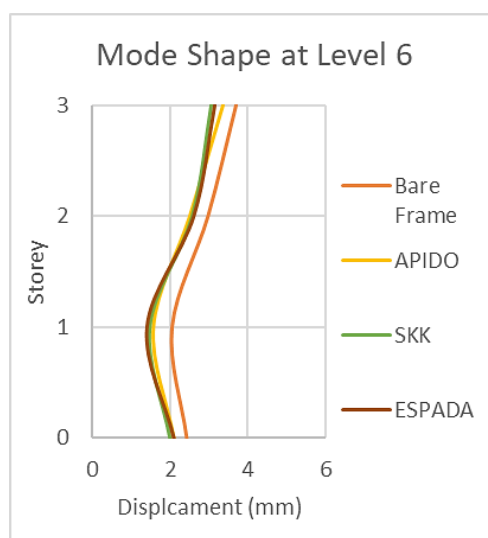


Figure 4.22: Mode Shape for Structures at Level 6.

In this study, Level 7 and Level 8 simulated the ground motion with short displacement and high aggressiveness. At Level 7, the bare frame structure shows a double curvature mode shape with the largest displacement among the testing models, as shown in Figure 4.23 (a), indicating the structures with dampers have better seismic performance compared to the bare frame structure. The damping system absorbs the seismic energy, reducing the structure's overall response during shaking. The structures with different brands of viscous dampers have similar ground movement but different rooftop displacement, showing that the effectiveness of viscous dampers in the reduction of rooftop displacement is varied. The structure with SKK dampers performs better than the structure with the APIDO and ESPADA damper since it has a double S curvature mode shape at Level 7. Thus, SKK dampers can spread the earthquake load uniformly to all floors of the structure, preventing load concentration on one floor that may lead to structural failure, while other dampers are not able to change the mode shape to double curvature at this level.

Figure 4.23 (b) shows that the structures with SKK dampers and ESPADA dampers behave similarly at Level 8. Both structures have similar mode shapes with identical ground movement and rooftop displacement. APIDO dampers have relatively low effectiveness in improving the seismic performance of the building at this level since there is only a slight reduction on the lower floors of the structure. However, the amplitude of vibrations observed on the top floor is more significant than in other models. The structures with

APIDO dampers and the bare frame structure both pose single curvature mode shapes that are undesired in seismic design due to the load concentration. The ground movement of the structure with APIDO dampers is smaller than the bare frame structure. However, its rooftop displacement is larger than the bare frame structure, meaning that the damping system does not dissipate the seismic energy.

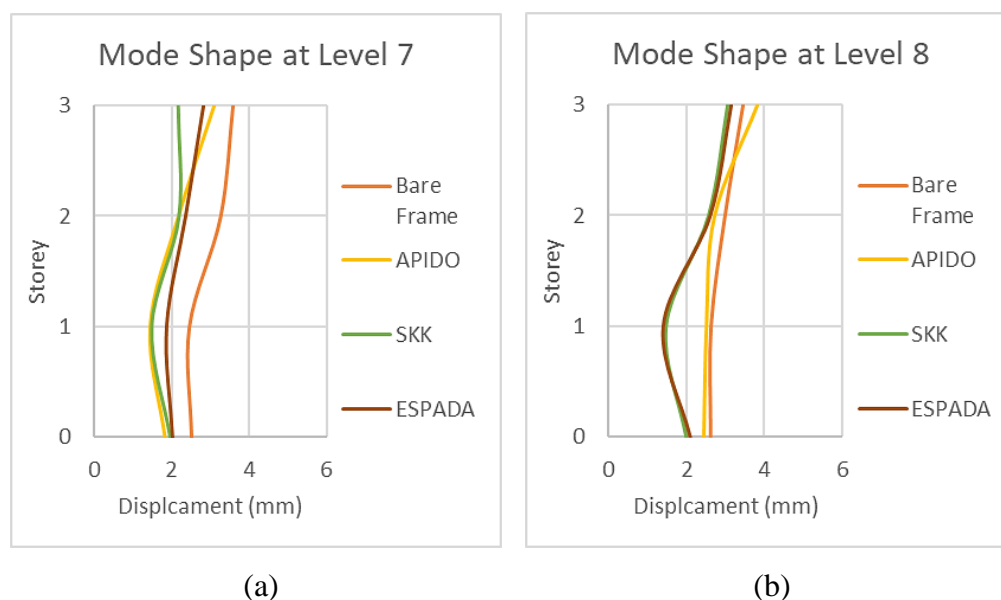


Figure 4.23: Mode Shape for Structures at (a) Level 7; (b) Level 8.

The last two levels in the shaking table test have a very high aggressiveness with low shaking displacement. Figure 4.24 shows that all the mode shapes of structures obtained at Level 9 and Level 10 have a double S curvature shape except for the structure with SKK dampers at Level 9. The structure with SKK dampers poses a straight mode shape with a difference in the ground and rooftop displacement that is less than 0.2 mm, indicating the inter-storey drift of the structure is very little. The relative translational displacement between two consecutive floors of the structure is minimal, which means the lateral forces due to earthquakes are distributed efficiently between its different floors, preventing excessive deformation and structural damage.

The structures with dampers show notable improvements in reducing the rooftop displacement at Level 10, indicating that the structure's vibration is less intense compared to the bare frame structure. Thus, the structure is more stable with the presence of a damping system since the braced dampers are

subjected to tension and compression forces rapidly and help in absorbing the seismic energy, reducing the dynamic response of the structure during an earthquake. Since the overall amplitude of lateral movement of the structure is found to be less than 2 mm, the structures are vibrated intensely instead of having significant lateral movement due to the high shaking frequency.

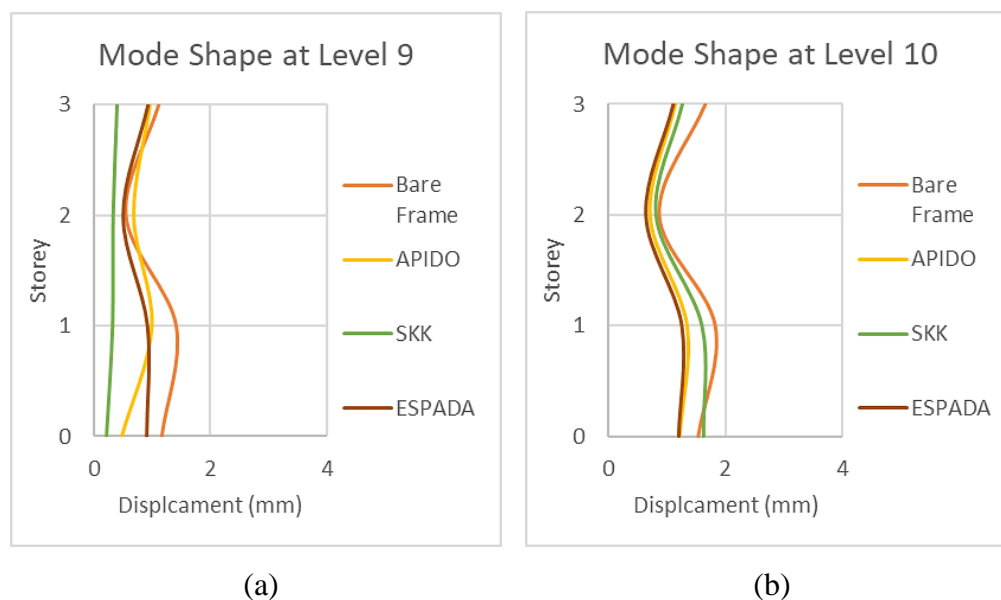


Figure 4.24: Mode Shape for Structures at (a) Level 9; (b) Level 10.

Table 4.6 shows the reduction percentage in rooftop displacement of each damper at all levels in the shaking table test. The results show general improvements in the reduction of rooftop displacement of the structure throughout most of the earthquake simulation. Level 5 represents the worst-case scenario of the experiment where all the dampers fail to reduce the dynamic response of the building. Level 5 is the intermediate level where the structure changes its behaviour from massive lateral movement to intense vibration when subjected to simulated pseudo dynamic load. Starting from Level 6, the rooftop displacements of the structure are smaller than 4 mm which is an insignificant lateral movement corresponding to the height of the structure, which is 1500 mm. Based on the results, the structure is observed to move horizontally when the shaking frequency is relatively low. On the other hand, the structure starts to vibrate in smaller amplitude when the shaking gets intense.

Table 4.6: Rooftop Displacement and Reduction Percentage of Each Damper at All Levels.

Level	Intensity		Rooftop displacement (mm)				Reduction percentage (%)		
	Displacement	Aggressiveness	Bare frame	APIDO	SKK	ESPADA	APIDO	SKK	ESPADA
1	Large	Very low	12.27	13.82	12.73	12.12	-12.61	-13.72	-11.21
2	Large	Low	15.16	14.86	13.97	14.45	-11.98	-11.83	-11.69
3	Moderate	Low	17.53	9.57	12.61	16.25	-45.43	-23.08	-7.32
4	Moderate	Low	18.26	11.88	14.85	16.86	-34.91	-18.66	-7.68
5	Moderate	Aggressive	7.10	10.01	8.15	7.28	-41.05	-14.81	-2.60
6	Short	Aggressive	3.71	3.36	3.05	3.16	-9.46	-17.91	-14.85
7	Short	Aggressive	3.58	3.09	2.18	2.83	-13.58	-39.11	-20.78
8	Short	Aggressive	3.45	3.82	3.15	3.43	-10.49	-8.91	-0.79
9	Short	Very high	1.10	0.97	0.40	0.92	-12.47	-63.44	-16.27
10	Short	Very high	1.66	1.14	1.27	1.10	-31.16	-23.71	-33.70

The outcome of the research shows that the SKK damper has the highest reduction percentage in rooftop displacement, up to 63.44% at Level 9. APIDO damper has the second greatest improvement to the rooftop displacement of the structure of 45.43% reduction at Level 3. ESPADA damper has the best performance at Level 10, with a reduction percentage in rooftop displacement of 33.70%.

One notable observation from the data is that the APIDO damper has the highest effectiveness in dissipating seismic energy when the shaking is low aggressiveness with moderate displacement compared to other brands of viscous dampers. SKK damper is found to enhance the seismic behaviour the best when the simulated earthquake motion is in high frequency and short distance. ESPADA damper performs moderately in most conditions regardless of the shaking intensities.

4.7 Prototype Displacement Response Prediction

This research selected the high school building as the prototype for the downscaled 1 bay 3-storey reinforced concrete building. The similitude relation between the full-scale prototype and scaled model was established by applying Similitude Theory and Buckingham's Pi Theorem when acquiring the model design and specifications. Hence, the results obtained from the shaking table test conducted on the downscaled model can be used to predict the dynamic

response of the full-scale prototype in this study. The value of the prototype's lateral movement and inter-storey drift can be determined by using experimental data since both systems are similar.

According to the Similitude Theory, only the dimensional scale factor, $S = 8$ is required in determining linear dimension in the system. Hence, the data obtained from the downscaled model is multiplied by the dimensional scale factor to get the corresponding values for the full-scale system. The actual full-scale deflection and the structural behaviour of the prototype during the earthquake with varying intensities can be investigated and studied in this way. Table 4.7 and Table 4.8 show the predicted value of the inter-storey drift for the full-scale prototype at each level of shaking using the results obtained from the downscaled model with and without dampers. The yellow highlighted value represents the highest inter-storey drift for each structure.

Table 4.7: Prototype Inter-Storey Drift Prediction for Bare Frame Structure and Structure with APIDO Dampers at All Levels.

Level	Bare frame structure			Structure with APIDO dampers		
	GF - 1F	1F - 2F	2F - 3F	GF - 1F	1F - 2F	2F - 3F
1	5.16	5.61	- 2.87	2.61	10.54	1.73
2	11.57	16.61	- 1.03	4.31	13.55	5.62
3	37.54	29.66	9.77	17.75	- 5.46	13.70
4	41.29	30.19	6.40	17.57	8.42	4.71
5	-10.11	26.99	9.07	17.98	18.14	16.78
6	- 3.05	7.48	5.86	- 4.24	7.51	6.88
7	- 0.45	6.37	2.50	- 3.04	5.79	7.31
8	0.08	2.89	3.75	0.53	1.65	8.80
9	1.98	- 6.87	4.46	4.11	- 2.49	2.22
10	2.34	- 7.71	6.35	1.03	- 5.20	3.54

Table 4.8: Prototype Inter-Storey Drift Prediction for Structure with SKK and ESPADA Dampers at All Levels.

Level	Structure with SKK dampers			Structure with ESPADA dampers		
	GF - 1F	1F - 2F	2F - 3F	GF - 1F	1F - 2F	2F - 3F
1	3.68	7.79	- 0.55	3.68	8.46	- 2.04
2	11.44	8.17	1.47	11.05	13.03	- 3.26
3	28.35	20.53	2.56	36.29	29.51	4.20
4	26.41	22.01	5.58	35.60	27.24	4.52
5	7.75	24.77	7.16	- 1.07	25.51	7.99
6	- 4.12	8.66	3.88	- 5.59	9.70	4.35
7	- 3.92	5.75	- 0.16	- 1.24	3.97	3.77
8	- 0.81	3.90	4.33	0.67	1.39	6.61
9	0.91	0.10	0.59	0.11	- 3.35	3.43
10	- 0.22	- 6.30	3.61	0.41	- 4.86	3.72

4.8 Summary

In summary, the inverted V diagonal braced-damper system is able to reduce the displacement response of the structure to earthquake ground motion. The data analysis reveals that there is a reduction in the rooftop displacement of the structure with dampers up to approximately 64% from the bare frame structure. During an earthquake, the viscous dampers absorb the seismic energy through a combination of fluid flow and mechanical friction when subjected to axial compression and tension forces. The inverted V shape of the braces increases the stiffness and strength of the structure, enhancing its ability to resist lateral forces and restrain structure sway. Hence, the damping system is beneficial in seismic design to enhance structural performance during an earthquake event.

CHAPTER 5

CONCLUSIONS AND RECOMMENDATIONS

5.1 Conclusions

In a nutshell, the shaking table tests were conducted to study the seismic behaviour of the structure with and without dampers in terms of inter-storey drift and mode shape of the structure. A few conclusions can be drawn corresponding to the objectives of this research.

The first objective is to construct a downscaled reinforced concrete 1 bay 3-storey model. The high school building prototype was selected to acquire model design and specifications in this study. A 1:8 downscaled model was constructed by using grade C30 concrete, and 3 mm steel bars were used for the reinforcement. Compressive strength tests were conducted for each concrete mix batch to ensure the constructed structure met the design requirements. Superplasticizers were utilised in this study to reduce the water-to-cement ratio while maintaining the quality and workability of the concrete. The constructed reinforced concrete building was successfully sustained throughout the study without collapsing.

The next objective is to access the building's inter-storey drift with and without dampers. 25 mm and 50 mm LVDTs were installed on the shaking table and each floor of the structure to measure and record the lateral movement of the structure. Three brands of viscous dampers were used in this study which are APIDO, SKK and ESPADA dampers. This research proves that viscous damping systems can improve the seismic resistance of the structure since there are general improvements in the displacement response of the structure. When the viscous damping systems were installed, the downscaled model's inter-storey drift was smaller. The results obtained from the shaking table test show that APIDO, SKK and ESPADA dampers can reduce a maximum of 45%, 63% and 34% of rooftop displacement, respectively.

The last research objective is to compare the mode shape of the building with and without dampers. The mode shape of the bare frame structure and structure with dampers were prepared to study the structural behaviour

under earthquake simulation with different intensities. When the shaking frequency and unit displacement of the shaking change, the structure behaviour is different, showing different mode shapes. Double S curvature and double curvature mode shape are preferable in seismic design since they provide greater stability and resistance to lateral load. The seismic forces are distributed more evenly and uniformly throughout the structure compared to a single curvature mode shape, reducing the load concentration on one floor, which is undesirable in structural design. Double curvature mode shapes allow the structure to absorb more energy and deform more before failure, preventing a sudden building collapse, which may cause catastrophic consequences.

5.2 Recommendations for Future Work

Although installing a damping system helps in improving the seismic performance of the building, the system is found ineffective when the building behaviour changes from significant lateral movement to intense vibration. Hence, there is room for improving the viscous damping system to enhance its performance under this condition. The effectiveness of the viscous dampers may be influenced by the dampers system's configurations in a building.

Besides, the seismic behaviour was investigated by using a 1 bay 3-storey structure in this study. Different types of structures can be further studied in the laboratory to assess their seismic performance under different shaking intensities. For example, low and high-rise buildings may result in different structural behaviour and seismic resistance during an earthquake. It is important to study the seismic performance of a high-rise building since it is more susceptible to failure and requires a seismic design which is not commonly considered in Malaysia. Other than that, 1 bay frame structures are not common for modern buildings, thus it is crucial to study the seismic performance of other types of structures.

REFERENCES

- Aly, A. M. and Abburu, S., 2015. On the Design of High-Rise Buildings for Multihazard: Fundamental Differences between Wind and Earthquake Demand. *Shock and Vibration*, Volume 2015, pp. 1-22.
- ASTM Standard 33, 2018. *Standard Specification for Concrete Aggregates*. West Conshohocken: ASTM International.
- ASTM Standard C150, 2012. *Standard Specification for Portland Cement*. West Conshohocken: ASTM International.
- Bayrak, B., Kaplan, G., Akarsu, O. and Aydin, A. C., 2022. The Plastic Hinge Length Prediction of RC Members by Using ANN.
- Bhat, E. A. and Azam, M. F., 2020. Effect of Shear Wall Area on Seismic Behaviour of Multistoried Building with Soft Storey At Ground Floor. *International Journal of Engineering Research and Technology (IJERT)*, 9(7), pp. 22-37.
- Boron, P., Chelmecki, J., Dulinska, J.M., Jurkowska, N., Ratajewicz, B., Stecz, P. and Tatara, T., 2023. On the Possibility of Using 3D Printed Polymer Models for Modal Tests on Shaking Tables: Linking Material Properties Investigations, Field Experiments, Shaking Table Tests, and FEM Modeling. *Materials*, 16(4), p. 1471.
- Casaburo, A., Petrone, G., Franco, F. and De Rosa, S., 2019. A Review of Similitude Methods for Structural Engineering. *Applied Mechanics Reviews*, 71(3).
- Constantinou, M. C. and Symans, M. D., 1992. Mechanical Properties of Fluid Dampers. In: *Experimental and Analytical Investigation of Seismic Response of Structures with Supplemental Fluid Viscous Dampers*. Buffalo, NY: National Center for Earthquake Engineering Research, pp. 1-22.
- Constantinou, M. C., Tsopeles, P., Hammel, W. and Sigaher, A. N., 2001. Toggle-Brace-Damper Seismic Energy Dissipation Systems. *Journal of Structural Engineering*, 127(2), pp. 105-112.
- Earle, S., 2015. *Physical Geology*. Victoria, B.C. : BCcampus.

Elhassan, K., 2018. *History's Deadliest Earthquake in Shaanxi 1556, Leveled Mountains and Reversed Rivers*. [Online] Available at: <https://historycollection.com/historys-deadliest-earthquake-in-shaanxi-1556-leveled-mountains-and-reversed-rivers/2/> [Accessed 5 August 2022].

Elias, S. and Matsagar, V., 2015. Optimum Tuned Mass Damper for Wind and Earthquake Response Control of High-Rise Building. *Advances in Structural Engineering*, pp. 1475-1487.

EN 1998-1, 2004. *Eurocode 8: Design of structures for earthquake resistance – Part 1: General rules, seismic actions and rules for buildings*. s.l.:British Standards Institution.

Gutierrez Soto, M. and Adeli, H., 2013. Tuned Mass Dampers. *Archives of Computational Methods in Engineering*, Volume 20, pp. 419-431.

Hamit, K. and Azeloğlu, O., 2020. Design of scaled down model of a tower crane mast by using similitude theory. *Engineering structures*, Volume 220, p. 110985.

Irfani, M. M. A. and Vimala, A., 2019. Collapse Mechanism of Strong Column Weak Beam Buildings of Varying Heights. *International Journal of Engineering and Advanced Technology*, 9(1), pp. 4144-4148.

Kashima, T. and Hirade, T., 2017. *Shaking Table Testing*. [Online] Available at: <https://iisee.kenken.go.jp/lna/?mod=viewandcid=E1-060-2009> [Accessed 3 September 2022].

Koçoğlu, E., Demir, F. B., Öteleş, Ü. U. and Özeren, E., 2023. Post-Earthquake Trauma Levels of University Students Evaluation: Example of 6 February Kahramanmaraş Earthquake. *Higher Education Studies*, 13(2).

Lee, D. and Taylor, D. P., 2001. Viscous damper development and future trends. *The Structural Design of Tall Buildings*, 10(5), pp. 311-320.

Lee, J.Y., Chow, T.L., Chong, F.L., Cheah, Y.B. and Lau, T.L., 2022. Development of Seismic Microzonation Maps for Low to Moderate Seismicity Regions Using Microtremor Observation Data.

Lu, X., Fu, G., Shi, W. and Li, W., 2008. Shake table model testing and its application. *The Structural Design of Tall and Special Buildings*, 17(1), pp. 181-201.

Martineau, M. O., Lopez, A. F. and Vielma, J. C., 2020. Effect of Earthquake Ground Motion Duration on the Seismic Response of a Low-Rise RC Building. *Advances in Civil Engineering*, Volume 2020, pp. 1-12.

Marto, A., Tan, C. S., Kasim, F. and Mohd Yunus, N. Z., 2013. Seismic impact in Peninsular Malaysia. *The 5th International Geotechnical Symposium-Incheon*, pp. 238-242.

Murty, C. V. R., Goswami, R., Vijayanarayanan, A. R. and Mehta, V., 2012. *Earthquake Behaviour of Buildings*. Gandhinagar: Gujarat State Disaster Management Authority.

Nabilah, A. B. and Balendra, T., 2012. Seismic Hazard Analysis for Kuala Lumpur, Malaysia. *Journal of Earthquake Engineering*, 16(7), pp. 1076-1094.

Nama, M. Y., Salem, L. A. and Mosa, A. M., 2023. Simplified Analytical Model and Shaking Table Test Validation for Seismic Analysis of Piled Raft Foundation. *International Journal of Science and Business*, 1(102-114), p. 22.

National Geographic Society, 2022. *Plate Tectonics and the Ring of Fire*. [Online] Available at: <https://education.nationalgeographic.org/resource/plate-tectonics-ring-fire> [Accessed 13 August 2022].

Nazaruddin, D. A. and Duerrast, H., 2021. Intraplate earthquake occurrence and distribution in Peninsular Malaysia over the past 100 years. *SN Applied Sciences*, 3(7), p. 693.

Ondrej, 2019. *Modal analysis*. [Online] Available at: <https://wiki.csiamerica.com/display/kb/Modal+analysis> [Accessed 6 September 2022].

Past é n, C., Campos, F., Ochoa - Cornejo, F., Ruiz, S., Valdebenito, G., Alvarado, D., Leyton, F. and Moffat, R., 2021. The Role of Site Conditions on the Structural Damage in the City of Valdivia during the 22 May 1960 Mw 9.5 Megathrust Chile Earthquake. *Seismological Research Letters*, 92(6), pp.3437-3451.

Pourzangbar, A., Vaezi, M., Mousavi, S. M. and Saber, A., 2020. Effects of Brace-viscous Damper System on the Dynamic Response of Steel Frames. *International Journal of Engineering*, 33(5), pp. 720-731.

Rajmani, A. and Guha, P., 2015. ANALYSIS OF WIND and EARTHQUAKE LOAD FOR DIFFERENT SHAPES OF HIGH RISE BUILDING. *International Journal of Civil Engineering and Technology (IJCIET)*, 6(2), pp. 38-45.

Serras, D., Kalapodis, N. A. and Muho, E. V., 2022. First Yield Inter-storey Drift Ratios of Composite (Steel/concrete) and Steel Frames for the Purposes of the Direct Displacement Based Design Method.

Severn, R. T., 2011. The development of shaking tables—a historical note. *Earthquake engineering and structural dynamics*, 40(2), pp. 195-213.

Tongkul, F., 2017. Active tectonics in Sabah – seismicity and active faults. *Bulletin of the Geological Society of Malaysia*, Volume 64, pp. 27-36.

Tongkul, F., 2021. An Overview of Earthquake Science in Malaysia. *ASM Science Journal*, Volume 14, pp. 1-12.

United States Geological Survey, 2022. *M 9.5 - 1960 Great Chilean Earthquake (Valdivia Earthquake)*. [Online] Available at: https://earthquake.usgs.gov/earthquakes/eventpage/official19600522191120_30/impact [Accessed 5 August 2022].

Wald, L., 2009. *The Science of Earthquakes*. [Online] Available at: <https://www.usgs.gov/programs/earthquake-hazards/science-earthquakes> [Accessed 10 August 2022].

Wang, T., Shao, J., Zhao, C., Liu, W. and Wang, Z., 2021. Shaking Table Test for Evaluating the Seismic Performance of Steel Frame Retrofitted by Buckling-Restrained Braces. *Shock and Vibration*, Volume 2021.

Yel, N.S., Arslan, M.H., Aksoylu, C., Erkan, İ.H., Arslan, H.D. and Işık, E., 2022. Investigation of the Earthquake Performance Adequacy of Low-Rise RC Structures Designed According to the Simplified Design Rules in TBEC-2019. *Buildings*, 12(10), p. 1722.

Yip, C. C. and Marsono, A. K., 2016. Structural seismic performance of reinforced concrete block system for two storeys safe house. *Jurnal Teknologi*, 78(2).

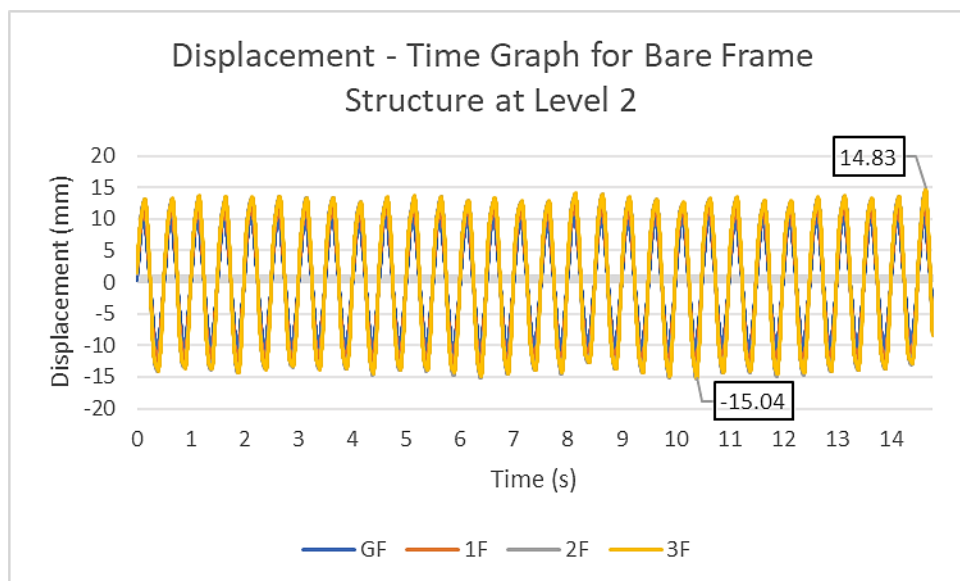
Yip, C. C., Marsono, A. K., Wong, J. Y. and Lee, S. C., 2017. Seismic performance of scaled IBS block column for static nonlinear monotonic pushover experimental analysis. *Jurnal Teknologi*, 80(1).

Yon, B., Sayin, E. and Onat, O., 2017. Earthquakes and Structural Damages. In: *Earthquakes - Tectonics, Hazard and Risk Mitigation*. Rijeka: InTech, pp. 319-339.

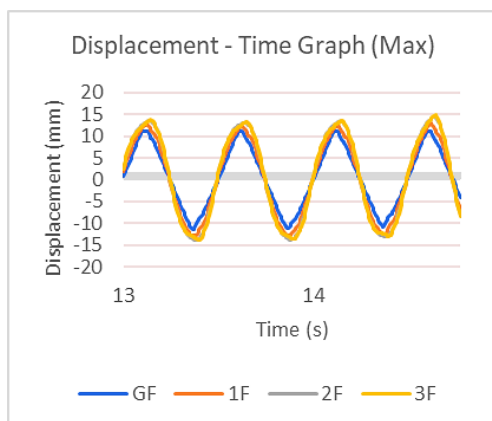
Zhang, Y., Xu, Y., Du, P., Li, W., Chen, L. and Tian, Q., 2020. The Volume Calculation Method of Rock Collapses and Loess Landslides Triggered by the 1556 AD Huaxian M 8 1/2 Earthquake in Shaanxi Province, China. *Earthquake Research in China*, 34(4).

APPENDICES

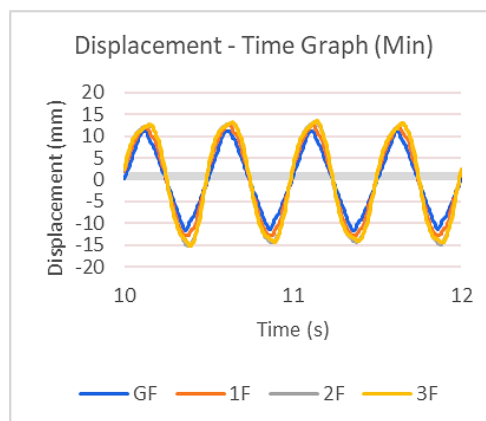
Appendix A: Graphs



(a)



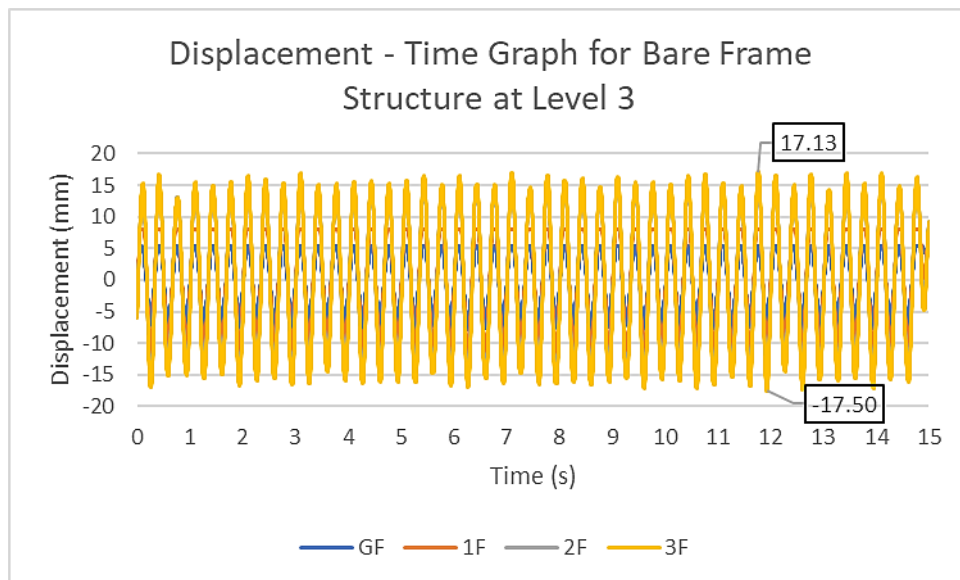
(b)



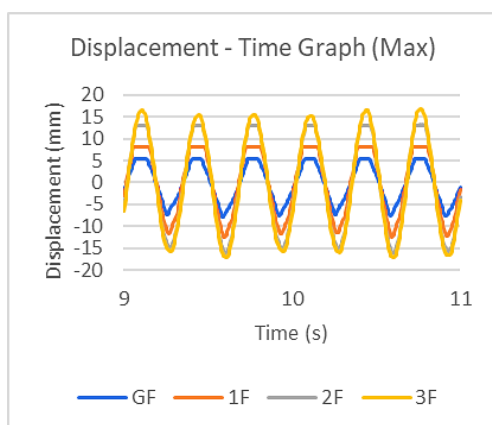
(c)

Graph A-1: Displacement – Time Graph for Bare Frame Structure at Level 2

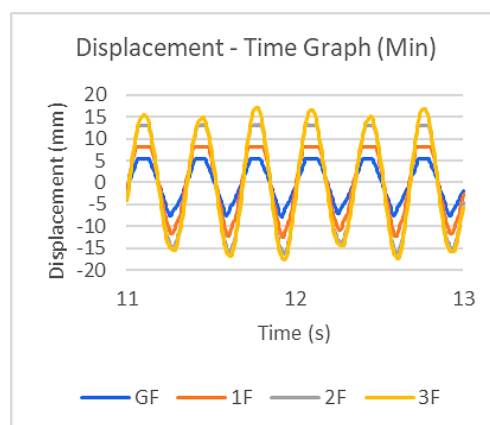
(a) Overall; (b) Maximum; (c) Minimum.



(a)

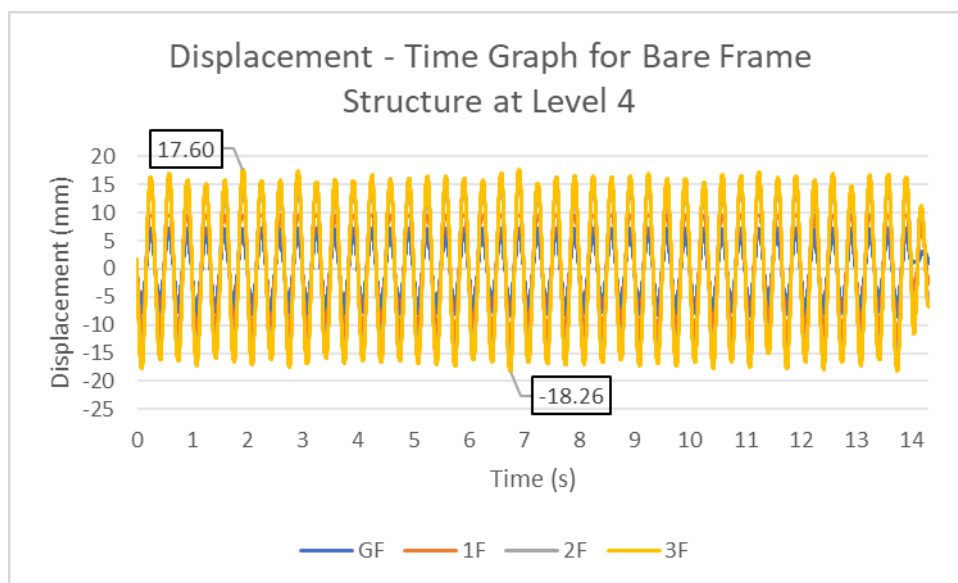


(b)

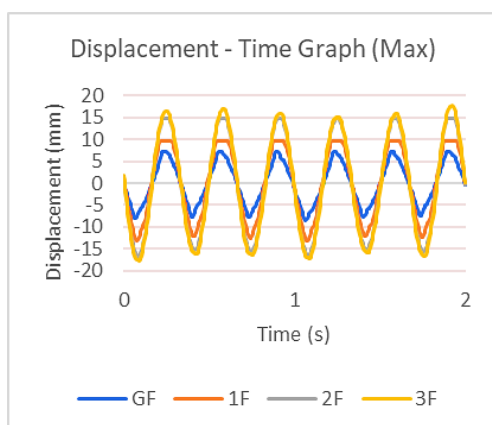


(c)

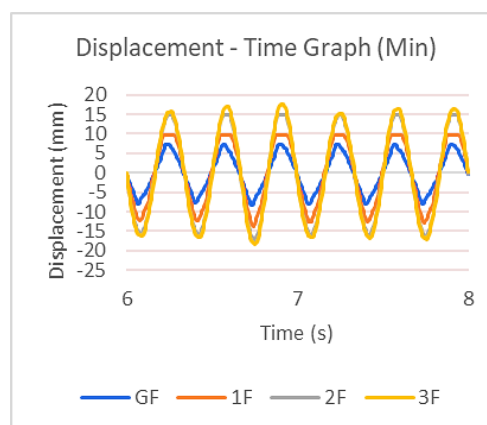
Graph A-2: Displacement – Time Graph for Bare Frame Structure at Level 3
 (a) Overall; (b) Maximum; (c) Minimum.



(a)

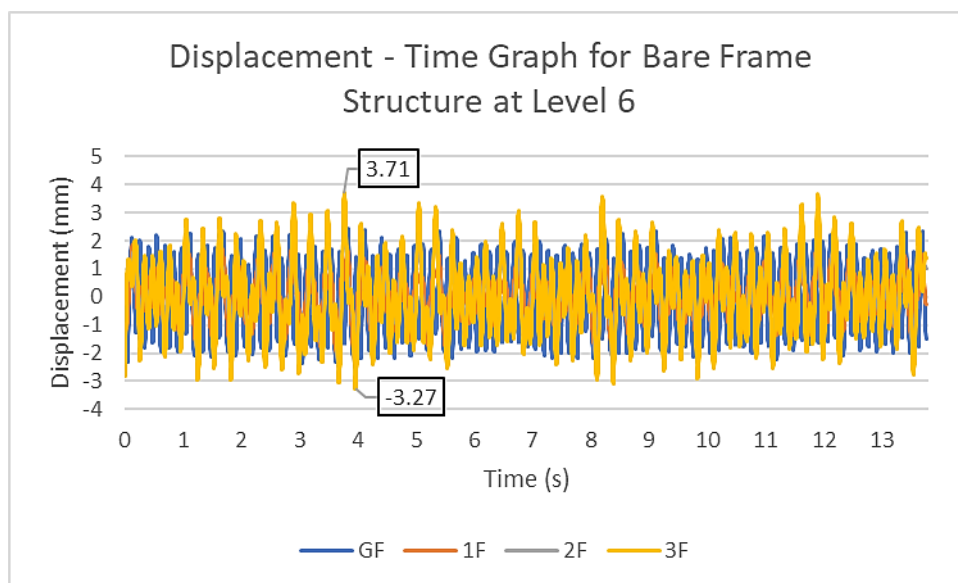


(b)

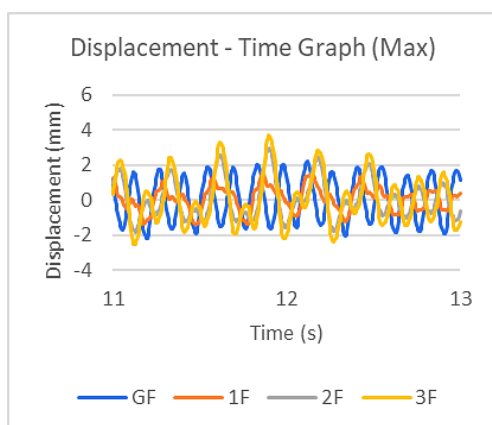


(c)

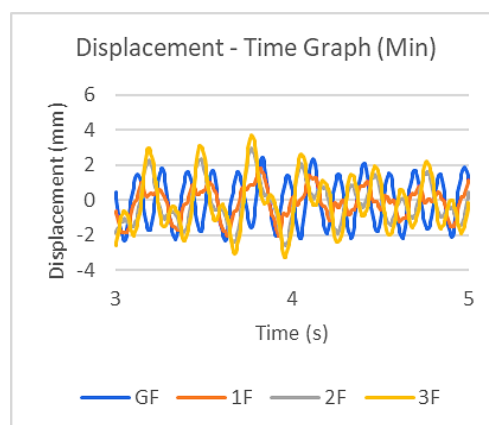
Graph A-3: Displacement – Time Graph for Bare Frame Structure at Level 4
 (a) Overall; (b) Maximum; (c) Minimum.



(a)

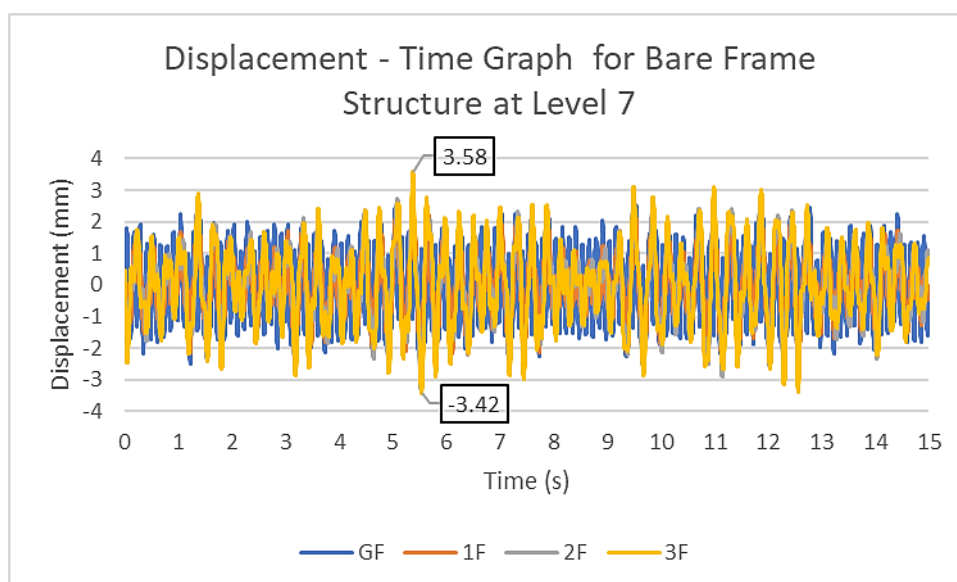


(b)

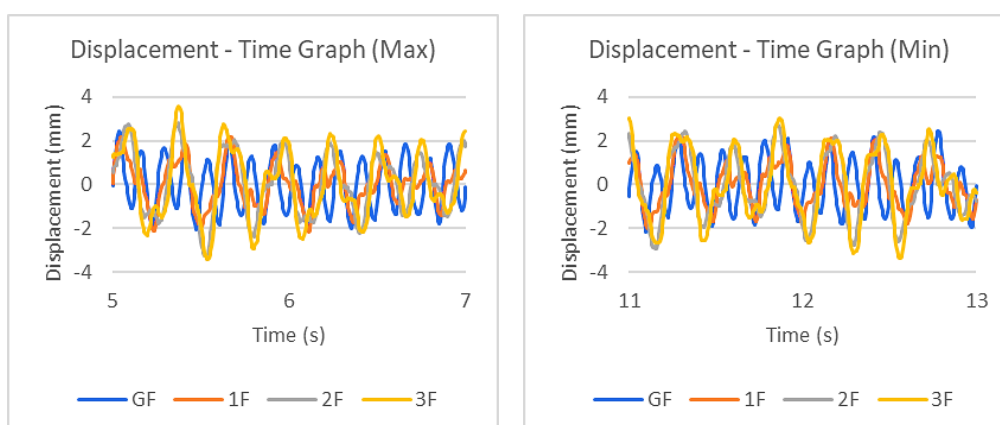


(c)

Graph A-4: Displacement – Time Graph for Bare Frame Structure at Level 6
 (a) Overall; (b) Maximum; (c) Minimum.



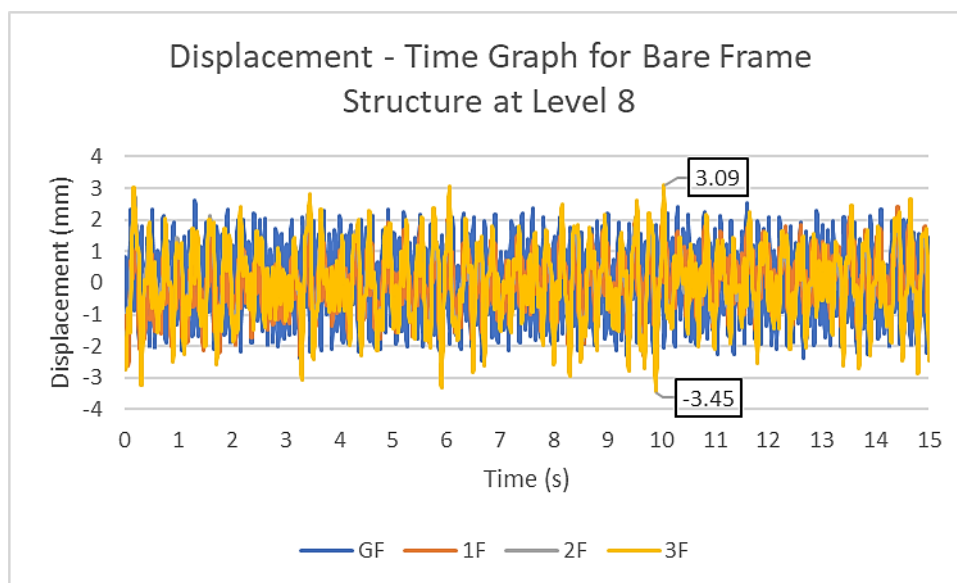
(a)



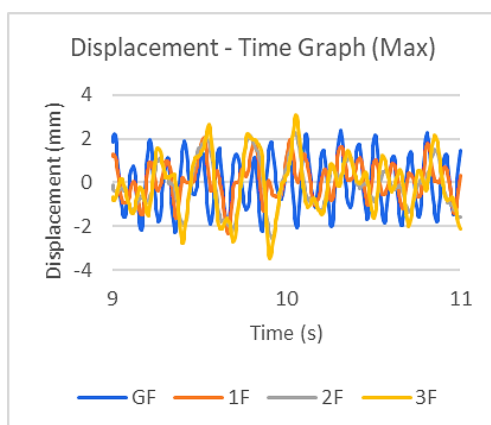
(b)

(c)

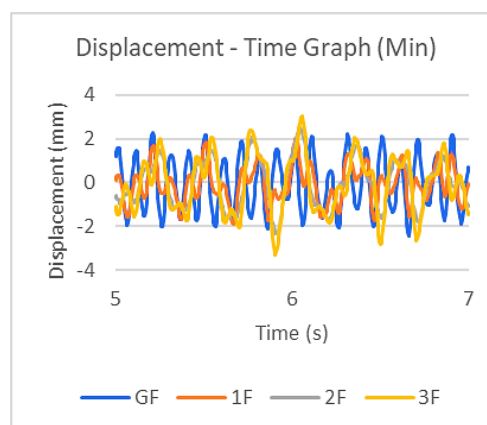
Graph A-5: Displacement – Time Graph for Bare Frame Structure at Level 7
 (a) Overall; (b) Maximum; (c) Minimum.



(a)

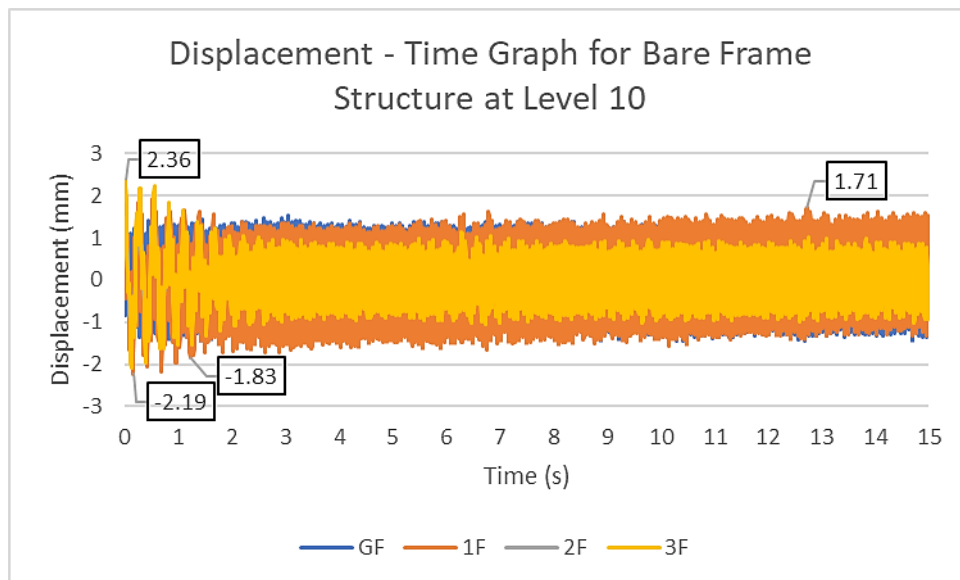


(b)

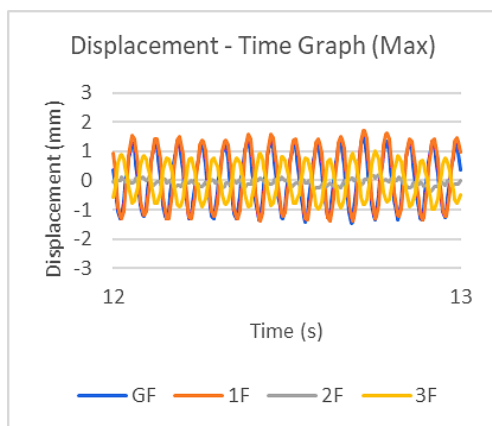


(c)

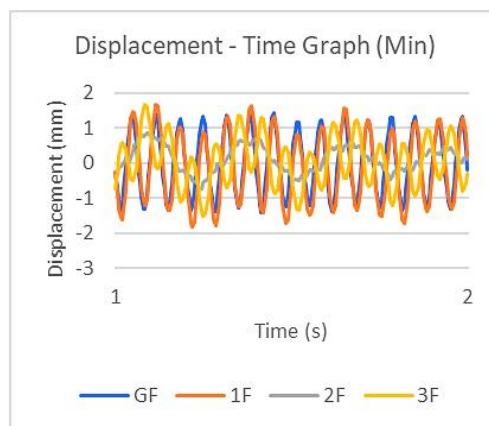
Graph A-6: Displacement – Time Graph for Bare Frame Structure at Level 8
 (a) Overall; (b) Maximum; (c) Minimum.



(a)

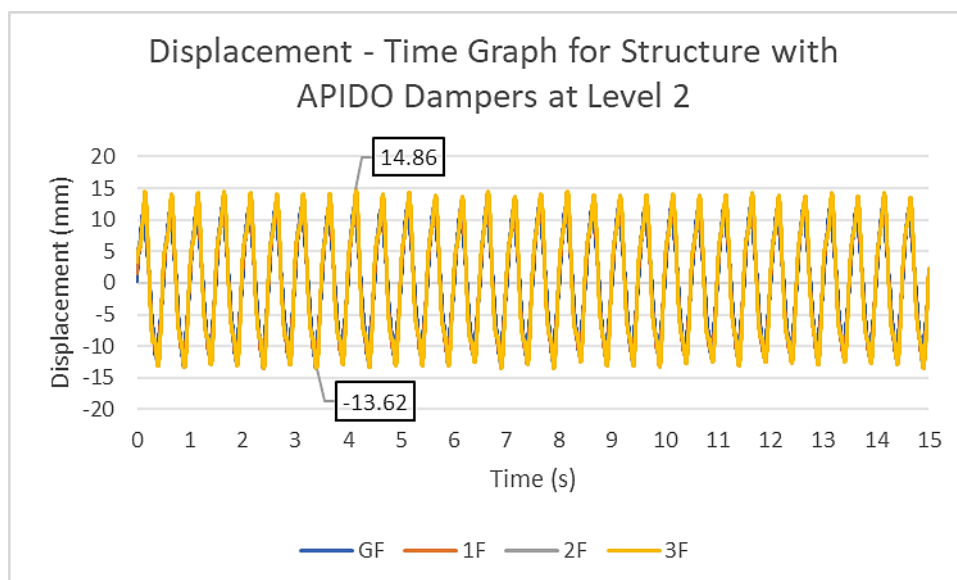


(b)

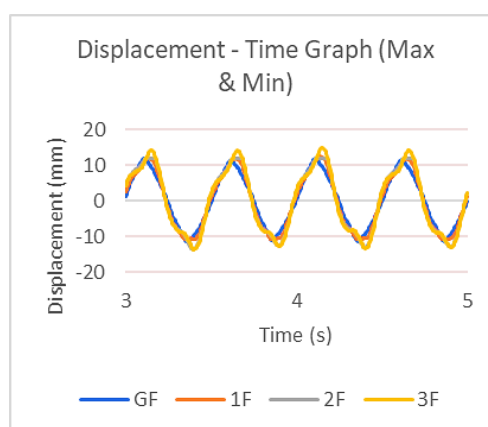


(c)

Graph A-7: Displacement – Time Graph for Bare Frame Structure at Level 10
 (a) Overall; (b) Maximum; (c) Minimum.

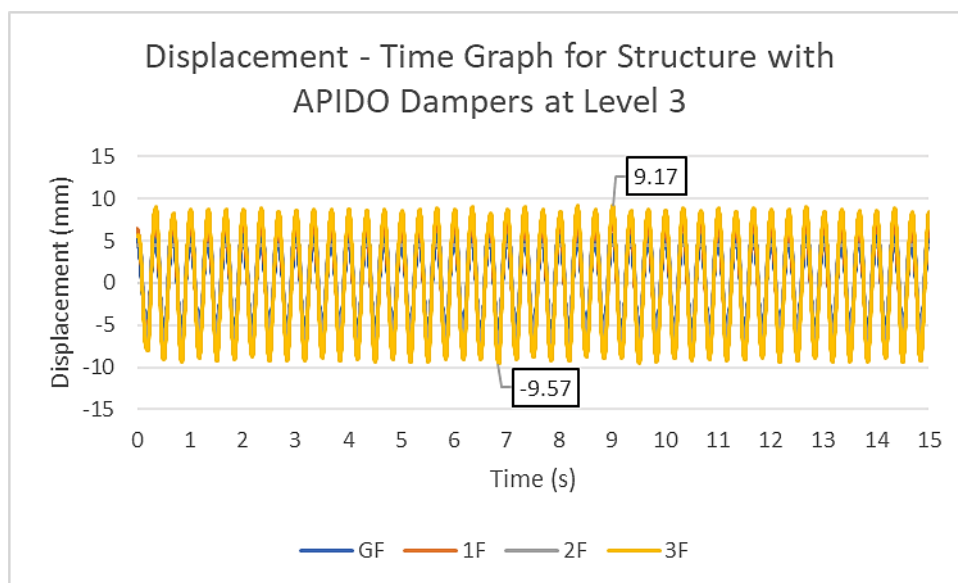


(a)

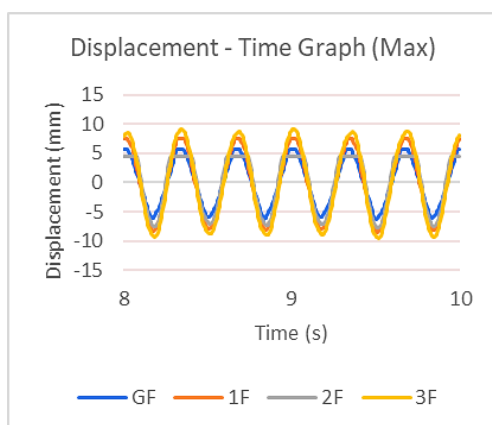


(b)

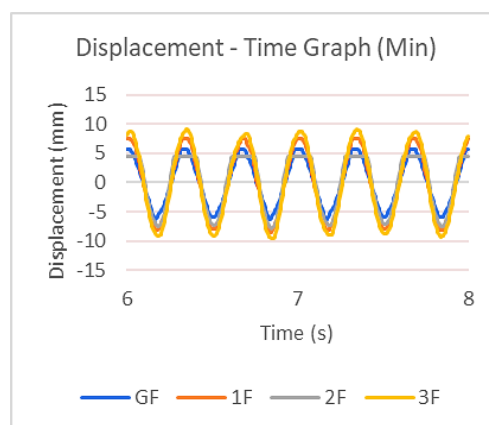
Graph A-8: Displacement – Time Graph for Structure with APIDO Dampers at Level 2 (a) Overall; (b) Maximum and Minimum.



(a)

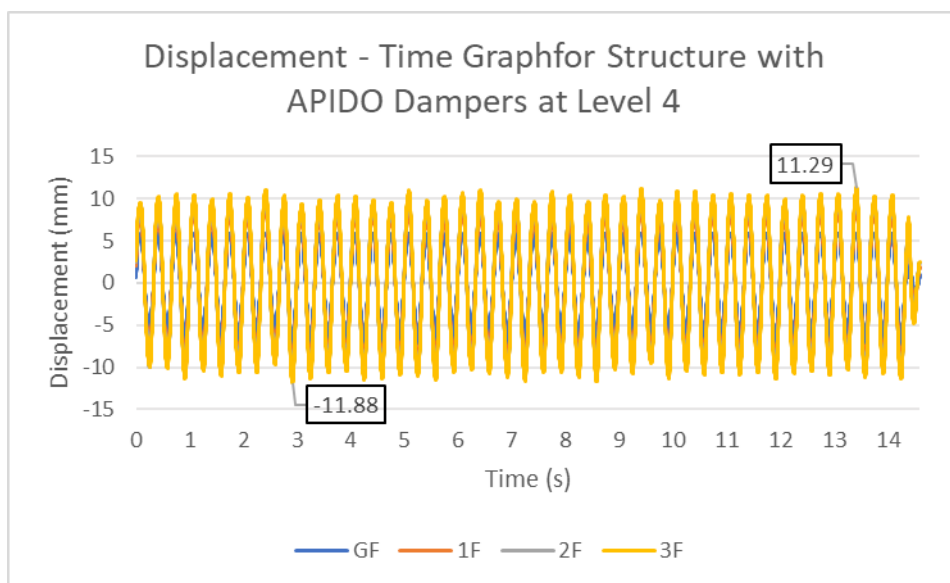


(b)

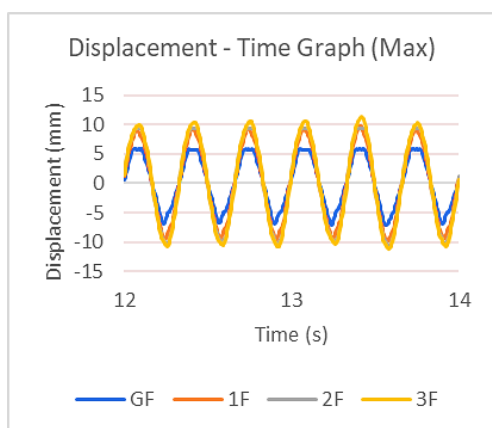


(c)

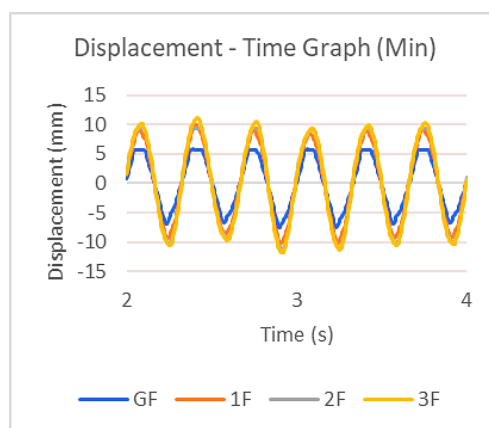
Graph A-9: Displacement – Time Graph for Structure with APIDO Dampers at Level 3 (a) Overall; (b) Maximum; (c) Minimum.



(a)

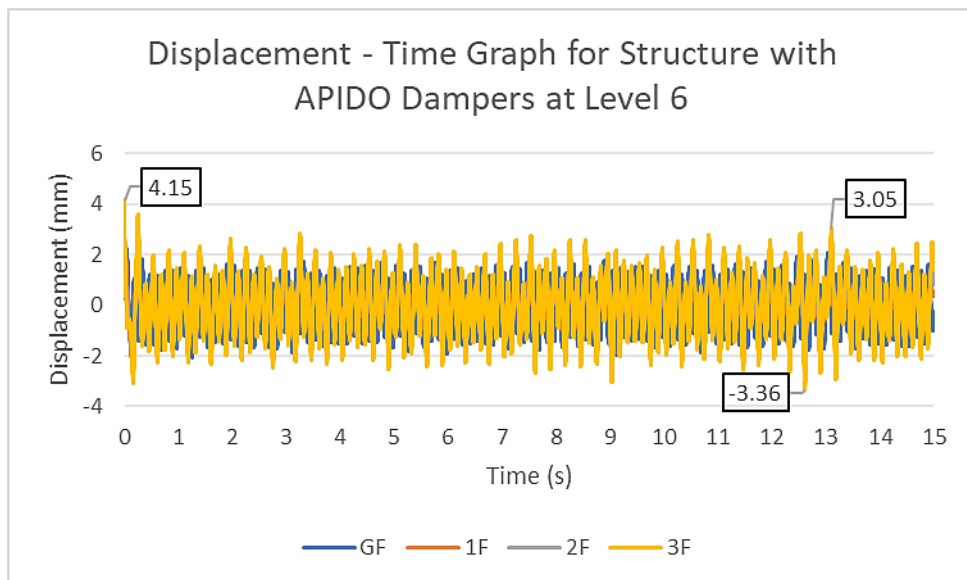


(b)

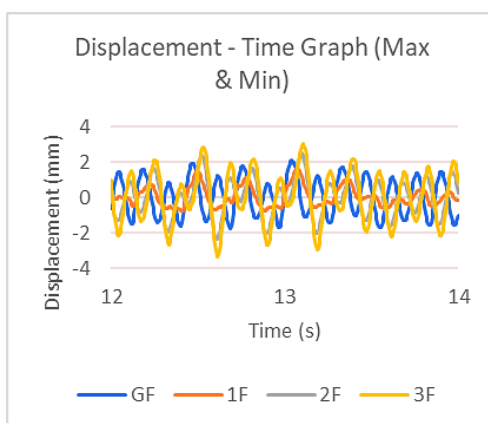


(c)

Graph A-10: Displacement – Time Graph for Structure with APIDO Dampers at Level 4 (a) Overall; (b) Maximum; (c) Minimum.

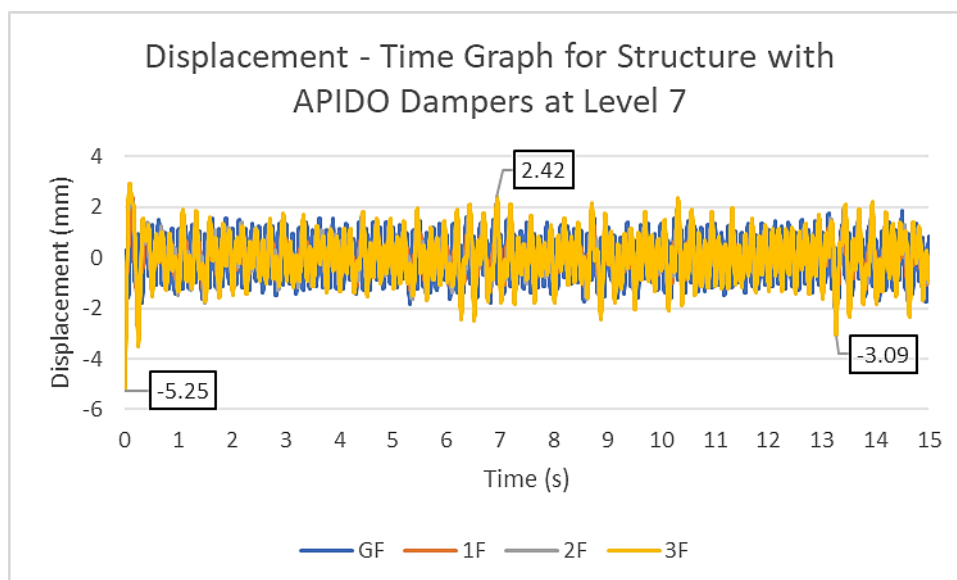


(a)

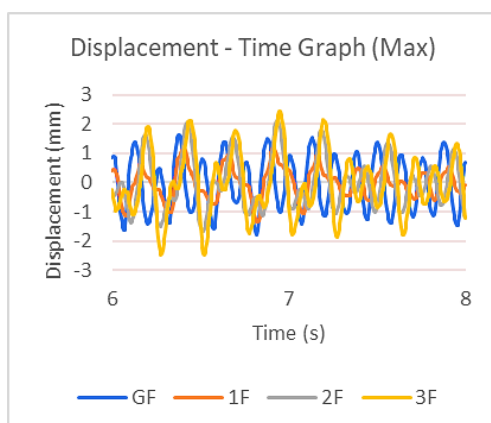


(b)

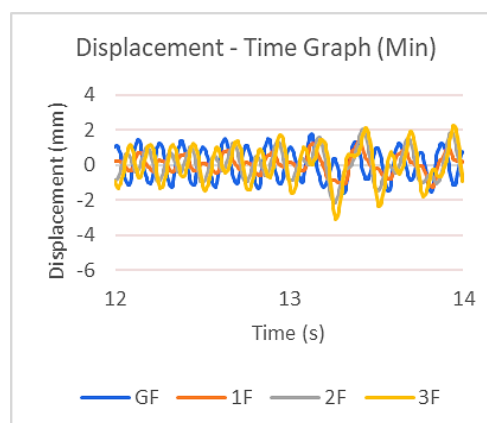
Graph A-11: Displacement – Time Graph for Structure with APIDO Dampers at Level 6 (a) Overall; (b) Maximum and Minimum.



(a)

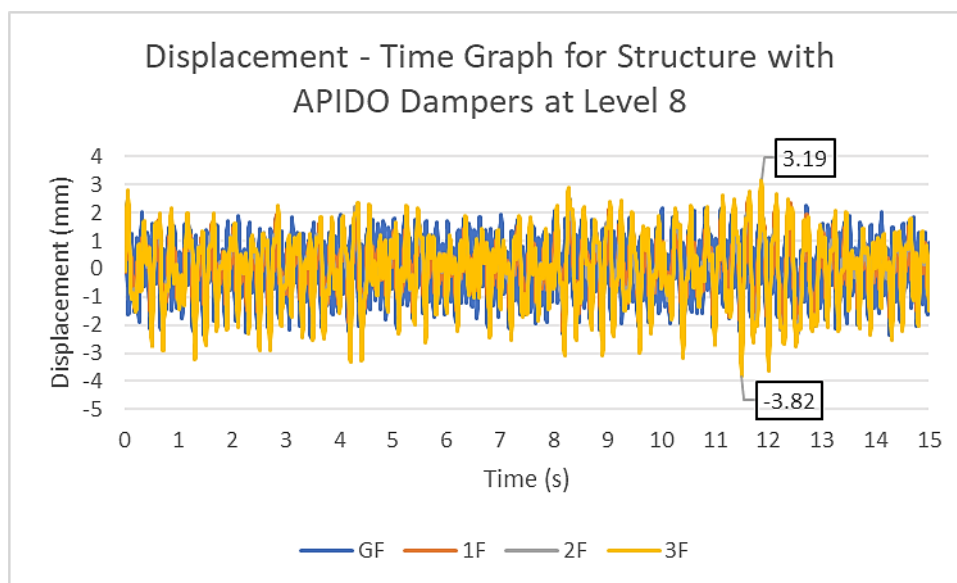


(b)

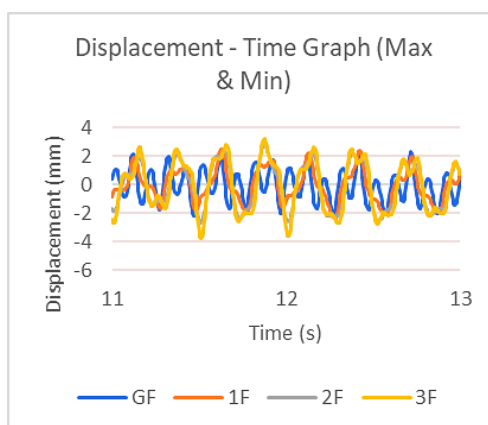


(c)

Graph A-12: Displacement – Time Graph for Structure with APIDO Dampers at Level 7 (a) Overall; (b) Maximum; (c) Minimum.

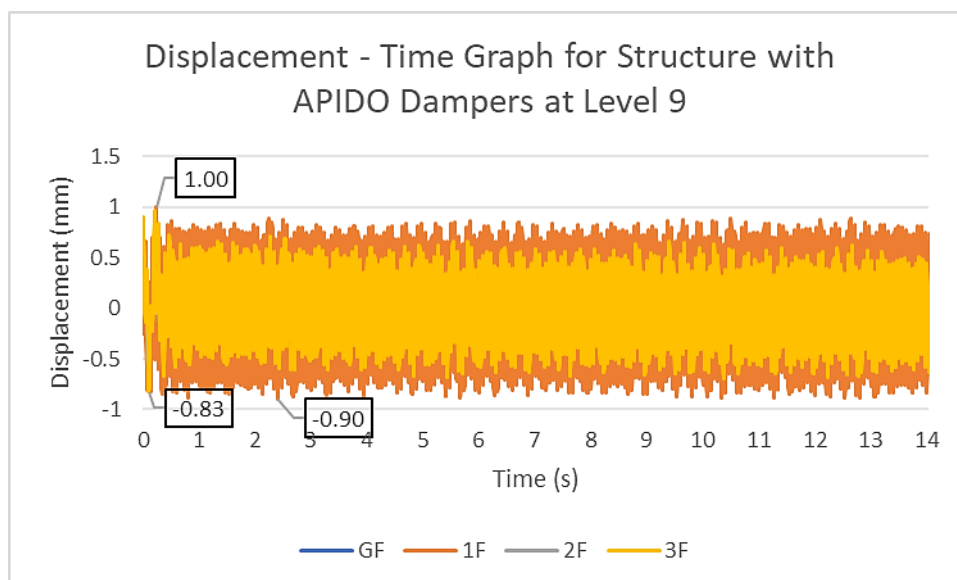


(a)

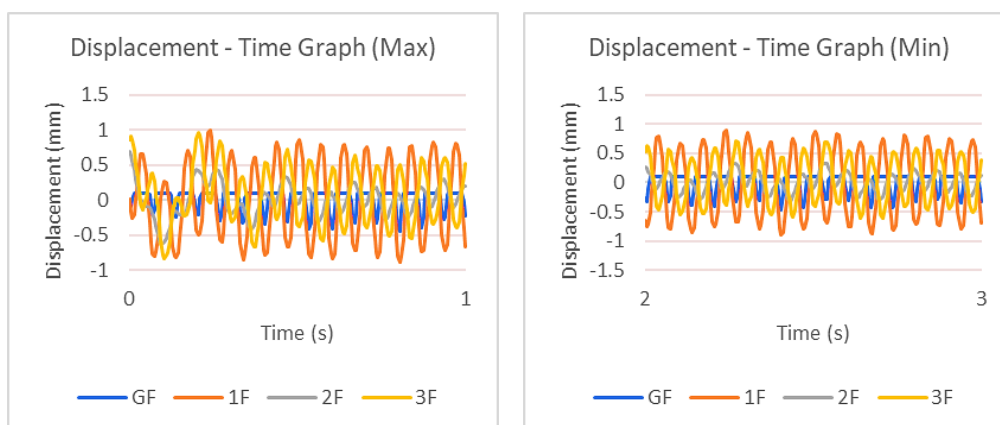


(b)

Graph A-13: Displacement – Time Graph for Structure with APIDO Dampers at Level 8 (a) Overall; (b) Maximum and Minimum.



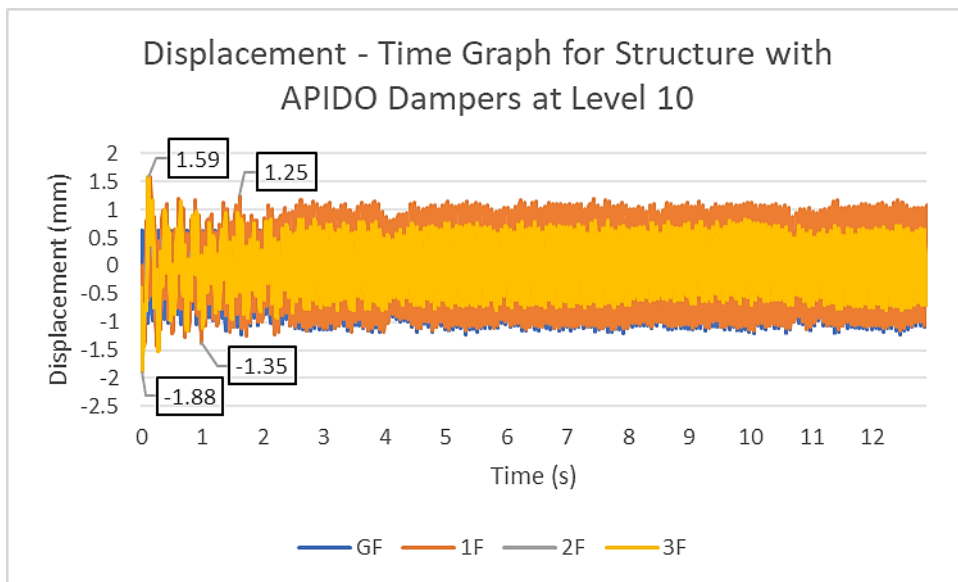
(a)



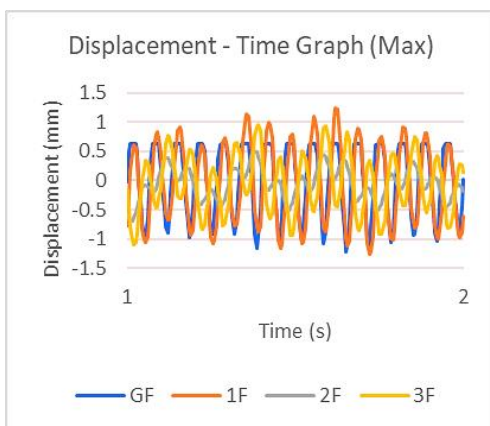
(b)

(c)

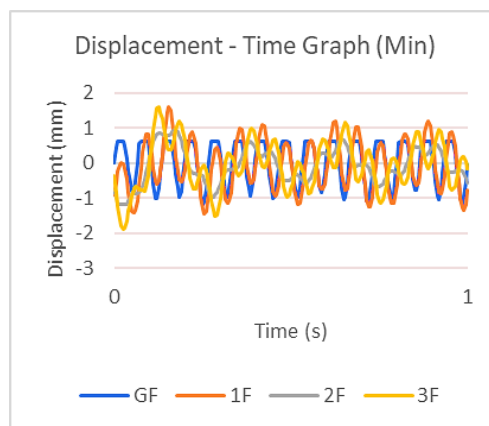
Graph A-14: Displacement – Time Graph for Structure with APIDO Dampers at Level 9 (a) Overall; (b) Maximum; (c) Minimum.



(a)

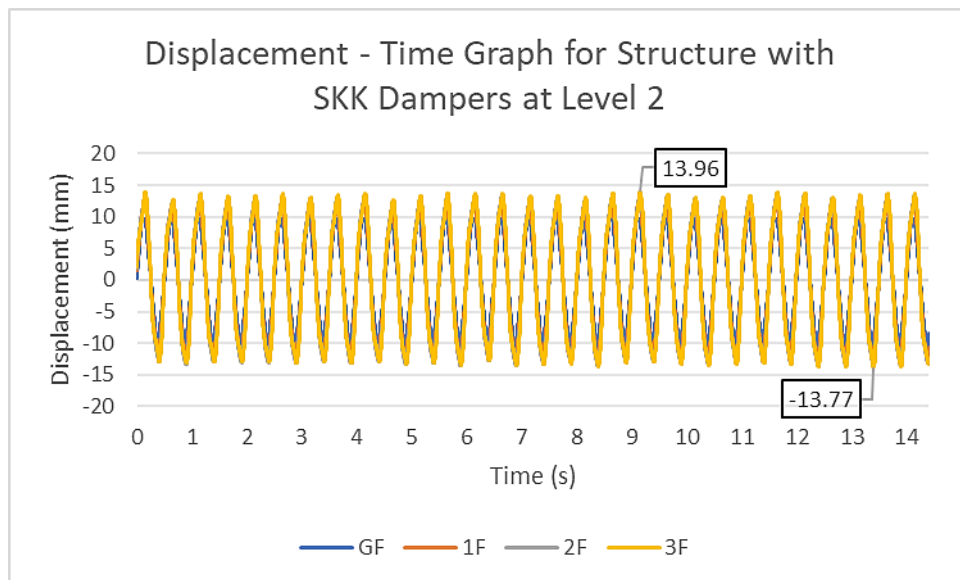


(b)

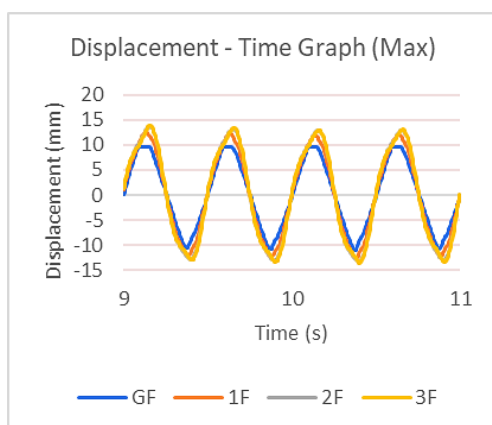


(c)

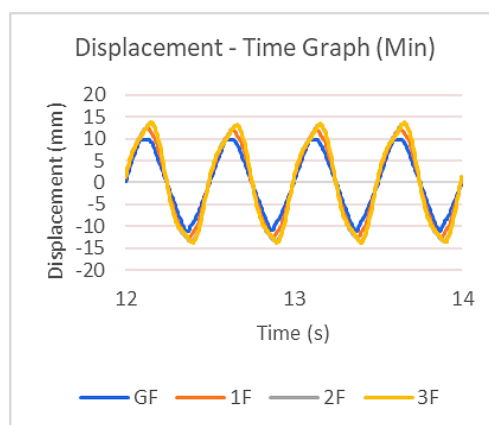
Graph A-15: Displacement – Time Graph for Structure with APIDO Dampers at Level 10 (a) Overall; (b) Maximum; (c) Minimum.



(a)

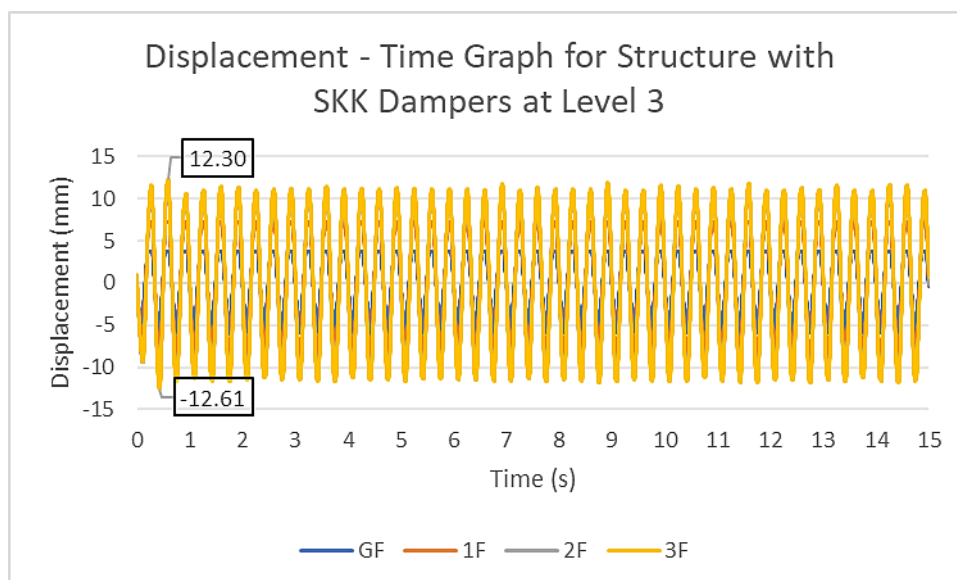


(b)

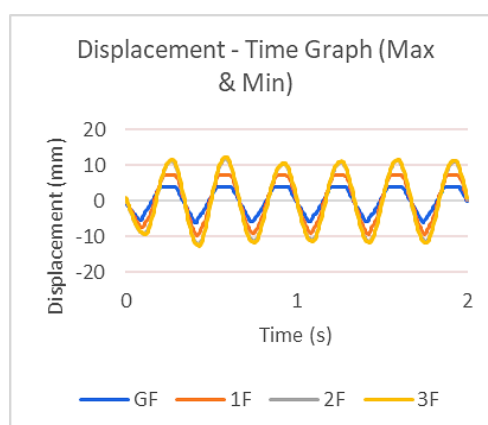


(c)

Graph A-16: Displacement – Time Graph for Structure with SKK Dampers at Level 2 (a) Overall; (b) Maximum; (c) Minimum.

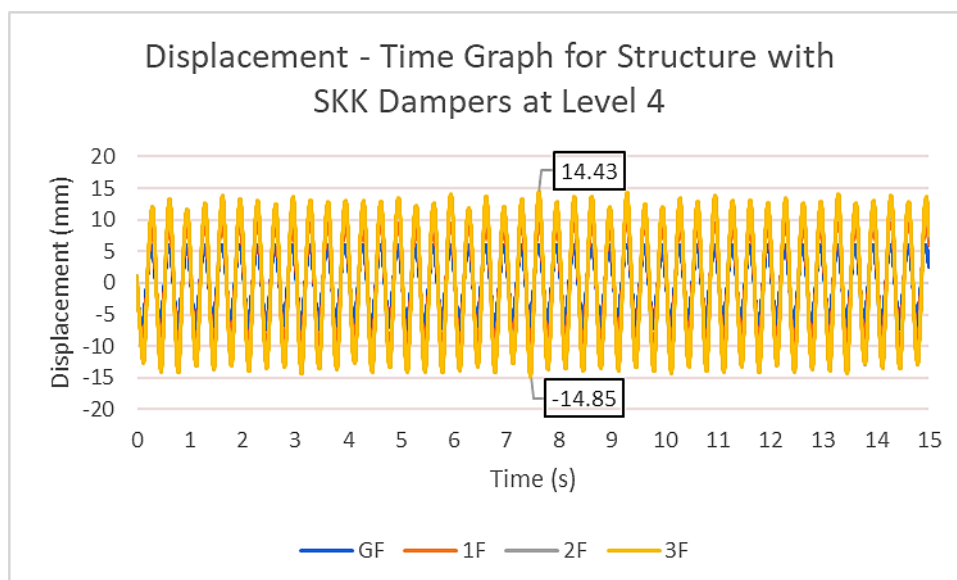


(a)

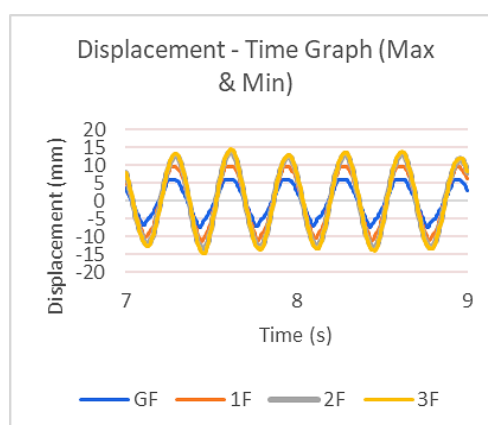


(b)

Graph A-17: Displacement – Time Graph for Structure with SKK Dampers at Level 3 (a) Overall; (b) Maximum and Minimum.

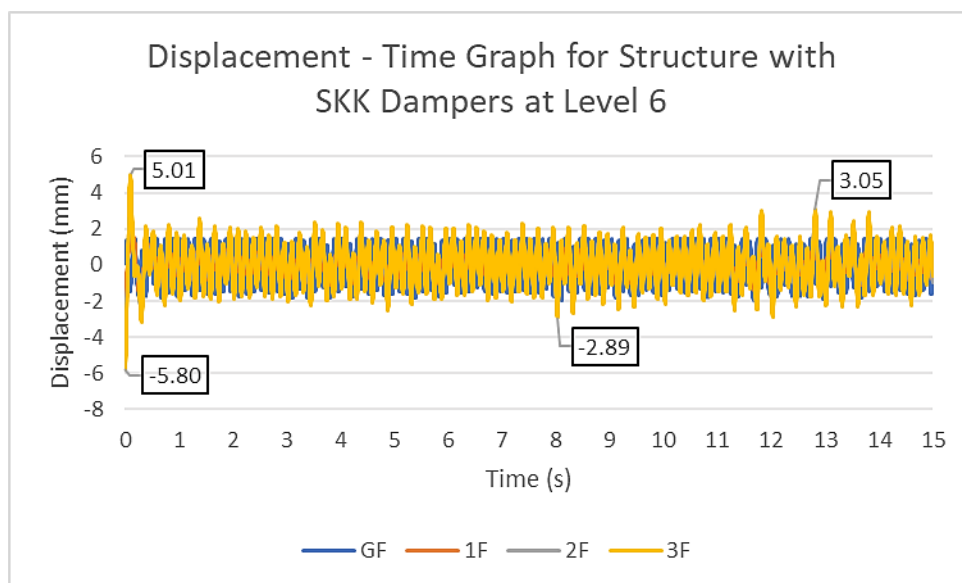


(a)

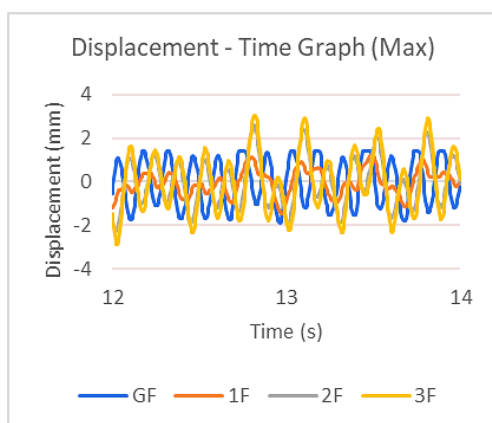


(b)

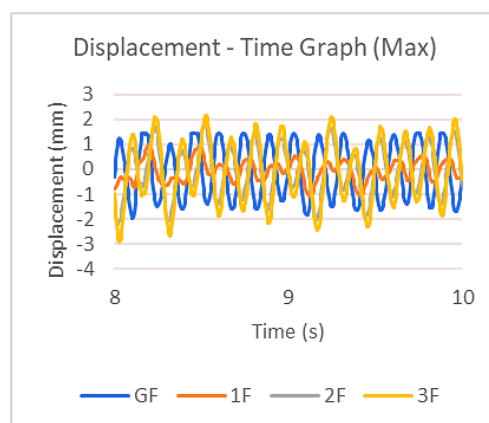
Graph A-18: Displacement – Time Graph for Structure with SKK Dampers at Level 4 (a) Overall; (b) Maximum and Minimum.



(a)

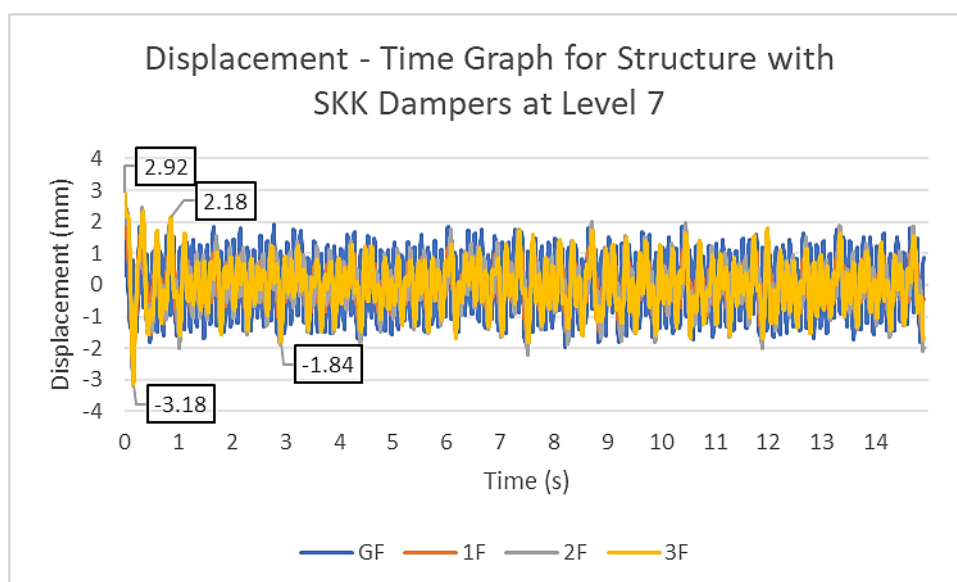


(b)

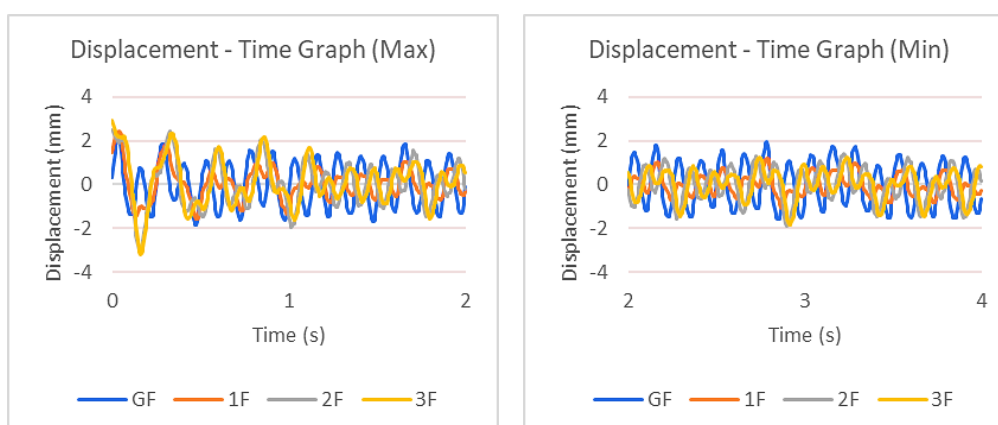


(c)

Graph A-19: Displacement – Time Graph for Structure with SKK Dampers at Level 6 (a) Overall; (b) Maximum; (c) Minimum.



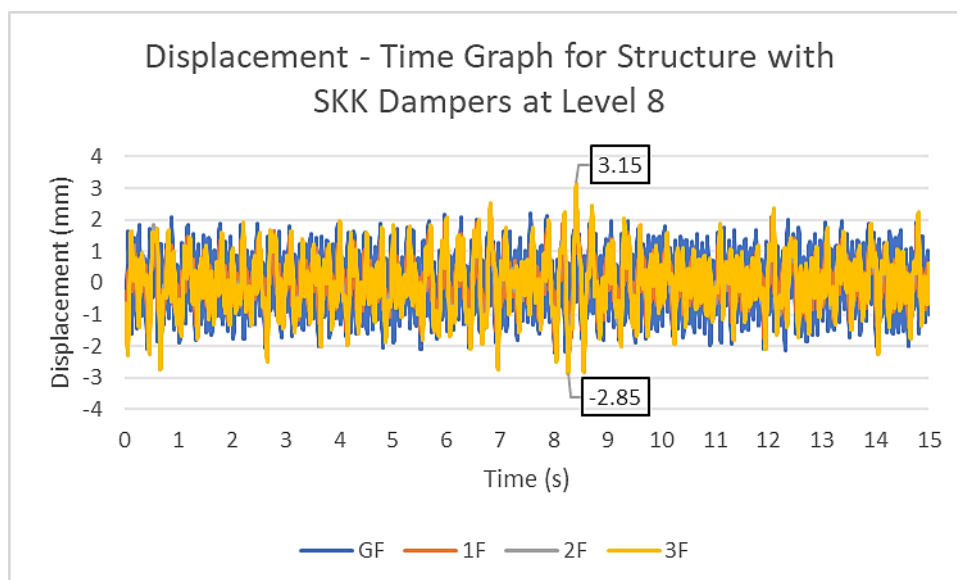
(a)



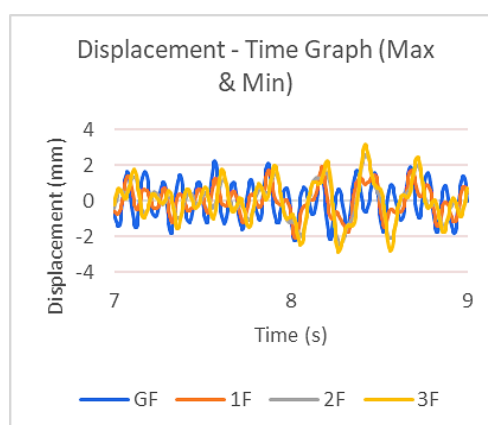
(b)

(c)

Graph A-20: Displacement – Time Graph for Structure with SKK Dampers at Level 7 (a) Overall; (b) Maximum; (c) Minimum.

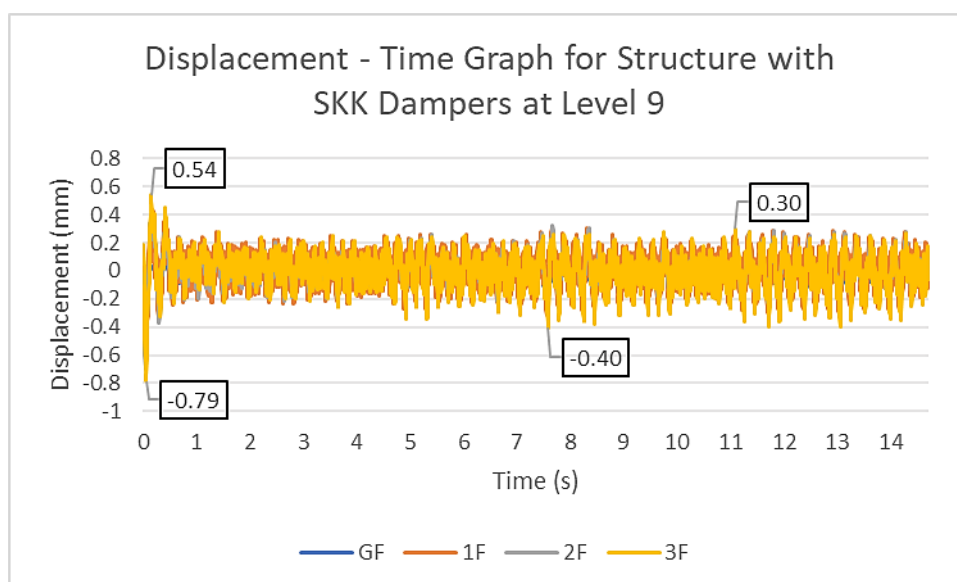


(a)

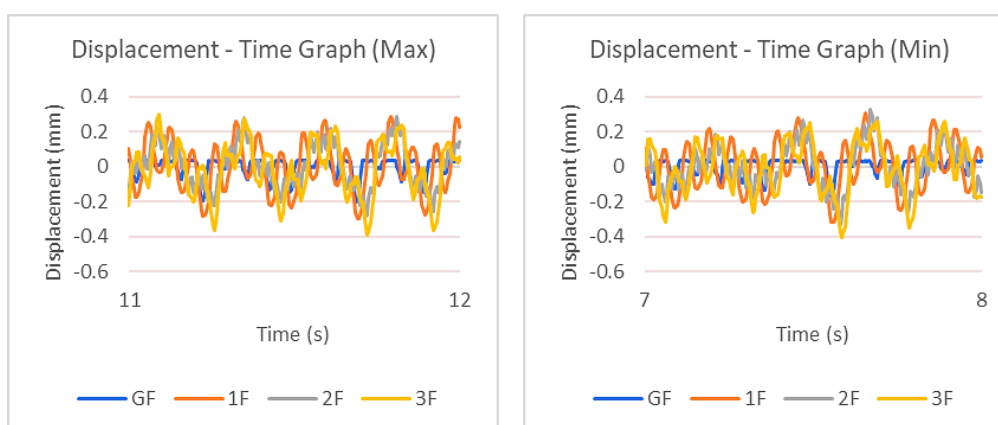


(b)

Graph A-21: Displacement – Time Graph for Structure with SKK Dampers at Level 8 (a) Overall; (b) Maximum and Minimum.



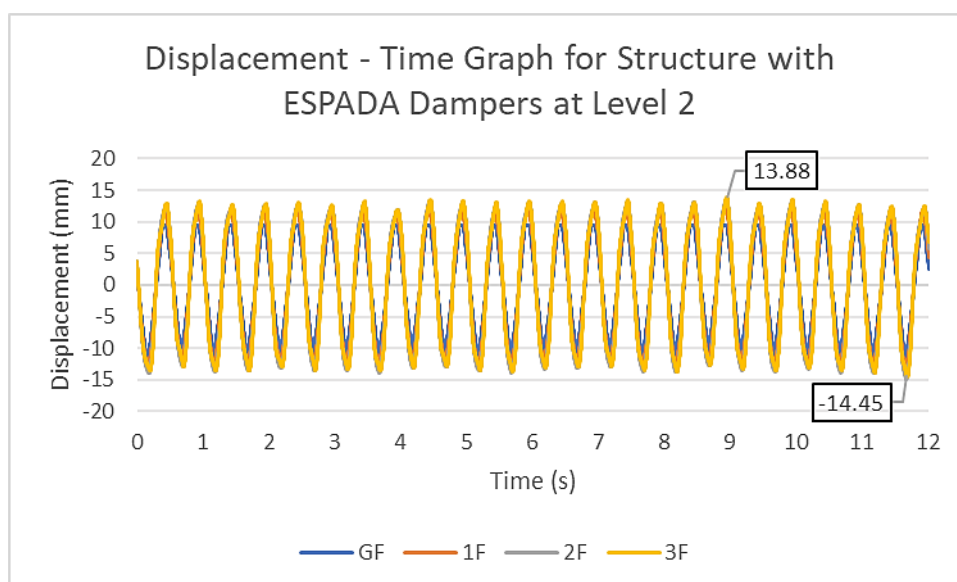
(a)



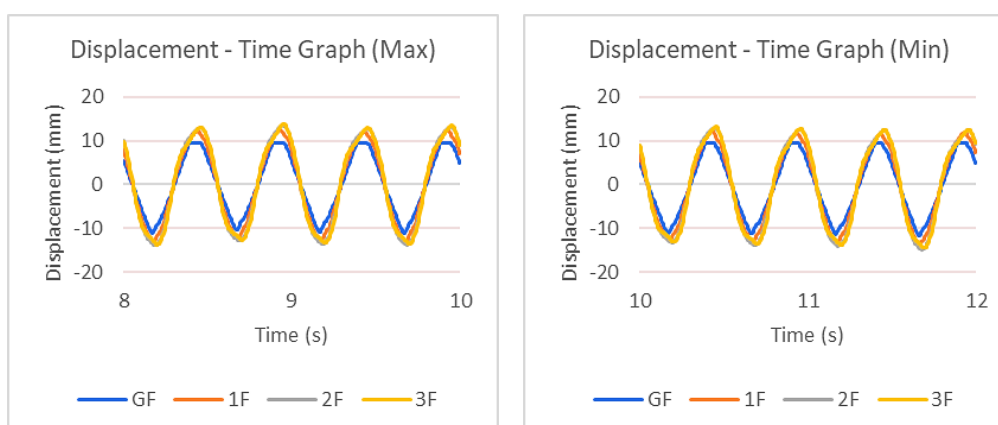
(b)

(c)

Graph A-22: Displacement – Time Graph for Structure with SKK Dampers at Level 9 (a) Overall; (b) Maximum; (c) Minimum.



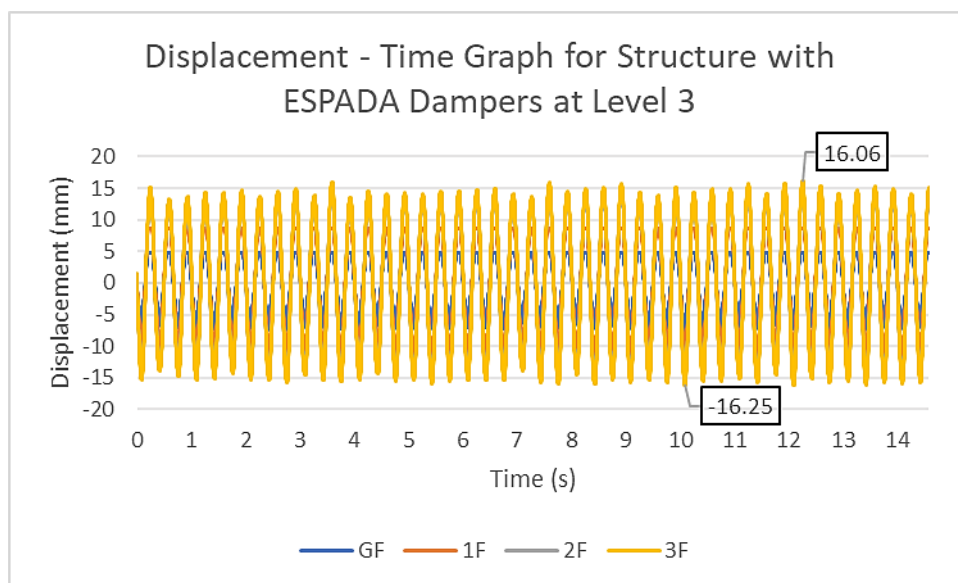
(a)



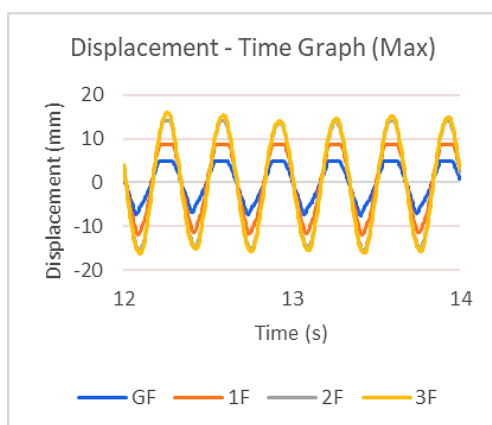
(b)

(c)

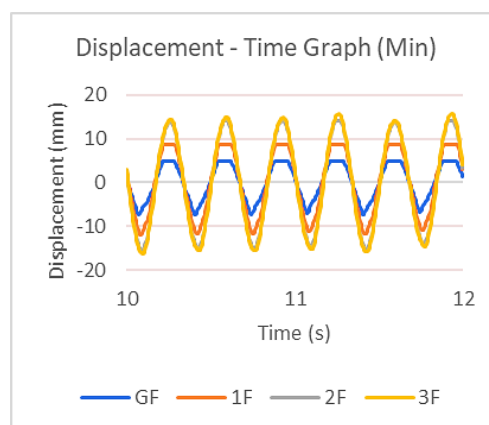
Graph A-23: Displacement – Time Graph for Structure with ESPADA Dampers at Level 2 (a) Overall; (b) Maximum; (c) Minimum.



(a)

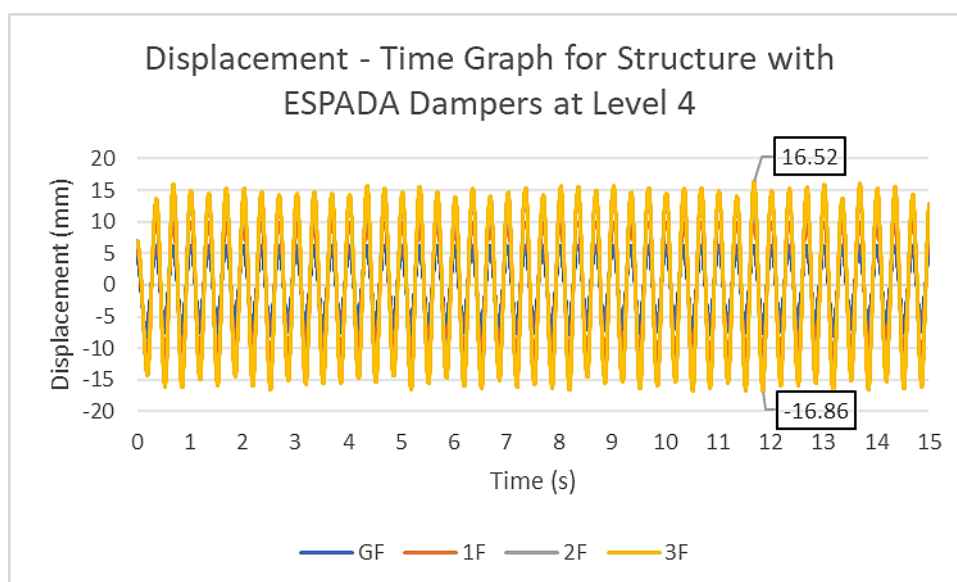


(b)

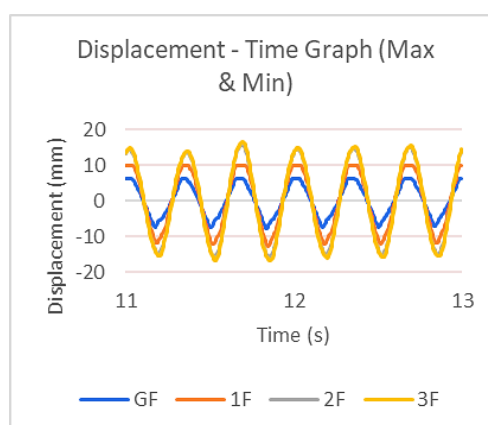


(c)

Graph A-24: Displacement – Time Graph for Structure with ESPADA Dampers at Level 3 (a) Overall; (b) Maximum; (c) Minimum.

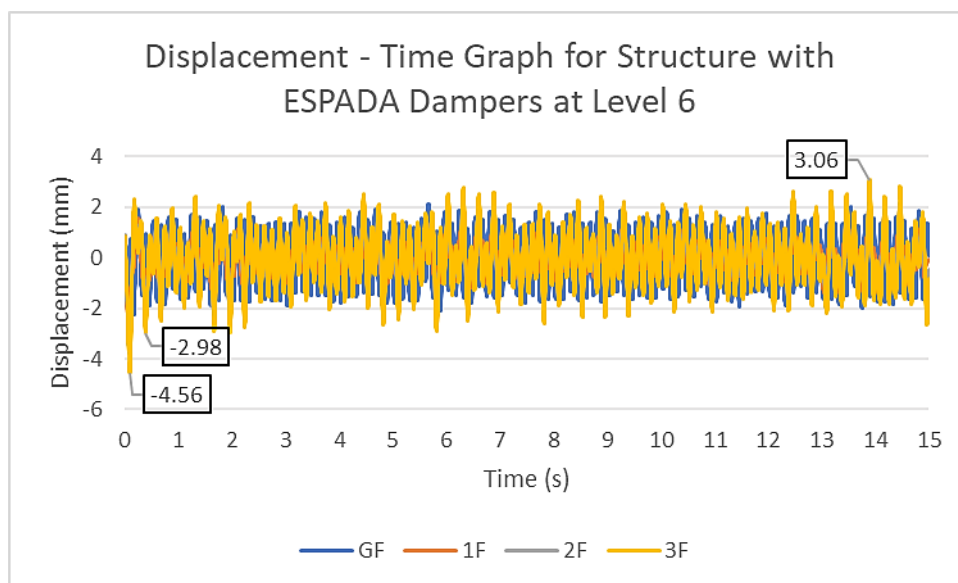


(a)

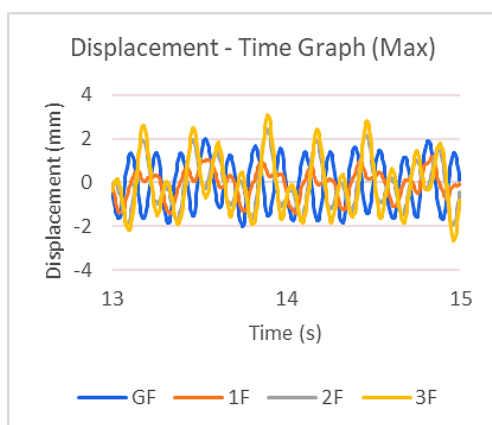


(b)

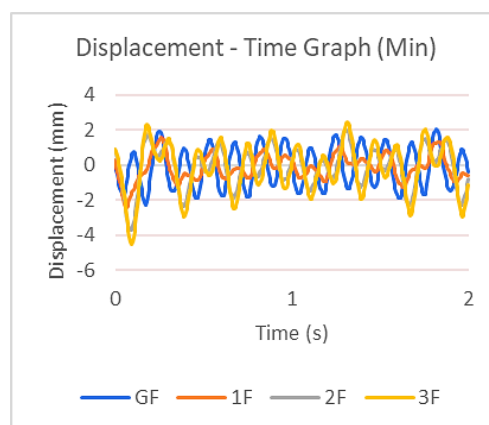
Graph A-25: Displacement – Time Graph for Structure with ESPADA Dampers at Level 4 (a) Overall; (b) Maximum and Minimum.



(a)

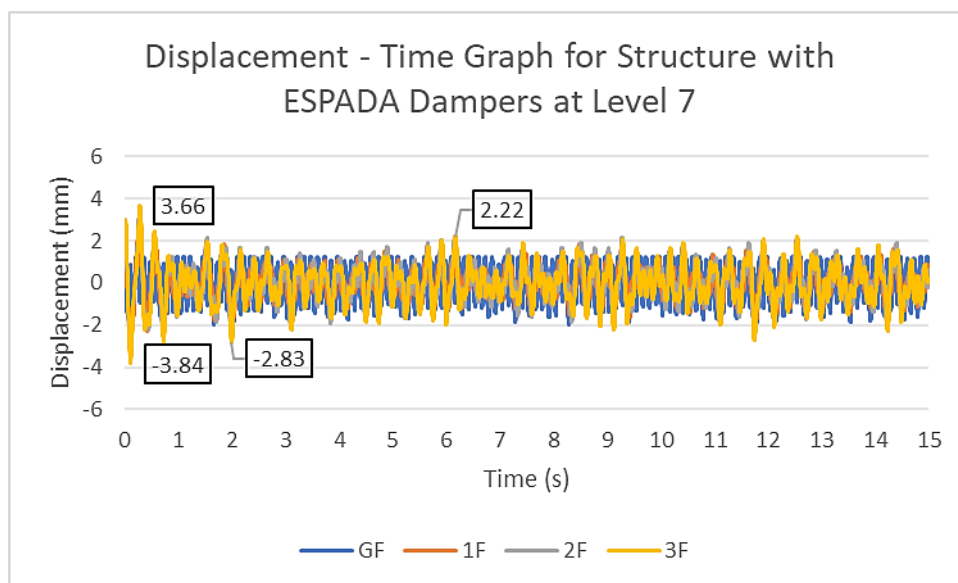


(b)

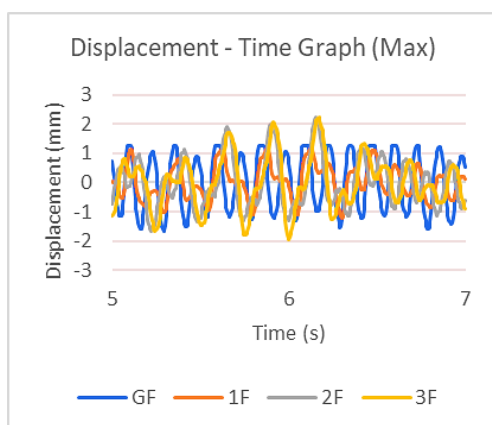


(c)

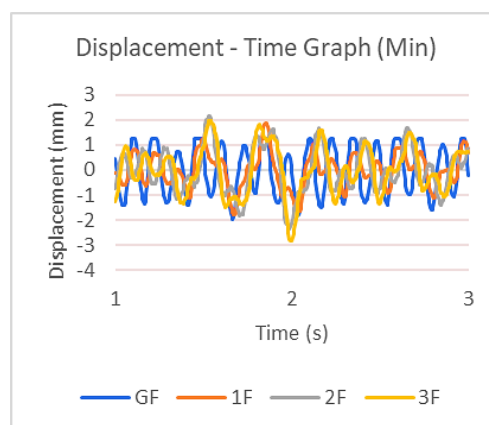
Graph A-26: Displacement – Time Graph for Structure with ESPADA Dampers at Level 6 (a) Overall; (b) Maximum; (c) Minimum.



(a)

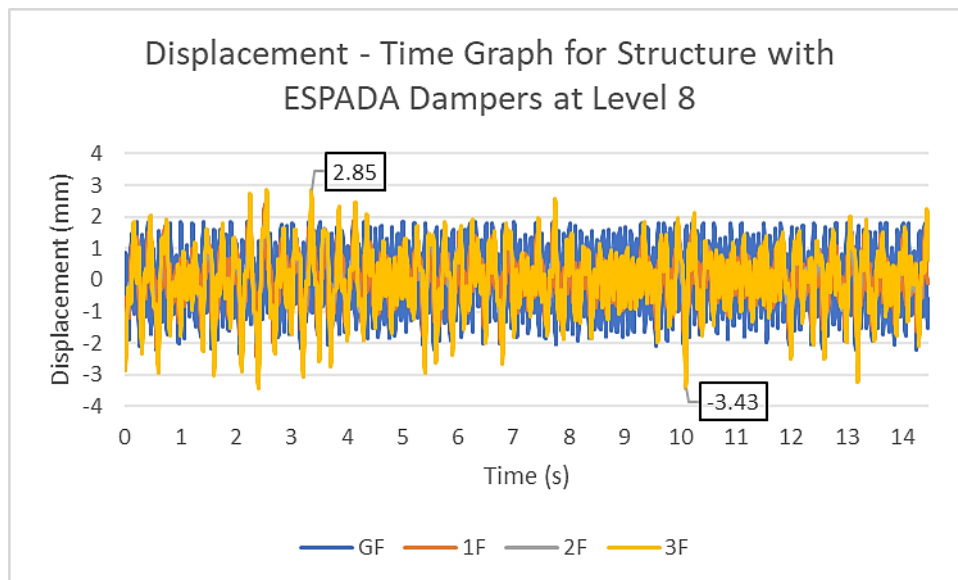


(b)

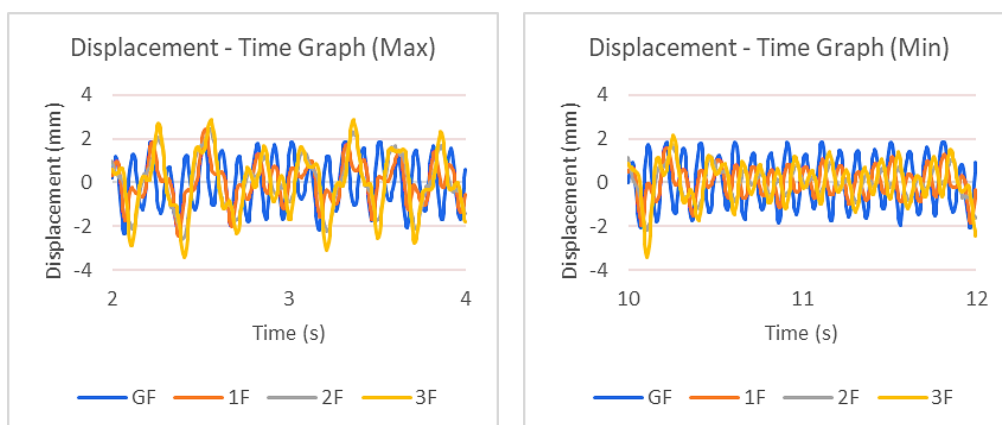


(c)

Graph A-27: Displacement – Time Graph for Structure with ESPADA Dampers at Level 7 (a) Overall; (b) Maximum; (c) Minimum.



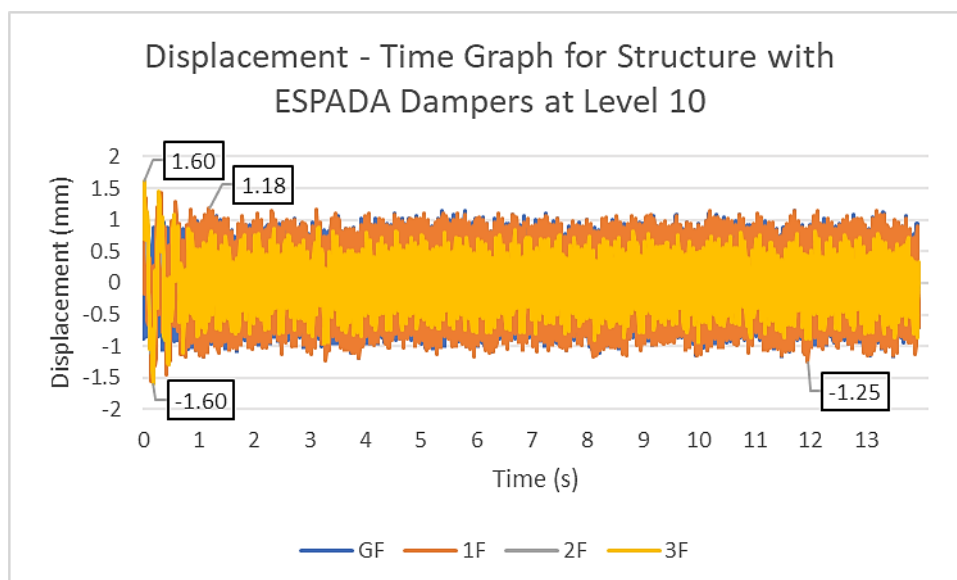
(a)



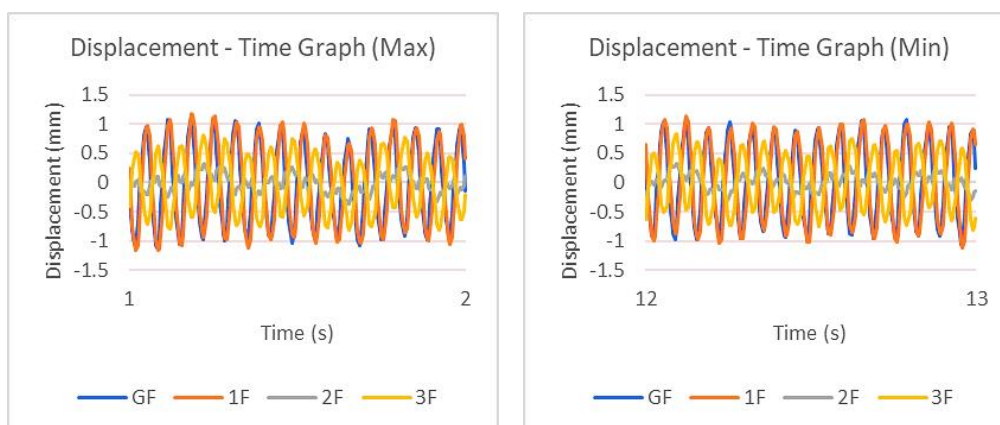
(b)

(c)

Graph A-28: Displacement – Time Graph for Structure with ESPADA Dampers at Level 8 (a) Overall; (b) Maximum; (c) Minimum.



(a)



(b)

(c)

Graph A-29: Displacement – Time Graph for Structure with ESPADA Dampers at Level 10 (a) Overall; (b) Maximum; (c) Minimum.